IMPROVING THE BIOACTIVITY OF POLYMERIC BONE REGENERATIVE SCAFFOLDS THROUGH PHYSICALLY AND CHEMICALLY INCORPORATED MOLECULES

By

XIAOHUAN WU

A dissertation submitted to the

School of Graduate Studies

Rutgers, The State University of New Jersey

In partial fulfillment of the requirements

For the degree of

Doctor of Philosophy

Graduate Program in Chemistry and Chemical Biology

Written under the direction of

Joachim Kohn

And approved by

_____

_____

_____

_____

New Brunswick, New Jersey

January, 2020

ABSTRACT OF THE DISSERTATION

Improving the Bioactivity of Polymeric Bone Regenerative Scaffolds Through Physically and Chemically Incorporated Molecules

By XIAOHUAN WU

Dissertation Director:

Professor Joachim Kohn

Although natural bone grafts including autografts and allografts are widely used in the clinics for the reconstruction of large bone defects, the development of bone graft substitutes (BGSs) continues to be an area of intense research. To apply the concept of tissue engineering in the development of BGSs, osteogenic growth factors and/or stem cells are incorporated into engineered scaffolds to mimic the bone tissue microenvironment. In the Kohn lab, BGSs based on E1001(1k), an intrinsically osteoconductive tyrosine-based polycarbonate, and beta-tricalcium phosphate (β-TCP) nanocrystals, were custom-fabricated (abbreviated as E1001(1k)/β-TCP scaffolds) and tested in various critical size calvarial models in combination with recombinant human bone morphogenetic protein 2 (rhBMP-2). To test the *in vivo* performance of this type of BGSs in long bone defect reconstruction, comparison study was conducted between E1001(1k)/β-TCP scaffolds and a clinically used β-TCP-based BGS (i.e., chronOS®) in a critical size sheep tibia model, with both constructs carrying a low dose of rhBMP-2 (1.1 mg per defect). It was found that

E1001(1k)/β-TCP scaffolds have comparable *in vivo* performance to chronOS®. More importantly, new bone regenerated in E1001(1k)/β-TCP scaffolds demonstrated a more physiological morphology, indicating ongoing bone remodeling into compact bone tissue.

A critical component in the bone microenvironment is the osteogenic growth factor (GF) phase. Though rhBMP-2 being one of the most studied GFs in the bone regeneration field, adverse effects associated with supraphysiological dosing is reported. Therefore, it is necessary to establish a reliable *in vitro-in vivo* correlation to determine the proper rhBMP-2 doses as well as to evaluate the efficacy of rhBMP-2 delivery systems. To date, the various study design in examining rhBMP-2 release profile *in vitro* has precluded comparative analyses. Due to the aforementioned concerns, a systematic evaluation of the most widely used *in vitro* rhBMP-2 activity assays is reported in **Chapter 3**. It was found that each model cell line (i.e., W-20-17, MC3T3 and C2C12) has an optimal dose-response range upon rhBMP-2 induction. In addition, a correlation between protein concentration (as measured by enzyme-linked immunosorbent assay) and protein activity (as measured by alkaline phosphatase induction from W-20-17 cells) was established. It was found that the expression system used to produce the rhBMP-2 had the most significant effect on its activity and stability *in vitro.*

In the previous *in vivo* studies, E1001(1k)/β-TCP scaffolds have been successfully utilized as carriers of rhBMP-2 to assist the healing process of critical size bone defects. However, the scaffold-only treatments typically demonstrate moderate osteoconductivity *in vivo* due to the lack of biological cues in synthetic polymers. On the other hand, owing to the unique redox chemistry, chelation capability with metal ions and Michael-type addition from thiols and amines, catechol functionality has triggered great interest in the

tissue engineering field. In **Chapter 4**, E1001(1k) analog polymers were functionalized with catechol side chains for enhanced bioactivity. It was found that the modified polymers were able to support mesenchymal stem cell, human osteoblast and MC3T3 cell growth. In addition, the surface anchoring catechol groups assist nano-sized silver deposition on the polymer surface by immersion-coating in silver nitrate solution, and the Ag-decorated surface has excellent antibacterial properties against *Escherichia coli* and *Staphylococcus aureus*. The versatile secondary functionality introduced by catechol modification makes the E1001(1k) analog polymers suitable for multiple bone-related applications.

DEDICATION

To my grandmother, Yunqing Di

ACKNOWLEDGMENTS

I'm grateful to my advisor Professor Joachim Kohn for giving me the opportunity to work in his lab. I appreciate his mentorship and support throughout my graduate school.

I would like to express my gratitude to my colleagues, especially Dr. Shuang Chen, for introducing me to the scaffold fabrication field; Dr. Koustubh S. Dube and Jarrod Cohen, for all the chemistry discussion; Stephanie L. Fung, for being a fantastic lab mate and her contribution to the rhBMP-2 related work; Dr. Yong Mao, for her help in biology-related questions; Dr. Maziar Shah Mohammadi, Dr. Ophir Ortiz, Dr. Alexandra K. Pastino and Dr. Antonio Merolli, Dr. Sangya Verma for all their help in the sheep study; Catherine Miles, Mariana Ries Nogueira de Lima, Joseph Molde, Christine Gwin for their great companion in Lab 210; Dr. Shruti Sexana, Dr. Wei Chang, Dr. Cemile Baktas, Dr. Sanjeeva Murthy, Dr. Divya Bhatnagar, Dr. Ritu Goyal, Dr. Tom Pashuck, Carmine Iovine, Dr. Zheng Zhang for their generous help and friendship. It is a great pleasure to work in such a friendly and supportive environment.

I would like to thank our collaborators Professor Changsheng Liu from East China University of Science and Technology for providing rhBMP-2; Professor Grace Elizabeth Pluhar at University of Minnesota Twin Cities for performing the sheep surgery; Dr. Timothy Bromage at New York University for doing the histology; Professor Gene Hall for allowing me to use ICP-OES instrument in his lab.

The sheep study and rhBMP-2 related work were supported by the Army, Navy, NIH, Air Force, VA, and Health Affairs to support the AFIRM II effort under Award No. W81XWH-14-2-0003. The rhBMP-2 research reported in this publication was also supported by the National Institute of Biomedical Imaging and Bioengineering of the

National Institutes of Health under Award Number P41EB001046. Note that the main body of Chapter 3 was published in *Tissue Engineering Part C: Methods* and reprinted with the permission from Mary Ann Liebert, Inc.

Last but not least, I would like to thank my committee members, Professor John Taylor, Professor Gene Hall, and Professor Adam J. Gormley for their attention and discussion about my research.

TABLE OF CONTENTS

LIST OF TABLES

LIST OF ILLUSTRATIONS

LIST OF ABBREVIATIONS

αMEM	Alpha Minimum Essential Medium
Ar	Argon
%	Percentage
±	Plus or minus
~	Approximately
^{13}C NMR	Carbon nuclear magnetic resonance
^{1}H NMR	Proton nuclear magnetic resonance
3D	Three-dimensional
ACURO	Animal Care and Use Review Office
AFIRM I	Armed Forces Institute of Regenerative Medicine I
$AgNO_3$	Silver nitrate
AgNP	Silver nanoparticle
ALP	Alkaline phosphatase
ANOVA	Single factor analysis of variance
AP	Anteroposterior
ASTM	American Society for Testing and Materials
BCA	Ticinchoninic acid
BGSs	Bone graft substitutes
BMPs	Bone morphogenetic proteins
CaP	Calcium phosphate
CHO cells	Chinese Hamster Ovary cells
CO_2	Carbon dioxide

CFU	Colony forming units
Da	Dalton
DCM	Methylene chloride
DI	Deionized
DIPEA	N, N-Diisopropylethylamine
DMEM	Dulbecco's Modified Eagle Medium
DMF	Dimethylformamide
DMSO-d_6	Deuterated dimethyl sulfoxide
DOPA	3,4-dihydroxy-l-phenylalanine
DSC	Differential scanning calorimetry
DT	Desaminotyrosyl-tyrosine
DTE	Desaminotyrosyl-tyrosine ethyl ester
DT*t*Bu	Desaminotyrosyl-tyrosine *tert*-butyl ester
E. coli	*Escherichia coli*
E1001(1k)	Poly(DTE -co-10%-DT-co-1%-PEG (1k))
ED50	Median effective dose
EDCI	1-Ethyl-3-(3- dimethylaminopropyl)carbodiimide
ELISA	Enzyme-linked immunosorbent assay
FBS	Fetal bovine serum
FDA	Food and Drug Administration
GF	Growth factor
GPC	Gel permeation chromatography
h	Hour

HA	Hydroxyapatite
hADSCs	Human adipose-derived stem cells
HCl	Hydrochloric acid
HEK-293	Human embryonic kidney 293 cells
HNO_3	Nitric acid
HPLC	High pressure liquid chromatography
HUASMCs	Human umbilical artery smooth muscle cell
HUVECs	Human umbilical vein endothelial cells
Hz	Hertz
ICP-OES	Inductively coupled plasma-optical emission spectrometry
IPA	Isopropanol
kDa	Kilodalton
kg	Kilogram
MeOH	Methanol
mg	Milligram
microCT	micro Computed Tomography
mins	Minutes
mL	Milliliter
mM	Millimole
mm	Millimeter
mmol	Millimole
Mn	Number averaged molecular weight
MSCs	Mesenchymal stem cells

M_w	Weight averaged molecular weight
N	Normality
NaCl	Sodium chloride
$NaNO_2$	Sodium nitrite
NaOH	Sodium hydroxide
ng	Nanogram
NHS	N-Hydroxysuccinimide
nm	Nanometer
ºC	Degree celcius
OD	Optical density
PBS	Phosphate-buffered saline
PCL	Polycaprolactone
pDA	Polydopamine
PEG	Poly(ethylene glycol)
PEG(1K)	Poly(ethylene glycol), molecular weight 1,000 Da
PLA	Polylactide
PLGA	Poly(lactic-*co*-glycolic acid)
PNPP	P-nitrophenyl phosphate
RH	Relative humidity
rhBMP-2	Recombinant human bone morphogenetic protein 2
rhBMP-7	Recombinant human bone morphogenetic protein 7
S. aureus	*Staphylococcus aureus*
SE	Standard error

SEM	Scanning electron microscope
TSB	Tryptic soy broth
TSA	Tryptic soy agar plates
TFA	Trifluoroacetic acid
TGF-b1	Transforming growth factor beta-1
WFI	Water for Injection
β-TCP	Beta-tricalcium phosphate
µg	Microgram
µL	Microliter
µm	Micrometer

1 Introduction

1.1 Scaffold-Based Bone Tissue Engineering for Large Bone Defects

Under healthy conditions, bone possesses intrinsic healing capacity without forming scar tissue. However, the regenerative process is impeded in the reconstruction of large bone defects caused by infection, trauma, tumor resection and diseases like osteoporosis.[1] Bone grafting is the primary treatment for augmenting the bone regeneration process in the cases mentioned above. The three types of bone grafts are autografts, allografts and bone graft substitutes (BGSs).[2] Generally, the regeneration capacity of bone grafts is measured by their osteoinductivity, osteoconductivity and osteointegration.[3] Osteoinduction implies recruitment of mesenchymal stem cells (MSCs) and stimulation of MSCs to differentiate into preosteoblasts.[3] Osteoconduction refers to the attachment and growth of bone cells on the bone graft surface.[3] Osseointegration means a structurally and functionally fused connection between the native bone and the orthopedic implant.[4] Bone grafting from either autografts and allografts is a common surgical procedure in orthopedic and maxillofacial surgeries.[5] Due to the quantity restrictions and the additional surgical procedure of autografts harvesting, and the immunogenicity as well as rejection reactions of allografts, the investigation of BGSs as bone graft alternatives has gained intense attention.

1.2 Application of Recombinant Bone Morphogenetic Protein 2

The components of the bone microenvironment include a matrix of hydroxyapatite nanocrystals and collagen fibers; a cellular phase of osteoblasts, osteoclasts, and osteocytes; and a biomolecule phase of growth factors and cytokines.[2, 6-8] To mimic the natural bone tissue, stem cells and/or growth factors are incorporated into scaffolds for enhanced osteoinductivity and osteoconductivity in the development of BGSs.

For the use of stem cells, adult MSCs are the most widely investigated cell type in the search of proper BGSs. Up to date, despite numerous promising reports on bone regeneration of critical size defects in various animal species, the use of MSCs for bone repair remains in a preclinical stage. A couple of critical issues need to be addressed before they are ready for clinical use: (1) the epigenetic and genetic changes of MSC population resulting from not standardized isolation protocols; (2) the genetic differences of MSCs isolated from various tissues and donors.[7]

Growth factors are proteins that bind to certain receptors on cell membranes and initiate a cascade of signaling inside cells. This cellular recognition leads to signal transduction to the nucleus, activating transcription factors and thus affecting gene expression. As a result, critical biological functions like matrix synthesis and tissue differentiation are manipulated.[8] Critical growth factors in the bone regeneration process include fibroblast growth factors (FGFs), vascular endothelial growth factor (VEGF), insulin-like growth factors (IGFs) and bone morphogenetic proteins (BMPs).[8] BMPs were isolated from the demineralized bone matrix by Urist in 1965,[9] and they were found to not only play a key role in embryonal development but also maintain and regenerate adult tissues and organs.[10-11] To this date, around 20 BMPs have been identified, with BMP-2

and BMP-7 having the most potent osteogenic ability to induce bone and cartilage formation.[12] In 2002, rhBMP-2/absorbable collagen sponge (ACS) loaded with a rhBMP-2 solution at 1.5-mg/mL (INFUSE® Bone Graft, Medtronic Spinal and Biologics, Memphis, TN) was approved by U.S. Food and Drug Administration (FDA) for spinal fusion procedures. Later, the same device was FDA-approved for open tibial fractures in 2004 and as an alternative to autografts for sinus augmentations as well as alveolar defects associated with extraction sockets in 2007.[13] The large share of preclinical and clinical research efforts together with triple FDA approvals directed particular attention to rhBMP-2, making it one of the most investigated, reported and significantly advanced growth factors in orthopedics. Though there is a vast amount of preclinical reports on the utilization of tissue-engineered scaffolds as carriers to deliver rhBMP-2 to the injury sites, a critical limitation to the current rhBMP-2 therapy is the need for supraphysiological doses due to the fast inactivation of proteins and local clearance.

Since rhBMP-2 could induce ectopic bone formation, it is evolutionarily designed to be a poorly soluble protein and binds strongly to the extracellular matrix to avoid exposure to responsive tissues during bone healing. However, vast amounts of local administration causes precipitation-rendered rhBMP-2 inactivation and excessive diffusion of rhBMP-2 into the surrounding tissue, which leads to high treatment costs and high risk of side effects such as infections, severe swelling, heterotopic ossification.[13-14] Therefore, in order to eliminate adverse effects, it is very important to develop proper carriers (i.e., scaffolds) that provide a sustained release of rhBMP-2 within the clinically relevant dose window.

Moreover, the source of rhBMP-2 influences its molecular structure and thus results in different osteogenic activity and stability. The extraction of native BMP from animal bones is impeded by its low concentration in bone tissues (~several mg per kg), different physiological properties due to species differences and risk of pathogen transfer. To satisfy the bulk demand of research and clinics, commercially available BMP-2s in the market are expressed as recombinant proteins from *Escherichia coli,*[15] Chinese Hamster Ovary (CHO) cells[16] and Human Embryonic Kidney 293 cells (HEK-293).[17] It should be noted that BMP-2 polypeptide expressed from CHO and HEK-293 cells undergo glycosylation, whereas polypeptides expressed from prokaryotic cells like *E. coli* do not have glycosylation.[18] Though all rhBMP-2s have exhibited bone-forming activities *in vivo*,[19-20] the lack of glycosylation reduces the solubility and bioactivity of *E. coli*-derived rhBMP-2 *in vitro*, thus having influences on its effective dose *in vivo* compared to mammalian cell-derived rhBMP-2s.[21] To date, there are not systematic literature comparisons on evaluating the efficacy of rhBMP-2 from different sources. On second thought, since it is necessary to establish an *in vitro* - *in vivo* correlation to help predict the performance of delivery systems as well as rhBMP-2 dosage window, a standardized protocol needs to be established for this purpose.

1.3 The Evolution of Biomaterials and Bone Graft Substitutes

As the knowledge of the bone tissue microenvironment has advanced in the past decades, the requirements and properties of BGSs have evolved and resulted in changes in the prerequisites of biomaterials used for implant devices fabrication. Hench defined the three generations of biomaterials throughout this evolution,[22] and it should be pointed out

that there is currently still active research for each generation of biomaterials. The first generation of biomaterials for BGSs requires bio-inert materials that have matching mechanical properties to the bone tissue, including metals such as titanium, ceramics such as alumina and polymers such as polypropylene and polymethylmethacrylate.[22] A common issue with these materials is the encapsulation of implants *in vivo* caused by inflammatory responses.[23]

Second generation BGSs aim to enhance to osteoconduction of devices and avoid fibrous tissue formation around the implants. To this point, biodegradable synthetic polymers like polylactide (PLA), poly(ε-caprolactone) (PCL), poly(lactic-*co*-glycolic acid) (PLGA) and natural polymers like chitosan and hyaluronic acid were applied in the fabrication of BGSs, the idea is to control the degradation of polymers into harmless byproducts as bone regeneration occurs. Composites made from polymers and bioactive ceramics were also introduced to improve the osteoconductivity and mechanical properties of the polymeric BGSs. Besides, to make polymer surfaces more "bioactive", either physically adsorbed or bioconjugated proteins/peptides can be modified onto device surfaces.[6, 24]

The third generation of biomaterials appeared at the same time as the scaffolds-based tissue engineering started to emerge,[25] with the ultimate goal of stimulating specific stem cell responses at the molecular level. Therefore, the combination of bioactivity and biodegradability become the most important characteristic of third-generation biomaterials. Although synthetic biodegradable polymers used in bone tissue engineering can be synthesized with tailored degradation rates and mechanical strength, they usually lack cell recognition sites and are hydrophobic. Owing to their limitations, secondary

functionalization on those polymers is necessary to improve their bioactivity in order to make them better candidates for BGS fabrication.[26]

1.4 Catechol-Modified Biomaterials

The inherent design of nature-inspired materials greatly advanced the development of functional materials with unique properties. Notably, the investigation of wet adhesion phenomenon of mussels leads to the discovery of 1,2-dihydroxybenzene (catechol) functionality in underwater adhesion, it was found that the synergistic effect from 3,4-dihydroxy-l-phenylalanine (DOPA) and lysine-enriched mussel foot proteins contribute to their extraordinary wet adhesion ability in the marine environment, with the catechol structure from DOPA mainly responsible for bridging attachments between surfaces.[27-31] With these intriguing findings, it was later discovered in 2007 that dopamine, with a similar chemical structure to DOPA, can undergo self-polymerization in alkaline aqueous conditions.[32] The resulting polydopamine (pDA) serves as a biocompatible coating on inorganic and organic substrates and allows for further functionalization with bioactive components.[33]

Catechol plays essential roles in many organisms as they interact with both inorganic (e.g., transition metal ions, metal oxides) and organic (e. g., amino acids) species through non-covalent forces (i.e., hydrogen bonding, π-stacking, chelation) and chemical reactions.[34] A unique property of catechol is its chelation with transition metals to give catechol-metal complexes.[34] Interestingly, it was reported that the catechol in polydopamine enriches calcium ions on the coating surface and facilitates the formation of hydroxyapatite (HA) in simulated body fluid, the orientation of HA crystals resembles natural HA in the bone tissue.[35]

Similar mineralization arising from the chelation between surface-anchoring catechol and zinc ions was also observed on poly(propylene carbonate)-*block*-poly(4-vinylcatechol acetonide) membranes.[36] pDA has been widely investigated as a bioactive orthopedic implant coating due to its surface-independent nature.

To date, the mechanism of pDA formation and the ultimate chemical structures of pDA remain a subject of debate.[37] The undefined structure of pDA gave rise to the exploration of other categories of catechol-containing biomaterials, where catechol groups are chemically introduced either to natural polymers such as chitosan,[38] alginate,[39] and hyaluronic acid[40] or synthetic polymers such as PEG-based polymers,[41] polymethacrylates,[41] polyacrylates,[41] and polyesters.[42-45] In the past decade, most mussel-inspired biomaterials are synthesized for their applications in bioadhesives and surface coatings in the biomedical field. Catechol-functionalized hydrogels from polysaccharides, polymethacrylates/polyacrylates and PEG-based polymers have been extensively tested for surgical sealants and glues in moist conditions.[46-48] For surface coatings-related applications, aside from the surface-independent pDA, catechol-functionalized polymers have between utilized to anchor macromolecules, functional groups or nanoparticles to device surfaces. Such medical applications include the creation of anticoagulant surfaces for cardiovascular devices[49] and antifouling surfaces for antibacterial needs in the orthopedic implant industry.[50]

Furthermore, due to the chemical reaction between catechol and its oxidized form (quinone) with amines and thiols from proteins, the interactions between catechol and cells were investigated and triggered intense interests in the tissue engineering field. For instance, it has been discovered that the adhesion and migration of NIH 3T3 fibroblasts cultured on

catechol-conjugated PCL-*block*-PEG nanofibers are proportional to the presence of catechol groups (nmol level) in a serum-free medium.[43] In a second study, a catecholized hyaluronic acid (CA-HA) hydrogel improved human adipose-derived stem cells (hADSCs)-induced angiogenesis in a critical limb ischemia mouse model. The same hydrogel promotes the best bone formation in a critical size mouse calvarial defect model in combination with rhBMP-2 compared to controls.[51] Moreover, it was found that pDA coating significantly promotes the attachment and proliferation of human umbilical vein endothelial cells (HUVECs) due to the quinone-mediated (oxidized catechol) fibrinogen adsorption on pDA. On the contrary, pDA coating also dramatically decreased the adhesion and proliferation of human umbilical artery smooth muscle cells (HUASMCs) owing to the presence of catechol groups in pDA. The redox chemistry of catechol in pDA is sable to control cell fates by altering specific protein adsorption.[52-53] The above mentioned *in vitro* and *in vivo* studies make catechol-containing materials particularly interesting for the development of third-generation biomaterials.

1.5 Thesis Organization

In this thesis, **Chapter 2** reports on the fabrication and characterization of 3 cm-long and tubular scaffolds made from a tyrosine-derived polycarbonate and β-TCP nanocrystals. The rhBMP-2 loading method and release profile were then investigated and developed for the human-sized scaffolds. The *in vivo* segmental bone regeneration performance of those scaffolds loaded with rhBMP-2 was compared to a clinically used chronOS® (TCP-based BGSs) with the same dose of rhBMP-2 (1.1 mg per defect) in a 30 mm critical size sheep tibia model. The current study aims at translating our previous

success in critical size calvarial defects to a long bone defect model in large animals. Bone formation in both treatment groups was assessed by microCT and histology analyses.

Then, a systematic investigation of the experimental parameters of the most widely used *in vitro* rhBMP-2 bioactivity assays is presented in **Chapter 3**. In this chapter, the dose-responses of model cell lines (W-20-17, MC3T3 and C2C12) upon rhBMP-2 induction were elaborated in terms of alkaline phosphatase (ALP) expression. In addition, a correlation between protein concentration (as measured by ELISA) and protein activity (as measured by ALP induction from W-20-17 cells) was established. Finally, the bioactivity and stability of rhBMP-2 from different resources were evaluated *in vitro*.

Though E1001(1k)/β-TCP scaffolds can be utilized as carriers for rhBMP-2 delivery in the reconstruction of critical size bone defects, the scaffold itself demonstrated limited osteoconductivity *in vivo* due to the lack of biological cues on the structure of E1001(1k).[54-55] In **Chapter 4**, E1001(1k) analog polymers were functionalized with catechol groups for enhanced bioactivity. The cell-material interaction was studied using human osteoblasts, MSCs and MC3T3 cells. In addition, the catechol-assisted silver deposition on the polymer surface was investigated, and the antibacterial capacity of the resulting polymer films was tested against *E. coli* and *S. aureus.*

1.6 References

1.Mauffrey, C.; Barlow, B. T.; Smith, W., Management of segmental bone defects. *The Journal of the American Academy of Orthopaedic Surgeons* **2015,** *23* (3), 143-53.
2.Brydone, A. S.; Meek, D.; Maclaine, S., Bone grafting, orthopaedic biomaterials, and the clinical need for bone engineering. *Proc Inst Mech Eng H* **2010,** *224* (12), 1329-43.
3.Albrektsson, T.; Johansson, C., Osteoinduction, osteoconduction and osseointegration. *Eur Spine J* **2001,** *10 Suppl 2*, S96-101.
4.LeGeros, R. Z.; Craig, R. G., Strategies to affect bone remodeling: osteointegration. *Journal of bone and mineral research : the official journal of the American Society for Bone and Mineral Research* **1993,** *8 Suppl 2*, S583-96.
5.Ho-Shui-Ling, A.; Bolander, J.; Rustom, L. E.; Johnson, A. W.; Luyten, F. P.; Picart, C., Bone regeneration strategies: Engineered scaffolds, bioactive molecules and stem cells current stage and future perspectives. *Biomaterials* **2018,** *180*, 143-162.
6.Polo-Corrales, L.; Latorre-Esteves, M.; Ramirez-Vick, J. E., Scaffold design for bone regeneration. *J Nanosci Nanotechnol* **2014,** *14* (1), 15-56.
7.Luby, A. O.; Ranganathan, K.; Lynn, J. V.; Nelson, N. S.; Donneys, A.; Buchman, S. R., Stem Cells for Bone Regeneration: Current State and Future Directions. *J Craniofac Surg* **2019,** *30* (3), 730-735.
8.Azevedo, H. S.; Pashkuleva, I., Biomimetic supramolecular designs for the controlled release of growth factors in bone regeneration. *Adv Drug Deliv Rev* **2015,** *94*, 63-76.
9.Urist, M. R., Bone: formation by autoinduction. *Science* **1965,** *150* (3698), 893-9.
10.Hogan, B. L., Bone morphogenetic proteins: multifunctional regulators of vertebrate development. *Genes Dev* **1996,** *10* (13), 1580-94.
11.Reddi, A. H., Role of morphogenetic proteins in skeletal tissue engineering and regeneration. *Nat Biotechnol* **1998,** *16* (3), 247-52.
12.El Bialy, I.; Jiskoot, W.; Reza Nejadnik, M., Formulation, Delivery and Stability of Bone Morphogenetic Proteins for Effective Bone Regeneration. *Pharm Res* **2017,** *34* (6), 1152-1170.
13.McKay, W. F.; Peckham, S. M.; Badura, J. M., A comprehensive clinical review of recombinant human bone morphogenetic protein-2 (INFUSE Bone Graft). *Int Orthop* **2007,** *31* (6), 729-34.
14.Carreira, A. C.; Lojudice, F. H.; Halcsik, E.; Navarro, R. D.; Sogayar, M. C.; Granjeiro, J. M., Bone morphogenetic proteins: facts, challenges, and future perspectives. *Journal of dental research* **2014,** *93* (4), 335-45.
15.Wozney, J. M.; Rosen, V.; Celeste, A. J.; Mitsock, L. M.; Whitters, M. J.; Kriz, R. W.; Hewick, R. M.; Wang, E. A., Novel regulators of bone formation: molecular clones and activities. *Science* **1988,** *242* (4885), 1528-34.
16.Kim, J. Y.; Kim, Y. G.; Lee, G. M., CHO cells in biotechnology for production of recombinant proteins: current state and further potential. *Appl Microbiol Biotechnol* **2012,** *93* (3), 917-30.
17.Chen, R.; Jeong, S. S.; Feng, H., Recombinant production of authentic human proteins using human cell expression systems. Google Patents: 2012.
18.Liu, C.; Lin, J.; Jiangchao, Q.; Yuan, Y., Optimized DNA sequences encoding recombinant human bone morphogenetic protein-2 (rhBMP-2), preparation method and the uses thereof. Google Patents: 2011.

19.Carragee, E. J.; Hurwitz, E. L.; Weiner, B. K., A critical review of recombinant human bone morphogenetic protein-2 trials in spinal surgery: emerging safety concerns and lessons learned. *Spine J* **2011,** *11* (6), 471-91.
20.Harada, Y.; Itoi, T.; Wakitani, S.; Irie, H.; Sakamoto, M.; Zhao, D.; Nezu, Y.; Yogo, T.; Hara, Y.; Tagawa, M., Effect of Escherichia coli-produced recombinant human bone morphogenetic protein 2 on the regeneration of canine segmental ulnar defects. *J Bone Miner Metab* **2012,** *30* (4), 388-99.
21.Kempen, D. H. R.; Lu, L.; Hefferan, T. E.; Creemers, L. B.; Maran, A.; Classic, K. L.; Dhert, W. J. A.; Yaszemski, M. J., Retention of in vitro and in vivo BMP-2 bioactivities in sustained delivery vehicles for bone tissue engineering. *Biomaterials* **2008,** *29* (22), 3245-3252.
22.Hench, L. L.; Polak, J. M., Third-generation biomedical materials. *Science* **2002,** *295* (5557), 1014-7.
23.Anderson, J. M., Biological responses to materials. *Annual review of materials research* **2001,** *31* (1), 81-110.
24.Ma, Z.; Gao, C.; Gong, Y.; Ji, J.; Shen, J., Immobilization of natural macromolecules on poly-L-lactic acid membrane surface in order to improve its cytocompatibility. *J Biomed Mater Res* **2002,** *63* (6), 838-47.
25.Amini, A. R.; Laurencin, C. T.; Nukavarapu, S. P., Bone tissue engineering: recent advances and challenges. *Critical Reviews™ in Biomedical Engineering* **2012,** *40* (5).
26.BaoLin, G.; Ma, P. X., Synthetic biodegradable functional polymers for tissue engineering: a brief review. *Sci China Chem* **2014,** *57* (4), 490-500.
27.Maier, G. P.; Rapp, M. V.; Waite, J. H.; Israelachvili, J. N.; Butler, A., Adaptive synergy between catechol and lysine promotes wet adhesion by surface salt displacement. *Science* **2015,** *349* (6248), 628-632.
28.Harrington, M. J.; Masic, A.; Holten-Andersen, N.; Waite, J. H.; Fratzl, P., Iron-clad fibers: a metal-based biological strategy for hard flexible coatings. *Science* **2010,** *328* (5975), 216-20.
29.Stewart, R. J.; Ransom, T. C.; Hlady, V., Natural Underwater Adhesives. *J Polym Sci B Polym Phys* **2011,** *49* (11), 757-771.
30.Waite, J. H.; Tanzer, M. L., Polyphenolic Substance of Mytilus-Edulis - Novel Adhesive Containing L-Dopa and Hydroxyproline. *Science* **1981,** *212* (4498), 1038-1040.
31.Waite, J. H.; Qin, X., Polyphosphoprotein from the adhesive pads of Mytilus edulis. *Biochemistry* **2001,** *40* (9), 2887-93.
32.Lee, H.; Dellatore, S. M.; Miller, W. M.; Messersmith, P. B., Mussel-inspired surface chemistry for multifunctional coatings. *Science* **2007,** *318* (5849), 426-430.
33.Lee, H. A.; Ma, Y. F.; Zhou, F.; Hong, S.; Lee, H., Material-Independent Surface Chemistry beyond Polydopamine Coating. *Accounts Chem Res* **2019,** *52* (3), 704-713.
34.Yang, J.; Stuart, M. A. C.; Kamperman, M., Jack of all trades: versatile catechol crosslinking mechanisms. *Chem Soc Rev* **2014,** *43* (24), 8271-8298.
35.Ryu, J.; Ku, S. H.; Lee, H.; Park, C. B., Mussel-Inspired Polydopamine Coating as a Universal Route to Hydroxyapatite Crystallization. *Adv Funct Mater* **2010,** *20* (13), 2132-2139.
36.Zhou, H.-J.; Yang, G.-W.; Zhang, Y.-Y.; Xu, Z.-K.; Wu, G.-P., Bioinspired Block Copolymer for Mineralized Nanoporous Membrane. *ACS nano* **2018,** *12* (11), 11471-11480.

37.Liu, Y.; Ai, K.; Lu, L., Polydopamine and its derivative materials: synthesis and promising applications in energy, environmental, and biomedical fields. *Chem Rev* **2014,** *114* (9), 5057-115.
38.Ryu, J. H.; Hong, S.; Lee, H., Bio-inspired adhesive catechol-conjugated chitosan for biomedical applications: A mini review. *Acta Biomaterialia* **2015,** *27*, 101-115.
39.Kim, Y. S.; Cho, S. W.; Ko, B.; Shin, J.; Ahn, C. W., Alginate-Catechol Cross-Linking Interferes with Insulin Secretion Capacity in Isolated Murine Islet Cells. *Diabetes Metab J* **2018,** *42* (2), 164-168.
40.Park, H. J.; Jin, Y.; Shin, J.; Yang, K.; Lee, C.; Yang, H. S.; Cho, S. W., Catechol-Functionalized Hyaluronic Acid Hydrogels Enhance Angiogenesis and Osteogenesis of Human Adipose-Derived Stem Cells in Critical Tissue Defects. *Biomacromolecules* **2016,** *17* (6), 1939-48.
41.Kord Forooshani, P.; Lee, B. P., Recent approaches in designing bioadhesive materials inspired by mussel adhesive protein. *J Polym Sci A Polym Chem* **2017,** *55* (1), 9-33.
42.Mehdizadeh, M.; Weng, H.; Gyawali, D.; Tang, L.; Yang, J., Injectable citrate-based mussel-inspired tissue bioadhesives with high wet strength for sutureless wound closure. *Biomaterials* **2012,** *33* (32), 7972-7983.
43.Choi, J. S.; Messersmith, P. B.; Yoo, H. S., Decoration of electrospun nanofibers with monomeric catechols to facilitate cell adhesion. *Macromol Biosci* **2014,** *14* (2), 270-9.
44.Jenkins, C. L.; Siebert, H. M.; Wilker, J. J., Integrating Mussel Chemistry into a Bio-Based Polymer to Create Degradable Adhesives. *Macromolecules* **2017,** *50* (2), 561-568.
45.Bilic, G.; Brubaker, C.; Messersmith, P. B.; Mallik, A. S.; Quinn, T. M.; Haller, C.; Done, E.; Gucciardo, L.; Zeisberger, S. M.; Zimmermann, R., Injectable candidate sealants for fetal membrane repair: bonding and toxicity in vitro. *American journal of obstetrics and gynecology* **2010,** *202* (1), 85. e1-85. e9.
46.Brubaker, C. E.; Messersmith, P. B., Enzymatically degradable mussel-inspired adhesive hydrogel. *Biomacromolecules* **2011,** *12* (12), 4326-4334.
47.Fullenkamp, D. E.; He, L.; Barrett, D. G.; Burghardt, W. R.; Messersmith, P. B., Mussel-inspired histidine-based transient network metal coordination hydrogels. *Macromolecules* **2013,** *46* (3), 1167-1174.
48.Barrett, D. G.; Bushnell, G. G.; Messersmith, P. B., Mechanically robust, negative-swelling, mussel-inspired tissue adhesives. *Advanced healthcare materials* **2013,** *2* (5), 745-755.
49.Liu, X.; Deng, J.; Ma, L.; Cheng, C.; Nie, C.; He, C.; Zhao, C., Catechol chemistry inspired approach to construct self-cross-linked polymer nanolayers as versatile biointerfaces. *Langmuir* **2014,** *30* (49), 14905-14915.
50.Ryu, J. Y.; Song, I. T.; Lau, K. A.; Messersmith, P. B.; Yoon, T.-Y.; Lee, H., New antifouling platform characterized by single-molecule imaging. *Acs Appl Mater Inter* **2014,** *6* (5), 3553-3558.
51.Park, H. J.; Jin, Y.; Shin, J.; Yang, K.; Lee, C.; Yang, H. S.; Cho, S. W., Catechol-Functionalized Hyaluronic Acid Hydrogels Enhance Angiogenesis and Osteogenesis of Human Adipose-Derived Stem Cells in Critical Tissue Defects. *Biomacromolecules* **2016,** *17* (6), 1939-1948.
52.Yang, Z.; Tu, Q.; Zhu, Y.; Luo, R.; Li, X.; Xie, Y.; Maitz, M. F.; Wang, J.; Huang, N., Mussel-inspired coating of polydopamine directs endothelial and smooth muscle cell fate for re-endothelialization of vascular devices. *Adv Healthc Mater* **2012,** *1* (5), 548-59.

53.Ding, Y. H.; Yang, Z. L.; Bi, C. W. C.; Yang, M.; Zhang, J. C.; Xu, S. L.; Lu, X.; Huang, N.; Huang, P. B.; Leng, Y., Modulation of protein adsorption, vascular cell selectivity and platelet adhesion by mussel-inspired surface functionalization. *J Mater Chem B* **2014,** *2* (24), 3819-3829.
54.Kim, J.; Magno, M. H.; Alvarez, P.; Darr, A.; Kohn, J.; Hollinger, J. O., Osteogenic differentiation of pre-osteoblasts on biomimetic tyrosine-derived polycarbonate scaffolds. *Biomacromolecules* **2011,** *12* (10), 3520-7.
55.Kim, J.; Magno, M. H.; Waters, H.; Doll, B. A.; McBride, S.; Alvarez, P.; Darr, A.; Vasanji, A.; Kohn, J.; Hollinger, J. O., Bone regeneration in a rabbit critical-sized calvarial model using tyrosine-derived polycarbonate scaffolds. *Tissue Eng Part A* **2012,** *18* (11-12), 1132-9.

2 Segmental Bone Regeneration with Tyrosine-Derived Polycarbonate/Beta-Tricalcium Phosphate Scaffolds in A Critical Size Sheep Tibial Model

2.1 Introduction

Segmental bone loss caused by high-energy trauma, infection and malignancy is particularly challenging to orthopedic surgeons and poses the threat of significant disability for patients. The gold standard for the reconstruction of long bone defects (< 5 cm) is autograft transplantation. However, the application of autografts is subjected to limited availability and donor site morbidity.[1] While allografts serve as an alternative to autografts, they are associated with possible disease transmission and immune rejection. These transplants may also result in insufficient integration, and the lack of internal stress-oriented remodeling could potentially lead to fracture at the allograft-host interface.[2]

The complications and shortcomings of autografts and allografts have motivated scaffold-based tissue engineering strategies for the development of bone graft substitutes (BGSs). Ideally, the synthetic bone regeneration scaffold should be made from an osteoconductive biomaterial that can be further enhanced with osteoinductive proteins and osteogenic cells.[1] Recombinant human bone morphogenetic proteins (rhBMPs), especially rhBMP-2, has been extensively used for this purpose,[3] while bone marrow or fat-derived mesenchymal stem cells (MSCs) are the preferred cell type used in prior studies.[4] The application of rhBMP-2 has been approved by the U.S. Food and Drug Administration (FDA) and European Medicines Evaluation Agency (EMEA) for anterior lumbar spinal fusion and open tibia fractures treatment.[5] Well-known disadvantages of the clinical use of

rhBMP-2 relate to the high cost of rhBMP-2 and the occurrence of side effects such as adipose tissue formation[6] and ectopic bone formation,[7] especially at higher doses. Thus, another area of active research is the development of carriers that require lower doses of rhBMP-2 while still leading to successful bone regeneration.[8]

Previously, tyrosine-derived polycarbonates composed of desaminotyrosyl-tyrosine ethyl ester (DTE), desaminotyrosyl-tyrosine (DT) and poly(ethylene glycol) (PEG) have been developed to provide proper mechanical properties, biodegradability, and biocompatibility for bone regeneration. Intrinsically osteoconductive poly(DTE -co-10%-DT-co-1%-PEG (1k)) (E1001(1k)) emerged as an excellent candidate for bone scaffolds, where the polymer is composed of 89 mol% DTE, 10 mol% DT and 1 mol% PEG with the molecular weight of 1000 Da.[9-11] The *in vivo* performance of E1001(1k) scaffolds doped with beta-tricalcium phosphate (β-TCP) nanocrystals and supplemented with rhBMP-2 has been investigated in critical size rat mandibular, rabbit calvarial and goat calvarial defect models.[6, 12-14] The scaffolds supplemented with rhBMP-2 were found to be biocompatible, bioresorbable and osteoconductive.[6, 9-10, 13-14] Interestingly, E1001(1k)/β-TCP scaffolds with 400 μg rhBMP-2 promoted complete filling of trabecular bone over 20 mm critical size goat calvarial defects at 16 weeks.[14]

To date, the clinical translation of tissue engineering strategies for segmental bone reconstruction is limited by the lack of robust findings from preclinical trials in large animal models. Very few papers compare the different augmentation strategies in the preclinical models, leaving the positive outcomes inconclusive.[15] Among the various animal species used for preclinical trials, adult sheep are considered reliable animal species for the evaluation of segmental bone regeneration due to the similarity in tibiae dimensions

and the degree of weight-bearing.[16] In the past decades, composite scaffolds fabricated from hydroxyapatite (HA), TCP, bioactive glass or polymers were intensively tested in sheep tibial defects ranging from 1 cm to 4.5 cm.[17] The majority treatments of segmental defect reconstruction involve incorporation of MSCs into scaffolds, whereas very few papers reported growth factor (GF, such as BMP-2 and BMP-7) application alone[18-22] or in combination with MSCs.[23] Particularly, for the critical size sheep tibial defect scaled at 3 cm, polycaprolactone (PCL) and TCP composite scaffolds (PCL/TCP) induced only limited new bone regeneration[21, 24] but had the comparable bone formation and superior strength to autografts when loaded with 3.5 mg rhBMP-7 at 12 months.[21] In a successive study, similar PCL/TCP scaffolds with honeycomb structures and 3.5 mg rhBMP-7 were able to accelerate and guide the formation of mechanically competent bone, resulting in increased mineral particles and collagen fiber orientation along the tibial axis at 12 months to allow proper weight-bearing.[22] Other osteogenic GFs have also been applied. For example, it has been reported that HA granules mixed with 2.5 mg rhBMP-7 were able to generate bone that has no comparable mechanical strength and bridging to autografts at 12 weeks.[19] Though the investigation *of in vivo* performance of synthetic scaffolds and osteogenic GFs is relatively rare, the effective dose of GFs is above 2 mg per 3 cm-defect.[18-23]

In the current study, we aimed to translate positive results from previous calvarial models to a more challenging 30 mm critical size sheep tibial defect model. To our knowledge, the dose of rhBMP-2 (1.1 mg per defect) applied is the lowest reported amongst comparable studies where acellular composite scaffolds and rhBMP-2 were applied.[25-28] Furthermore, the formulation of trabecular bone mimetic E1001(1k)/β-TCP

scaffolds and rhBMP-2 was compared to a clinically used β-TCP-based BGS (chronOS®) with the same dose of rhBMP-2. Segmental bone regeneration and the remodeling process were investigated for 17 weeks by radiographic, micro computed tomography and histological analyses. The morphology of newly formed bone was qualitatively examined to assess the bone remodeling process.

2.2 Materials and Methods

2.2.1 Materials

E1001(1k) was synthesized by Cyalume Technologies Holdings, Inc. (Ft. Lauderdale, FL, USA). β-TCP nanocrystals came from Berkeley Advanced Biomaterials, Inc. (San Leandro, CA, USA). Custom-made punches and fixtures for scaffold fabrication were assembled by F&A Machine Co. (Middlesex, NJ, USA). β-TCP granules were from ChronOS DePuy Synthes Products (West Chester, PA, USA). rhBMP-2 loaded to E1001(1k)/β-TCP was provided by Dr. Changsheng Liu at East China University of Science and Technology (ECUST, Shanghai, China). rhBMP-2 loaded to β-TCP granules was from Medtronic (Minneapolis, MN, USA). 1, 4-dioxane, sodium chloride (NaCl), sodium hydroxide (NaOH), bovine serum albumin (BSA), penicillin/streptomycin were from Sigma Aldrich (St. Louis, MO, USA). Dulbecco's Modified Eagle Medium (DMEM) and L-glutamine came from Life Technologies (Carlsbad, CA, USA). Fetal bovine serum (FBS) came from Atlanta Biologicals (Flowery Branch, GA, USA). Dulbecco's phosphate-buffered saline (DPBS) and Water for Injection (WFI) for Cell Culture were purchased from Thermo Fisher Scientific (Waltham, MA, USA). P-nitrophenyl phosphate (PNPP) was purchased from VWR (Vadnor, PA, USA). Enzyme-linked immunosorbent assay

(ELISA) kit comes from PeproTech (Rocky Hill, NJ, USA). The W-20-17 rat stromal cell line was obtained from ATCC (Manassas, VA, USA). For histology analyses, methylmethacrylate was purchased from Fisher Scientific Company (Suwanne, GA, USA). EXAKT methylmethacrylate histology slide was from EXAKT Technologies, Inc. (Oklahoma City, OK, USA). Chemicals for staining came from Alfa Aesar (Ward Hill, MA, USA).

2.2.2 Scaffold Fabrication and Characterization

The porous E1001(1k)/β-TCP scaffolds used for the sheep tibial study were fabricated by a combination of solvent casting, porogen leaching and phase separation techniques according to previously described procedures.[9] Briefly, β-TCP nanocrystals (Berkeley Advanced Biomaterials, Inc.; San Leandro, CA) and 212 - 425 μm NaCl particles (Sigma Aldrich; St. Louis, MO) were mixed with E1001(1k) solution in 1,4-dioxane (Sigma Aldrich; St. Louis, MO) and deionized (DI) water. 30% of β-TCP nanocrystals and 70% E1001(1k) polymer by weight were used. The mixture was then cast into Teflon molds, frozen in liquid nitrogen and lyophilized (Labconco LFZ-2.5L, Hampton, NH). Tubular scaffolds were shaped from the dry molds by using custom-made punches and fixtures (F&A Machine Co.; Middlesex, NJ) to give dimensions of 30 mm (length) × 15 mm (outer diameter) × 8 mm (inner diameter). The cores punched out of the cylinders were reserved for characterization.

The NaCl was then leached out from the mold in DI water and the salt-free scaffolds were dried under vacuum. The skin (2 mm from the surface) of scaffolds was removed by razor blades in a custom-made shaping mold. To ensure consistent pore

architecture and β-TCP distribution throughout the construct as well as the reproducibility of lab-scale fabrication, E1001(1k)/β-TCP scaffolds, together with the corresponding cores generated during fabrication, were sectioned into three 10 mm-long segments (i.e., top, middle and bottom) (Figure 2.1). Scaffolds from three different batches were characterized. The pore architecture of each section from a single scaffold was examined by scanning electron microscope (SEM, Phenom ProX, Nanoscience Instruments, Alexandria, VA, USA). The weight percentage of β-TCP in scaffold sections and open porosity of core sections were quantified by Thermal Gravimetric Analysis (TGA, Mettler Toledo, LLC., Columbus, OH, USA) and micro Computed Tomography (microCT, SkyScan 1172, Bruker, Kontich, Belgium), respectively.

2.2.3 *In Vitro* rhBMP-2 Loading and Release

To examine the release kinetics of rhBMP-2 from E1001(1k)/β-TCP scaffolds, model scaffolds with the dimensions of 2.6 mm (thickness) x 15 mm (outer diameter) x 8 mm (inner diameter) were fabricated. rhBMP-2 (ECUST) solution in DI water was loaded to the scaffolds through a semi-vacuum loading method (80 μg/scaffold, n = 4). To mimic *in vivo* conditions, the center of scaffolds was blocked by 30 mm-long pieces from intramedullary rods. The scaffolds were placed into 3 mL assay medium of W-20-17 cells (ATCC; Manassas, VA) that was prepared according to ASTM Standard F2131-02 and incubated at 37 ºC and 5% CO_2. The basal medium was prepared according to ASTM Standard F2131-02 (Dulbecco's Modified Eagle Medium (DMEM) supplemented with 200 mM L-glutamine (Life Technologies; Carlsbad, CA), 10% fetal bovine serum (FBS; Atlanta Biologicals; Flowery Branch, GA) and 0.5% gentamicin (Sigma Aldrich; St. Louis,

MO)). E1001(1k)/β-TCP scaffolds loaded with DI water served as negative controls. The assay medium was collected and changed on Day 1, 2, 3, 5, 7 and 14. The collected media containing released rhBMP-2 was stored at -80 ºC till further analyses. The rhBMP-2 concentration in the release media was quantified by ELISA (PeproTech; Rocky Hill, NJ). The bioactivity of released rhBMP-2 was determined using ASTM Standard F2131-02. Briefly, W-20-17 cells were plated at a density of 10^5 cells/cm^2 in 96-well tissue culture plates. After 24 h of incubation at 37 ºC, the media was replaced with 100 µL of sample/well and incubated at 37 ºC for another 24 h. The media was aspirated and wells were washed with 200 µL/well DPBS (Thermo Fisher Scientific; Waltham, MA) once. Cells were lysed in 50 µL water for injection (WFI) and lysed through two freeze-thaw cycles. An equal volume of P-nitrophenyl phosphate (PNPP) solution (VWR; Vadnor, PA) was added to each well for development. The PNPP solution was prepared at 3.4 mg/mL in glycine buffer according to ASTM Standard F2131-02. The plates were developed at room temperature for 1 h and the reaction was stopped by the addition of 100 µL/well 0.2 N NaOH solution. Absorbance was measured at 405 nm.

2.2.4 *In Vivo* Study

Twelve skeletally mature sheep with a mean body weight of 70 kg were used. The sheep were cared for in accordance with the guidelines of, and in an animal facility approved by The Animal Care and Use Review Office (ACURO). Anaesthesia was induced with intravenous ketamine (2.2 mg/kg) and diazepam (0.1 mg/kg) and maintained by isoflurane and oxygen inhalation after endotracheal intubation. Prophylactic cephazolin antibiotic (1 g intravenously) was given at induction and at the end of surgery. The surgical

procedure involved a medial approach to the tibia and removal of a 30 mm mid-diaphyseal osteoperiosteal tubular segment. The distal bone segment was reamed with 6 mm and 8 mm reamers until an 8 mm nail could be accommodated. E1001(1k)/ β-TCP scaffolds were implanted in the sheep tibia and periosteum was stripped off the site to avoid interference in interpreting growth results. The rhBMP-2 solution was loaded into E1001(1k)/β-TCP scaffolds prior to surgery using a custom-made semi-vacuum loading chamber to give a dose of 1.1 mg rhBMP-2 per scaffold. rhBMP-2 loaded in E1001(1k)/β-TCP scaffolds was provided by Dr. Changsheng Liu at East China University of Science and Technology (ECUST, Shanghai, China). rhBMP-2 loaded to β-TCP granules was sourced from Medtronic (Minneapolis, MN, USA). ChronOS® granules (DePuy Synthes Products; West Chester, PA) were mixed with the rhBMP-2 solution (Medtronic, 1.1 mg) and packed around the defect. The distal ends were stabilized using an intramedullary nail (Innovative Animal Products, Rochester, Minnesota) with two 4.5 mm cortical screws at each end. Within all treatment groups, animals were randomly assigned for a total of 6 per group. Transdermal fentanyl patches (150 μg/hr) and oral phenylbutazone (1 g once daily) were used for 72 hours after surgery to minimize pain and inflammation. Animals were examined twice daily for signs of pain and the ability to weight-bear following surgery.

2.2.5 Radiological Analysis

Mediolateral radiographs were taken immediately after surgery to document the position of the defect and to confirm the correct nail placement. Radiographs of the reconstructed sites in anteroposterior view and mediolateral view were taken at 4, 8, 12

and 17 weeks post-operation so that the progress of bone regeneration and remodeling could be assessed.

2.2.6 Micro Computed Tomography (microCT) Analyses

Scans were performed on a microCT scanner (Skyscan 1172, Bruker-microCT, Belgium) at a resolution of 10 μm, a voltage of 60 kVp, a current of 170 mA, and with a 0.5 mm aluminum filter (ImageIQ; Cleveland, Ohio USA). Projection image reconstruction was performed using Skyscan system software. Bone volume was quantified using CTAn v.1.13 software.

2.2.7 Histology and Histomorphometry Analyses

Midshaft tibia bone blocks were subject to graded ethanol substitution and infiltrated with methyl methacrylate (Fisher Scientific; Suwanne, GA) that was polymerized by exposure to ultraviolet light. The polymerized block was cut along the sagittal plane to give antero/posterior sections with a Buehler Isomet 1000 Precision Saw (Buehler, Lake Bluff, IL) and the cut surface of one block ground to a uniform 1200 grit finish using a Buehler Metaserv 250 Grinder-Polisher. The ground surface was mounted to an EXAKT methylmethacrylate histology slide (EXAKT Technologies, Inc.; Oklahoma City, OK) with cyanoacrylate adhesive, sawn through with the Exakt 300 CP Band System, and ground to ca. 110 μm thickness with the Exakt 400CS Grinding System. The sections were then polished using diamond suspension on the Buehler Metaserv to a 1 μm surface finish and approximately 100 μm final section thickness.

Histological sections were surface-stained with Stevenel's Blue[29] and counterstained with van Gieson's picrofuchsin (Alfa Aesar; Ward Hill, MA). Conventional light microscopy (LM) and circularly polarized light (CPL) using a Leica-Leitz DMRX/E Universal Microscope (Leica Microsystems, Wetzlar, Germany) employing a Leica PL Fluotar 5/0.12 objective lens were used to image the histology slides. LM and CPL images of approximately 10,000 x 50,000 pixels at 1.29 μm/pixel for anterior and posterior cortices each were acquired with a QIClick color video camera (QImaging, Surrey, BC) and automated Marzhauser stage (Märzhäuser Wetzlar, Wetzlar, Germany) using Objective Imaging Surveyor montaging software (Objective Imaging, Cambridge, UK).

A region of interest was identified that encompassed the area between the stumps. A custom electronic mask was created for each slide and was positioned similarly onto every slide. High magnification images of interfaces at the proximal and distal ends as well as the bone regenerate were taken. The following measurements were taken as a percentage of the region of interest: new bone area, trabecular area, trabecular thickness, trabecular number, trabecular separation, trabecular surface (perimeter), marrow space area, area of cartilage tissue, and the area of fibrous tissue.

2.2.8 Statistical Analysis

All statistical analyses were carried out in GraphPad Prism 7 software. Single factor analysis of variance (ANOVA) was performed followed by a multiple comparison post-hoc test (Tukey-Kramer method) with an established significance of $p \leq 0.05$. Data were reported as mean ± standard error (SE).

2.3 Results and Discussion

2.3.1 E1001(1k)/β-TCP Scaffold Fabrication and Characterization

Bioengineered scaffolds hold great potential for bone regeneration applications because of the wide variety of fabrication techniques and materials of reproducible strength. An optimal scaffold requires proper osteoinduction, osteoconduction, and osteointegration. Although polymers and ceramics have their advantages for osteogenic applications, they are also subjected to certain drawbacks (e.g., ceramics are brittle). Consequently, calcium phosphate is incorporated into the polymer matrix to increase the osteointegration potential of scaffolds.[30]

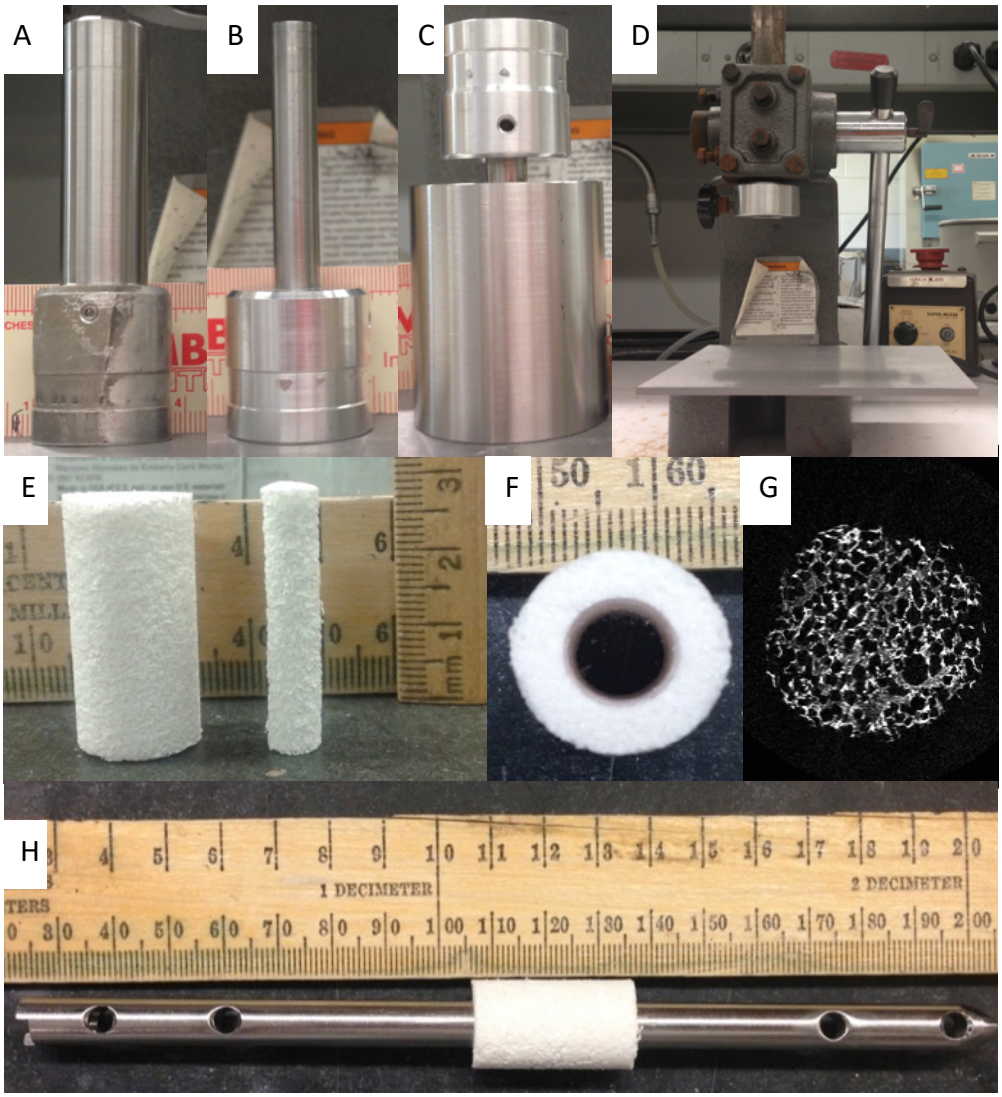

Figure 2.1 Molds for scaffold fabrication: 15 mm punch (A); 8 mm punch (B); 8 mm punch in 15 mm cylinder holder (C); modified arbor press for punches (D). Demonstration of tubular scaffolds for critical size sheep tibial model: E1001(1k)/β-TCP scaffolds and the core punched out of the cylindrical mold (E); top view of the scaffold (F); representative transverse section of the core constructed from microCT scans, interconnected pore architecture can be observed (G); scaffold fitted into 8mm intramedullary nail used for the tibial defect model (H).

Table 2.1 Open porosity of top, middle and bottom parts from a single long, tubular E1001(1k)/β-TCP scaffold.

Open porosity (%)	Scaffold 1	Scaffold 2	Scaffold 3
Top	90.72	91.12	89.46
Middle	91.61	91.70	91.35
Bottom	92.14	91.73	91.63
Average	91.49	91.52	90.81
Standard Error	0.41	0.20	0.68

Table 2.2 Weight percent of β-TCP of top, middle and bottom parts from a single long, tubular E1001(1k)/β-TCP scaffold.

β-TCP Content (%)	Scaffold 1	Scaffold 2	Scaffold 3
Top	26.4	25.9	26.7
Middle	24.4	21.9	21.9
Bottom	24.7	25.2	23.2
Average	25.2	24.3	23.9
Standard Error	0.63	1.21	1.45

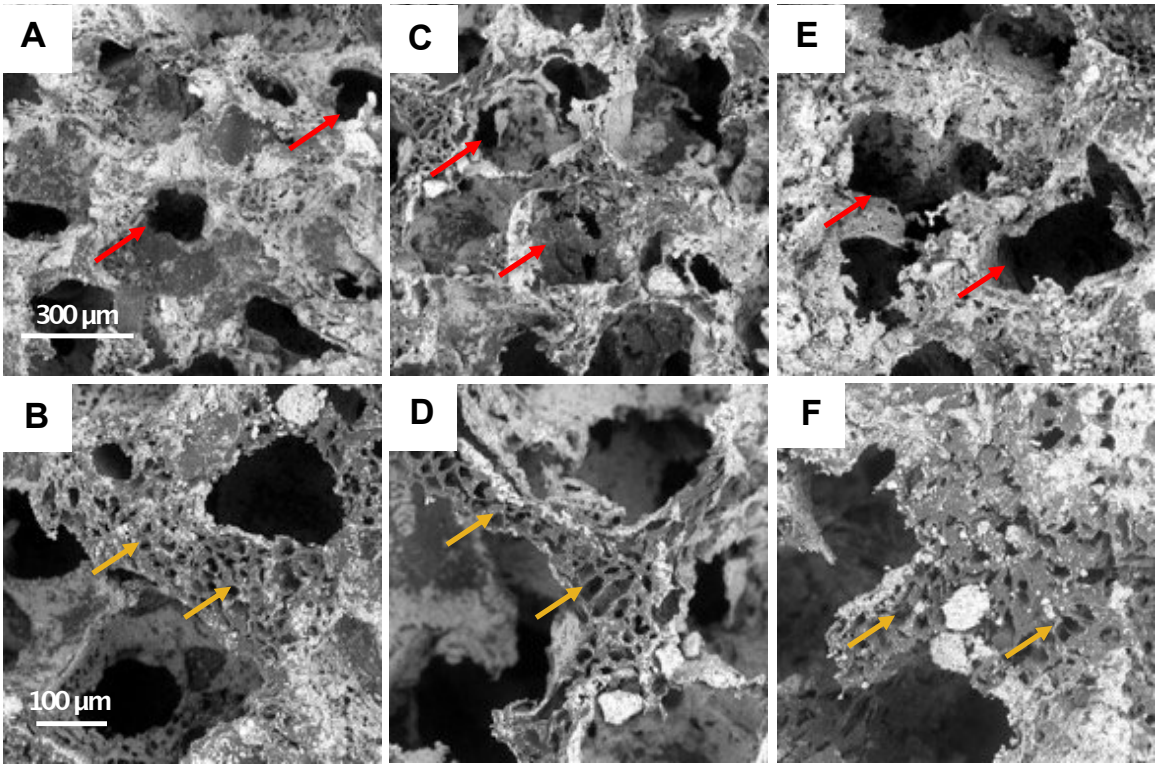

Figure 2.2 Representative SEM images of long, tubular E1001(1k)/β-TCP scaffolds: Top section (A-B), middle section (C-D), bottom section (E-F). The scaffolds have bimodal pore architecture, with macro-pores (red arrows) between 200 - 400 µm and micro-pores (yellow arrows) positioned on the walls of macro-pores at around 20 µm. β-TCP (white granules) distributes on the surface of the polymer network.

Herein, we developed a composite scaffold made of a biodegradable tyrosine-derived polymer (E1001(1k)) with β-TCP nanocrystals[30]. The punches and fabrication devices are demonstrated in Figure 2.1 A-D. As demonstrated in Figure 2.1E-H, the tubular scaffolds are shaped for the size of adult sheep tibiae and would be fixed on intramedullary nails in the sheep tibial defects.

To ensure excellent reproducibility of scaffold fabrication on a lab-scale, E1001(1k)/β-CTP scaffolds from three different batches were sectioned and examined, the average values of top, middle and bottom sections of a single scaffold were compared. The average open porosity and β-TCP wt% remained constant at around 91% (Table 2.1) and 26% (Table 2.2), respectively. The consistency in open porosity and β-TCP contents throughout the E1001(1k)/β-TCP bone scaffolds suggested a reproducible fabrication procedure in the lab. In the meanwhile, the morphology of porous network and distribution of CaP inside scaffolds were investigated by SEM. The interconnected macropore network (200-400 μm) of E1001(1k))/β-TCP scaffolds mimicked cancellous bone morphology (Figure 2.1G, Figure 2.2A-C) and can thus provide topographical and physical cues for osteoblast lineage progression. The micropore structure (Figure 2.2B-F) would be an ideal platform for the transportation of nutrients and benefit long-term fixation of bone implants in terms of osteointegration with the native bone.[30]

Tubular and porous E1001(1k)/β-TCP scaffolds with dimensions of 30 mm (length) × 15 mm (outer diameter) × 8 mm (inner diameter) were engineered and fabricated for a 30 mm critical size sheep tibial model (Figure 2.1). The scaffold was designed to be implanted in the defect area with an 8 mm intramedullary rod and bolts. SEM images demonstrated that for a single E1001(1k)/β-TCP scaffold, all three sections have bimodal pore size distribution, with macropores (200 - 400 μm) and 20 μm micropores positioned along the walls of macropores. In addition, β-TCP particles were distributed evenly on the surface of scaffolds as white particles (Figure 2.2). A representative section of micro-CT scans performed on E1001(1k)/β-TCP scaffolds showed the interconnected pore structure

(Figure 2.1G). Each E1001(1k)/β-TCP scaffold has a homogeneous pore network with open porosity of approximately 91% and 25 wt% β-TCP particles (Table 2.1, Table 2.2).

2.3.2 *In Vitro* Release and Bioactivity of rhBMP-2 from Scaffolds

To enhance the osteogenic potential of the E1001(1k)/β-TCP scaffolds, the scaffolds were employed as carriers for rhBMP-2. In our previous study, full bone regeneration was achieved by using 400 μg rhBMP-2 in a 20 mm critical size goat calvarial model.[31] To maintain a comparable dose per unit volume, the E1001(1k)/β-TCP bone scaffold was loaded with 1.1 mg of rhBMP-2 in the current study, and to our knowledge, this dose among the lowest in comparable segmental defect large animal models.

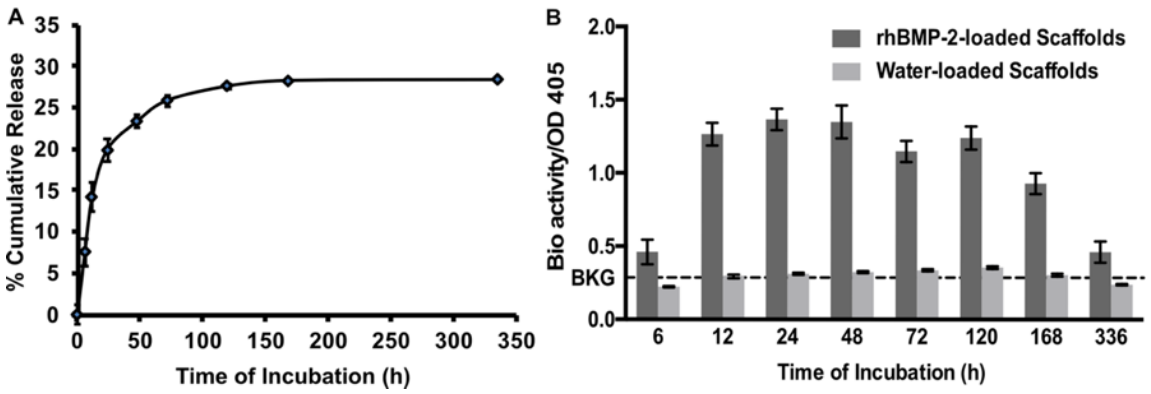

Figure 2.3 RhBMP-2 release from E1001(1k)/β-TCP scaffolds *in vitro*. The release profile was measured over 14 days. The % cumulative release of rhBMP-2, concentration in supernatants was quantified by ELISA at each time points (n = 4) (A); bioactivity of released rhBMP-2 in supernatants, measured as rhBMP-2-induced ALP expression from W-20-17 cells (B), the dotted line indicates background (BKG) OD readings at 405 nm (n = 4).

To apply the concept of tissue engineering, scaffolds were employed as carriers for rhBMP-2. For the current study, we intended to translate our previous success in various critical size calvarial defect models into a half weight-bearing segmental defect model in large animals. Previous studies showed that full bone regeneration was achieved by using 400 μg rhBMP-2 in a 20 mm critical size goat calvarial model.[14] Therefore, to maintain similar dose window, 1.1 mg of rhBMP-2 was loaded into each scaffold for the *in vivo* study, and to our knowledge, this dose among the lowest in comparable segmental defect large animal models where the use of acellular scaffolds and rhBMP-2 were implanted.[25-28] Ideally, effective rhBMP-2 treatment requires sustained delivery from the carrier during the first couple of weeks and maintenance of the local concentration within the therapeutic window.[3] The *in vitro* release kinetics of rhBMP-2 from E1001(1k)/β-TCP

model scaffolds were interpreted by measuring the cumulative percentage of rhBMP-2 in the culture media as a function of time. The scaffolds demonstrated a biphasic rhBMP-2 release profile. An initial burst release over 5 days was observed, where ~27% of the loaded protein was released. This was followed by a sustained release over 14 days (Figure 2.3A), suggesting possible protein adsorption to the hydrophobic polymeric scaffold surface.[10] In addition, E1001(1k)/β-TCP scaffolds have higher porosity (c.a. 90%) compared to chronOS® granules (72 ± 6%), thus providing larger surface area for physical binding of rhBMP-2 and increased retention of rhBMP-2 inside the scaffold matrix.

Since the release of a biomolecule from a carrier does not ensure biological activity because conformational changes can inactivate proteins,[3] the bioactivity of released rhBMP-2 was measured by ALP induction in W-20-17 cells. The ALP induction was compared to the background signal from water-loaded scaffolds at the same time points. In Figure 2.3B, results showed that the rhBMP-2 released from the scaffolds was active up to 14 days ($p < 0.05$, $n = 4$), whereas supernatant from control scaffolds loaded with water yielded no ALP response and have comparable signals to background (Figure 2.3B). Therefore, E1001(1k)/β-TCP scaffolds release active rhBMP-2 over the course of 14 days, which is imperative for appropriate bone regeneration.

2.3.3 Radiolucent Scaffolds for Monitoring of New Bone Growth *In Vivo*

In order to qualitatively assess bone formation *in vivo*, radiographs were taken immediately after the surgery and monthly over the course of the study. The radiographs are collected in Figure 2.4.

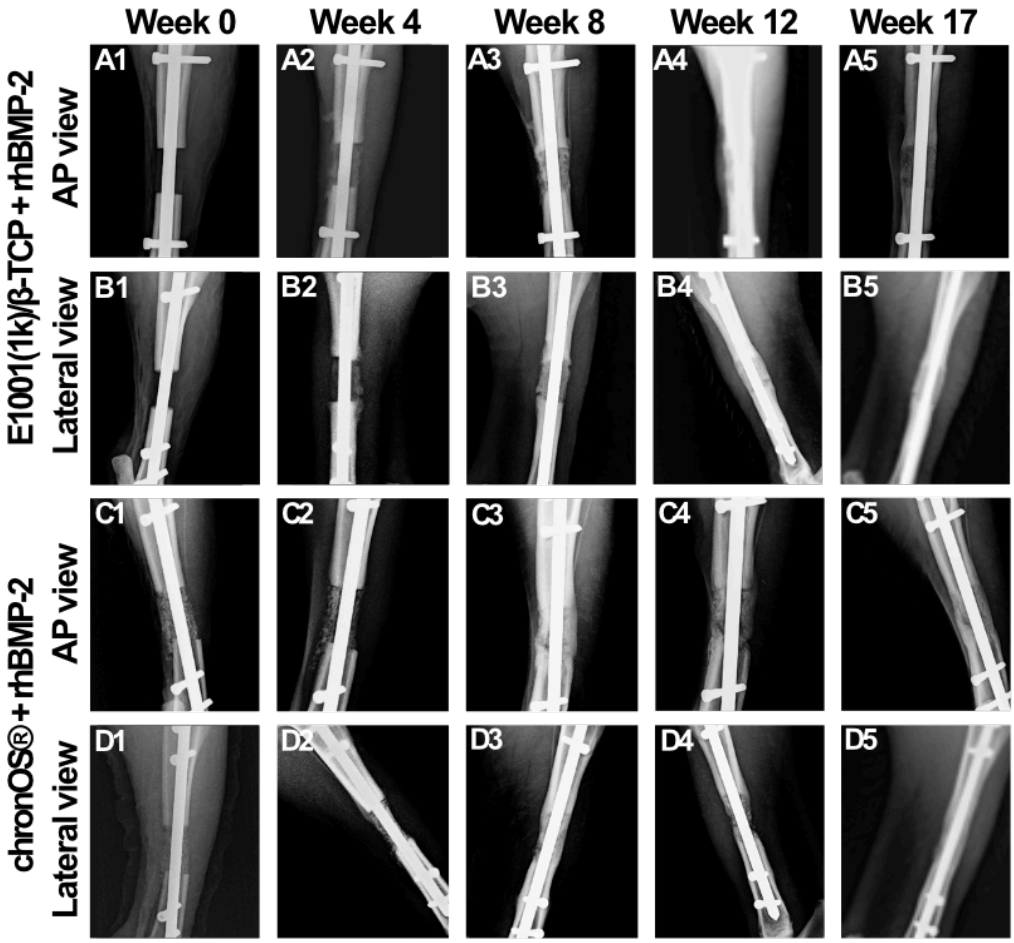

Figure 2.4 Representative radiological images of the critical size segmental defects at 0, 4, 8, 12 and 17 weeks post-operation: anteroposterior (AP) view (A1-5) and lateral view (B1-5) of the E1001(1k)/β-TCP + rhBMP-2 group; AP view (C1-5) and lateral view (D1-5) of the chronOS® + rhBMP-2 group. For the E1001(1k)/β-TCP + rhBMP-2 group, radiolucent scaffolds were not visible right after surgery, and bone formation was observed starting at 4 weeks. The bridging was observed as early as 8 weeks, signs of consolidation and remodeling were demonstrated between 8-17 weeks. Due to the radio-opacity of β-TCP granules, the healing process was not clearly visible for the chronOS® + rhBMP-2 group.

In contrast to the chronOS® + rhBMP-2 group, the radiolucent nature of E1001(1k) and relatively low β-TCP content (25 wt%) in the formulation allows for monitoring of the bone remodeling progress over the course of the 17-week experiment. The E1001(1k)/β-TCP composite scaffolds were radiolucent immediately following implantation (Figure 2.4A1, B1), and new bone formation was observed in the center of defects as early as at 4 weeks (Figure 2.4A2, B2). This could be due to the early burst release of bioactive rhBMP-2 promoting the healing process (Figure 2.3). Mineralization and remodeling of the newly formed bone were seen from 8 weeks to 17 weeks (Figure 2.4A3-5, B3-5). Although β-TCP in chronOS® appeared radiopaque at week 0 (Figure 2.4C1, D1), an increase in radiopacity associated with new bone formation was observed in the defect area (Figure 2.4C2-C5, D2-D5). The radiolucent nature of our composite scaffolds is beneficial for patient assessment post orthopedic surgeries in the clinical setting.

2.3.4 MicroCT Analysis

In order to provide a higher resolution to the bone regenerative capabilities of the E1001(1k)/β-TCP scaffolds and chronOS®, micro-CT scans were performed on the 17-week explants. Qualitative and quantitative results are summarized in Figure 2.5.

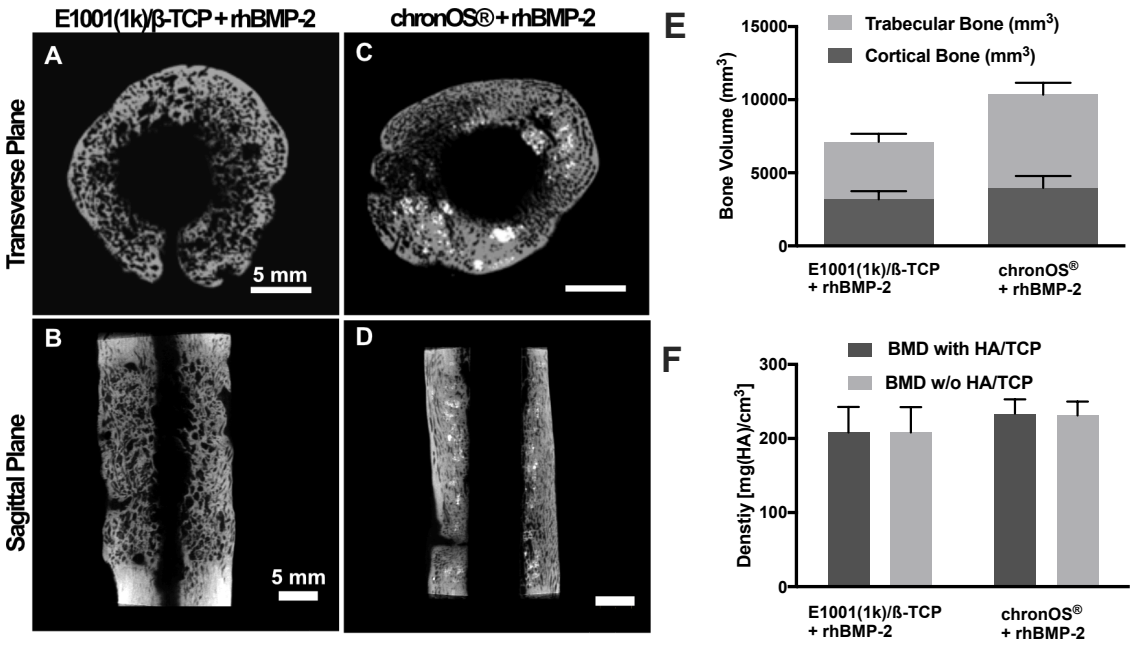

Figure 2.5 Representative reconstructed microCT images of 17-week sheep tibia explants: transverse (A) and sagittal (B) section from the E1001(1k)/β-TCP + rhBMP-2 group; transverse (C) and sagittal (D) section from the chronOS®+ rhBMP-2 group. Quantitative analyses on the reconstructed region of interests: trabecular bone and cortical bone volumes (E); bone mineral density with or without β-TCP contents from BGS materials (F). No significant difference was found between the two treatment groups (n = 6).

All treatments gave satisfactory bone bridging in 3 out of 6 cases without a clear discontinuity between the native cortical bone and the new bone regenerated (Figure 2.5B, D), the rest of the samples have partial bridging according to the reconstructed 3D image (data not shown here). Transverse sections in the middle of defects showed bone ingrowth from the native tibial bone into the constructs (Figure 2.5A-B). The morphology of newly formed bone within E1001(1k)/β-TCP scaffolds resembles trabecular bone (Figure 2.5B), whereas the new bone in chronOS® appears dense (Figure 2.5D). In addition, residual β-TCP granules in chronOS® are visible as bright spots in scans from the chronOS®+rhBMP-2 group (Figure 2.5C-D), indicating the β-TCP filling is not completely resorbed by surrounding tissue at 17 weeks. Furthermore, quantitative 3D morphometry analysis on the reconstructed representations of explants was conducted. It should also be noted that the quantitative microCT analyses are difficult to some degree, owing to the need to distinguish between the CaPs residual in the defects at 17 weeks and the mineral content in new bone. Therefore, the quantitative mciroCT results should be carefully reviewed. The total bone volume and bone mineral density (BMD) with or without β-TCP were not statistically different between E1001(1k)/β-TCP + rhBMP-2 and chronOS® + rhBMP-2 groups (Figure 2.5E-F). No significant difference was found between the two treatment groups, indicating comparable bone regeneration performance of E1001(1k)/β-TCP scaffolds to that of chronOS®.

2.3.5 Histological Analyses

Histology images of both study groups were summarized in Figure 2.6 and Figure 2.7, and were taken at different magnifications to assess the morphology of the newly regenerated bone as well as the interface of native tissue and newly formed mineralized tissue. Histomorphometry data are presented in Figure 2.8.

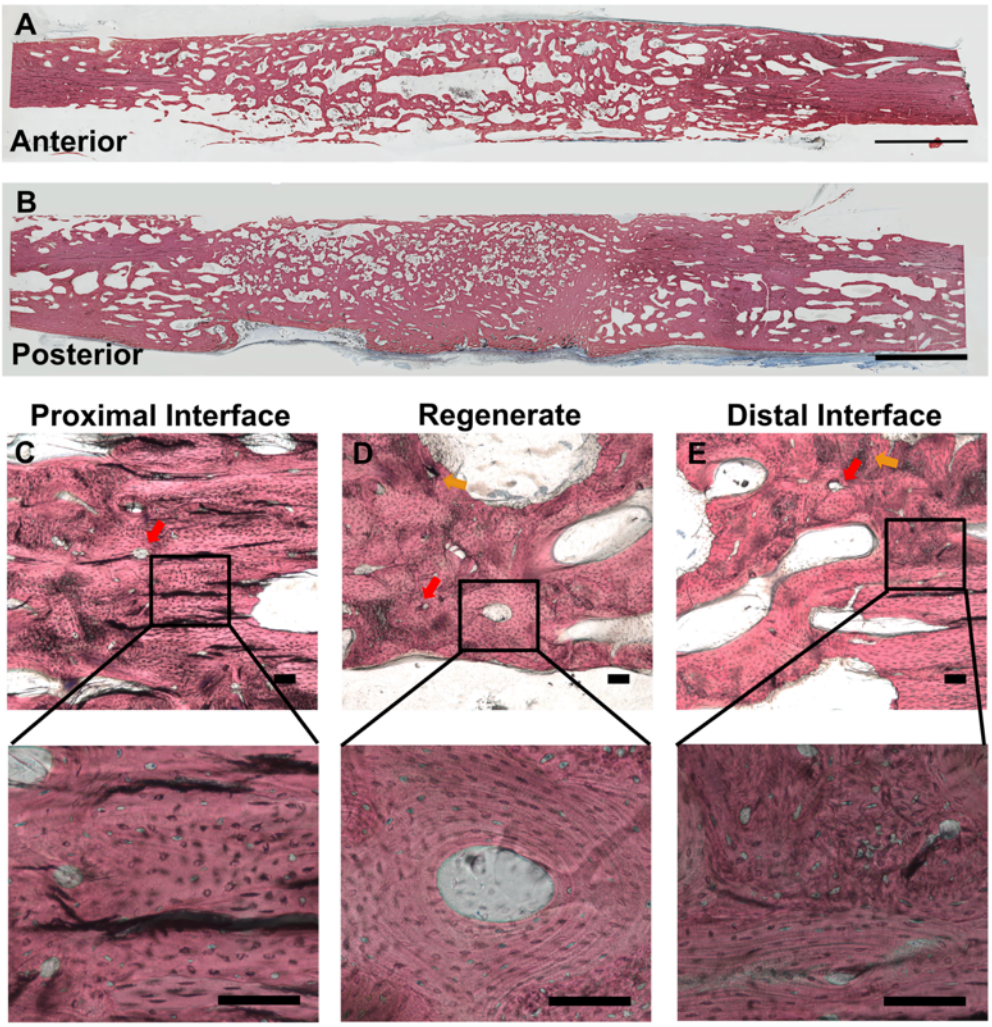

Figure 2.6 Representative histological images of explants from the E1001(1k)/β-TCP scaffolds + rhBMP-2 group: (A-B) Anterior and posterior section along the sagittal plane; (C-E) zoomed-in images (5X and 20X) of the proximal interface, regenerate and distal interface. Mineralized tissue stains red, nonmineralized structure stains various shades of blue, residual calcium minerals from scaffold materials stains black (yellow arrows). Newly-formed Haversian-like systems can be easily identified in the 20X images, and indicated in 5X images (5x). Scale bars are 200 μm.

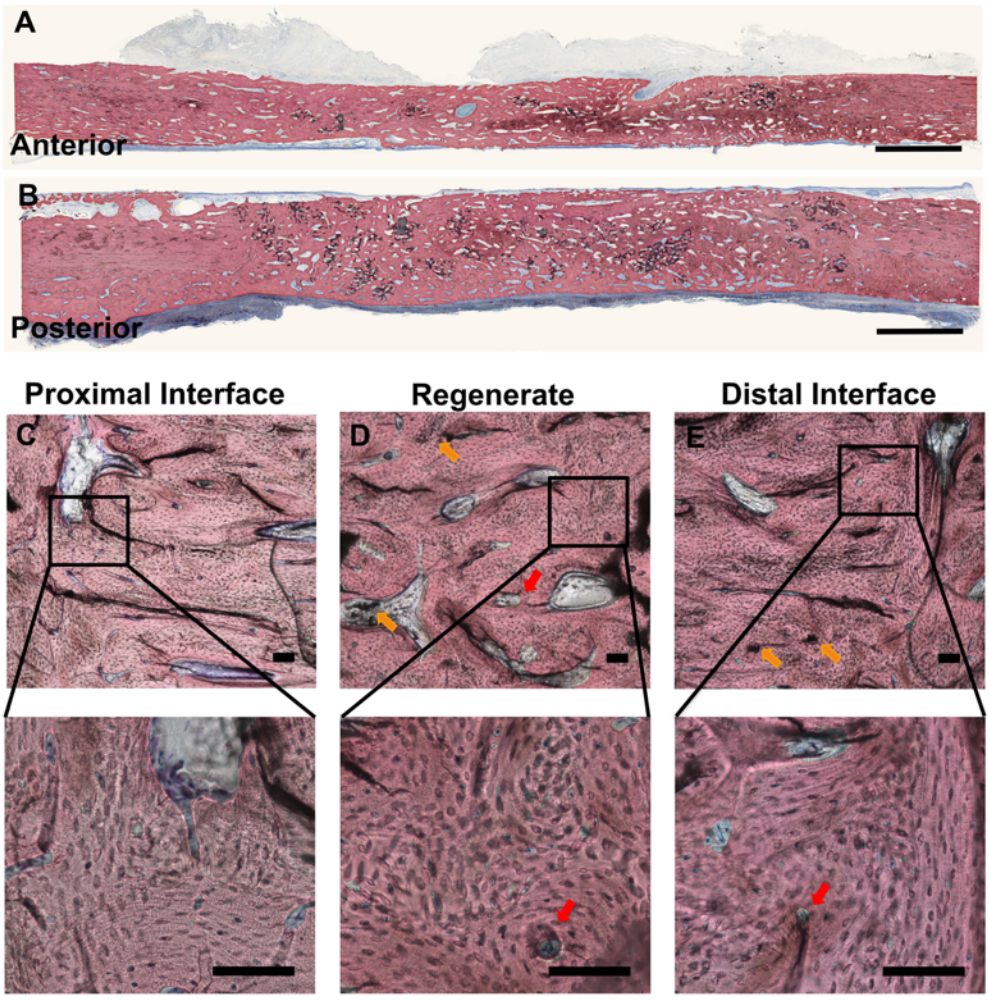

Figure 2.7 Representative histological images of explants from the chronOS® + rhBMP-2 group: (A-B) Anterior and posterior section along the sagittal plane; (C-E) zoomed-in images (5X and 20X) of proximal Interface, regenerate and distal interface. Mineralized tissue stains red, nonmineralized structure stains various shades of blue, residual calcium minerals from scaffold materials stains black (yellow arrows), newly formed Haversian-like systems is pointed out by red arrows. Scale bars are 200 µm.

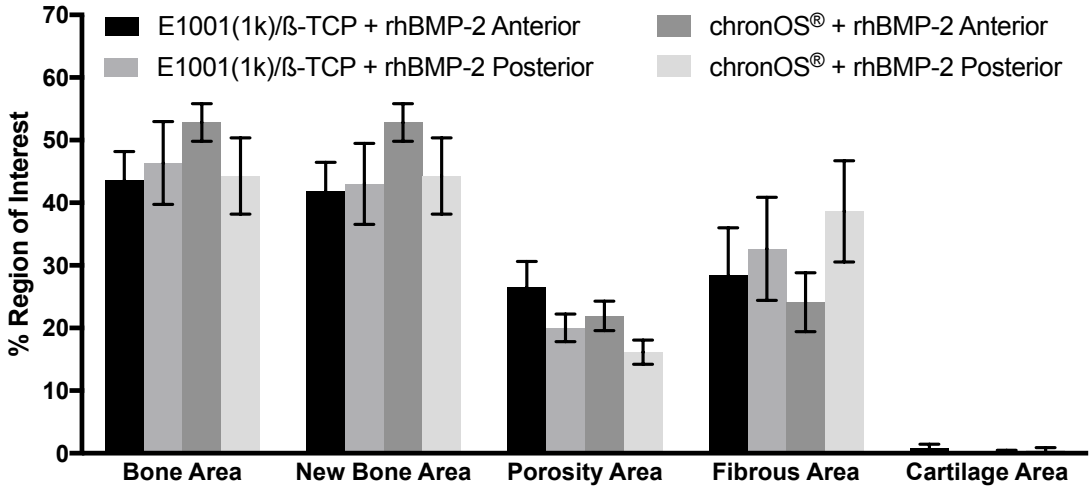

Figure 2.8 Summary of 2D histomorphometric analyses on the sagittal histology sections, both anterior and posterior parts were stained and quantified. The % bone area, % new bone formation, % porosity area, % fibrous area, % cartilage area within the region of interest (ROI) were not significantly different between the anterior and posterior sections from the same explant and between the two treatment groups (n = 6).

The histology analyses give a similar picture of bone regeneration from the microCT scans. Bridging on both sides with newly regenerated bone was observed in 50% of the cases (3 out of 6) at 17 weeks in both treatment groups, the rest samples either had bridging on one side or had bone ingrowth. Residual β-TCP crystals present in the E1001(1k)/β-TCP (Figure 2.6D-E, blue arrow) and chronOS® (Figure 2.7B, blue arrow) formulations were detected in the newly formed bone. Since the structure and arrangement of the existing bone can have a significant effect on its mechanical competence, the morphology of native bone-scaffold interfaces and that of the regenerated bone was examined. Defects treated with E1001(1k)/β-TCP scaffolds + rhBMP-2 provide the best-remodeled interface between native and new bone (Figure 2.6C, E). The aligned texture of

the native cortical bone blends evenly into the newly formed bone, and new Haversian-like systems can be easily identified in the sections from the E1001(1k)/β-TCP + rhBMP-2 group (Figure 2.6C-E). Slides from the ChronOS®+rhBMP-2 group provide a similar remodeled interface (Figure 2.7C, E). However, the new bone has a coarser texture and appeared denser compared to that formed within the E1001(1k)/β-TCP scaffolds (Figure 2.7A-B). This may reflect a less than physiological hyperstimulation of bone formation and/or a reduction in the rate of bone remodeling within the chronOS® construct.

To quantitatively assess the extent of new bone regeneration within each construct, 2D histomorphometry analyses were performed on the histology slides from all six animals in each group. The % new bone area in the region of interest (ROI) was quantified as follows: 53% for E1001(1k)/β-TCP + rhBMP-2 and 57% for chronOS® + rhBMP-2 (Figure 2.8). The evaluation of % fibrous area gives 16% for E1001(1k)/β-TCP + rhBMP-2 and 21% for chronOS® + rhBMP-2 (Figure 2.8). No statistical difference was observed between the two treatment groups. Histomorphometry shows that the bone regeneration performance of the E1001(1k)/β-TCP + rhBMP-2 formulation is akin to that of chronOS® + rhBMP-2 (Figure 2.8). It should be noted that this study concentrates on evaluating the bone regeneration capacity of E1001(1k)/β-TCP scaffolds carrying a low dose of rhBMP-2 in comparison to clinically relevant formulations, namely chronOS® + rhBMP-2, in a segmental large animal model. Although the time period of *in vivo* study is relatively short for the investigation of the long-term reconstruction of segmental bone defects,[1, 32-34] and the dose of rhBMP-2 delivered to the 30 mm gap in sheep tibiae is far lower than the reported values in literature,[27] this study does suggest that E1001(1k)/β-TCP scaffolds have

comparable bone regeneration performance to clinical relevant controls (chronOS®) based on qualitative and quantitative microCT and histological analyses on the explants.

2.4 Conclusion

In conclusion, we compared the *in vivo* performance of the E1001(1k)/β-TCP scaffolds to clinically applied chronOS® with an extremely low dose of rhBMP-2 (281 ng/mm^3) for 17 weeks in a human-like critical size sheep tibial model. The porous scaffolds are custom-shaped into 30 mm long tubes for sheep tibiae and show proper pore sizes inter-connected pore network that resembles native cancellous bone for optimal cell infiltration and proliferation. *In vitro* release studies demonstrated that the scaffolds were able to sustain a release of bioactive rhBMP-2 over 2 weeks, providing early biological cues for bone regeneration. Radiographs on the defects from the E1001(1k)/β-TCP + rhBMP-2 revealed callus tissue formation as early as 4 weeks due to the radiolucent nature of E1001(1k)/β-TCP scaffolds. Histomorphometry analyses revealed that the bone regenerated from the E1001(1k)/β-TCP scaffolds were not significantly different from the bone regenerated using chronOS® implants. Qualitative microCT and histology analyses on the explants revealed that both groups have comparable bone regeneration interfaces. However, histology sections from the E1001(1k)/β-TCP + rhBMP-2 group show more signs for physiological remodeling into compact bony tissue than those from the chronOS® + rhBMP-2 group. It should be noted that the use of a human-like sheep model makes these results highly translational for the prediction of clinical outcomes and suggest that E1001(1k)/β-TCP scaffolds are promising candidates for the reconstruction of long bone defects with considerably low amounts of osteogenic factors.

2.5 Reference

1.Mauffrey, C.; Barlow, B. T.; Smith, W., Management of segmental bone defects. *The Journal of the American Academy of Orthopaedic Surgeons* **2015,** *23* (3), 143-53.
2.Enneking, W. F.; Campanacci, D. A., Retrieved human allografts : a clinicopathological study. *The Journal of bone and joint surgery. American volume* **2001,** *83-a* (7), 971-86.
3.Carreira, A. C.; Lojudice, F. H.; Halcsik, E.; Navarro, R. D.; Sogayar, M. C.; Granjeiro, J. M., Bone morphogenetic proteins: facts, challenges, and future perspectives. *Journal of dental research* **2014,** *93* (4), 335-45.
4.Ho-Shui-Ling, A.; Bolander, J.; Rustom, L. E.; Johnson, A. W.; Luyten, F. P.; Picart, C., Bone regeneration strategies: Engineered scaffolds, bioactive molecules and stem cells current stage and future perspectives. *Biomaterials* **2018,** *180*, 143-162.
5.James, A. W.; LaChaud, G.; Shen, J.; Asatrian, G.; Nguyen, V.; Zhang, X.; Ting, K.; Soo, C., A Review of the Clinical Side Effects of Bone Morphogenetic Protein-2. *Tissue engineering. Part B, Reviews* **2016,** *22* (4), 284-97.
6.Shen, J.; James, A. W.; Zhang, X.; Pang, S.; Zara, J. N.; Asatrian, G.; Chiang, M.; Lee, M.; Khadarian, K.; Nguyen, A.; Lee, K. S.; Siu, R. K.; Tetradis, S.; Ting, K.; Soo, C., Novel Wnt Regulator NEL-Like Molecule-1 Antagonizes Adipogenesis and Augments Osteogenesis Induced by Bone Morphogenetic Protein 2. *Am J Pathol* **2016,** *186* (2), 419-34.
7.Zara, J. N.; Siu, R. K.; Zhang, X.; Shen, J.; Ngo, R.; Lee, M.; Li, W.; Chiang, M.; Chung, J.; Kwak, J.; Wu, B. M.; Ting, K.; Soo, C., High doses of bone morphogenetic protein 2 induce structurally abnormal bone and inflammation in vivo. *Tissue engineering. Part A* **2011,** *17* (9-10), 1389-99.
8.Ball, A. N.; Donahue, S. W.; Wojda, S. J.; McIlwraith, C. W.; Kawcak, C. E.; Ehrhart, N.; Goodrich, L. R., The challenges of promoting osteogenesis in segmental bone defects and osteoporosis. *Journal of Orthopaedic Research* **2018,** *36* (6), 1559-1572.
9.Kim, J.; Magno, M. H.; Alvarez, P.; Darr, A.; Kohn, J.; Hollinger, J. O., Osteogenic differentiation of pre-osteoblasts on biomimetic tyrosine-derived polycarbonate scaffolds. *Biomacromolecules* **2011,** *12* (10), 3520-7.
10.Magno, M. H. R.; Kim, J.; Srinivasan, A.; McBride, S.; Bolikal, D.; Darr, A.; Hollinger, J. O.; Kohn, J., Synthesis, degradation and biocompatibility of tyrosine-derived polycarbonate scaffolds *J. Mater. Chem.* **2010,** *20*, 8885-8893.
11.James, K.; Levene, H.; Parsons, J. R.; Kohn, J., Small changes in polymer chemistry have a large effect on the bone-implant interface: evaluation of a series of degradable tyrosine-derived polycarbonates in bone defects. *Biomaterials* **1999,** *20* (23-24), 2203-12.
12.Kim, J.; Magno, M. H.; Waters, H.; Doll, B. A.; McBride, S.; Alvarez, P.; Darr, A.; Vasanji, A.; Kohn, J.; Hollinger, J. O., Bone regeneration in a rabbit critical-sized calvarial model using tyrosine-derived polycarbonate scaffolds. *Tissue engineering. Part A* **2012,** *18* (11-12), 1132-9.
13.Guda, T.; Darr, A.; Silliman, D. T.; Magno, M. H.; Wenke, J. C.; Kohn, J.; Brown Baer, P. R., Methods to analyze bone regenerative response to different rhBMP-2 doses in rabbit craniofacial defects. *Tissue engineering. Part C, Methods* **2014,** *20* (9), 749-60.
14.Chen, S. S.; Ortiz, O.; Pastino, A. K.; Wu, X.; Hu, B.; Hollinger, J. O.; Bromage, T. G.; Kohn, J., Hybrid Bone Scaffold Induces Bone Bridging in Goat Calvarial Critical

Size Defects Without Growth Factor Augmentation. *Regen. Eng. Transl. Med.* **10.1007/s40883-019-00144-z**.
15.Reichert, J. C.; Saifzadeh, S.; Wullschleger, M. E.; Epari, D. R.; Schutz, M. A.; Duda, G. N.; Schell, H.; van Griensven, M.; Redl, H.; Hutmacher, D. W., The challenge of establishing preclinical models for segmental bone defect research. *Biomaterials* **2009,** *30* (12), 2149-63.
16.Peric, M.; Dumic-Cule, I.; Grcevic, D.; Matijasic, M.; Verbanac, D.; Paul, R.; Grgurevic, L.; Trkulja, V.; Bagi, C. M.; Vukicevic, S., The rational use of animal models in the evaluation of novel bone regenerative therapies. *Bone* **2015,** *70*, 73-86.
17.Roffi, A.; Krishnakumar, G. S.; Gostynska, N.; Kon, E.; Candrian, C.; Filardo, G., The Role of Three-Dimensional Scaffolds in Treating Long Bone Defects: Evidence from Preclinical and Clinical Literature-A Systematic Review. *Biomed Res Int* **2017,** *2017*, 8074178.
18.Gao, T. J.; Lindholm, T. S.; Kommonen, B.; Ragni, P.; Paronzini, A.; Lindholm, T. C.; Jalovaara, P.; Urist, M. R., The use of a coral composite implant containing bone morphogenetic protein to repair a segmental tibial defect in sheep. *Int Orthop* **1997,** *21* (3), 194-200.
19.den Boer, F. C.; Wippermann, B. W.; Blokhuis, T. J.; Patka, P.; Bakker, F. C.; Haarman, H. J., Healing of segmental bone defects with granular porous hydroxyapatite augmented with recombinant human osteogenic protein-1 or autologous bone marrow. *J Orthop Res* **2003,** *21* (3), 521-8.
20.Maissen, O.; Eckhardt, C.; Gogolewski, S.; Glatt, M.; Arvinte, T.; Steiner, A.; Rahn, B.; Schlegel, U., Mechanical and radiological assessment of the influence of rhTGFbeta-3 on bone regeneration in a segmental defect in the ovine tibia: pilot study. *J Orthop Res* **2006,** *24* (8), 1670-8.
21.Reichert, J. C.; Cipitria, A.; Epari, D. R.; Saifzadeh, S.; Krishnakanth, P.; Berner, A.; Woodruff, M. A.; Schell, H.; Mehta, M.; Schuetz, M. A.; Duda, G. N.; Hutmacher, D. W., A tissue engineering solution for segmental defect regeneration in load-bearing long bones. *Sci Transl Med* **2012,** *4* (141), 141ra93.
22.Cipitria, A.; Wagermaier, W.; Zaslansky, P.; Schell, H.; Reichert, J. C.; Fratzl, P.; Hutmacher, D. W.; Duda, G. N., BMP delivery complements the guiding effect of scaffold architecture without altering bone microstructure in critical-sized long bone defects: A multiscale analysis. *Acta Biomater* **2015,** *23*, 282-294.
23.Decambron, A.; Fournet, A.; Bensidhoum, M.; Manassero, M.; Sailhan, F.; Petite, H.; Logeart-Avramoglou, D.; Viateau, V., Low-dose BMP-2 and MSC dual delivery onto coral scaffold for critical-size bone defect regeneration in sheep. *J Orthop Res* **2017,** *35* (12), 2637-2645.
24.Reichert, J. C.; Wullschleger, M. E.; Cipitria, A.; Lienau, J.; Cheng, T. K.; Schutz, M. A.; Duda, G. N.; Noth, U.; Eulert, J.; Hutmacher, D. W., Custom-made composite scaffolds for segmental defect repair in long bones. *Int Orthop* **2011,** *35* (8), 1229-36.
25.Welch, R. D.; Jones, A. L.; Bucholz, R. W.; Reinert, C. M.; Tjia, J. S.; Pierce, W. A.; Wozney, J. M.; Li, X. J., Effect of recombinant human bone morphogenetic protein-2 on fracture healing in a goat tibial fracture model. *Journal of bone and mineral research : the official journal of the American Society for Bone and Mineral Research* **1998,** *13* (9), 1483-90.

26.Kirker-Head, C. A.; Gerhart, T. N.; Schelling, S. H.; Hennig, G. E.; Wang, E.; Holtrop, M. E., Long-term healing of bone using recombinant human bone morphogenetic protein 2. *Clinical orthopaedics and related research* **1995,** (318), 222-30.
27.Sachse, A.; Wagner, A.; Keller, M.; Wagner, O.; Wetzel, W. D.; Layher, F.; Venbrocks, R. A.; Hortschansky, P.; Pietraszczyk, M.; Wiederanders, B.; Hempel, H. J.; Bossert, J.; Horn, J.; Schmuck, K.; Mollenhauer, J., Osteointegration of hydroxyapatite-titanium implants coated with nonglycosylated recombinant human bone morphogenetic protein-2 (BMP-2) in aged sheep. *Bone* **2005,** *37* (5), 699-710.
28.Kirker-Head, C. A.; Gerhart, T. N.; Armstrong, R.; Schelling, S. H.; Carmel, L. A., Healing bone using recombinant human bone morphogenetic protein 2 and copolymer. *Clinical orthopaedics and related research* **1998,** (349), 205-17.
29.del Cerro, M.; Cogen, J.; del Cerro, C., Stevenel's Blue, an excellent stain for optical microscopical study of plastic embedded tissues. *Microsc Acta* **1980,** *83* (2), 117-21.
30.Karageorgiou, V.; Kaplan, D., Porosity of 3D biomaterial scaffolds and osteogenesis. *Biomaterials* **2005,** *26* (27), 5474-91.
31.Zhang, W.; Zhang, Z.; Chen, S.; Macri, L.; Kohn, J.; Yelick, P. C., Mandibular Jaw Bone Regeneration Using Human Dental Cell-Seeded Tyrosine-Derived Polycarbonate Scaffolds. *Tissue Eng Part A* **2016,** *22* (13-14), 985-93.
32.Keating, J. F.; Simpson, A. H.; Robinson, C. M., The management of fractures with bone loss. *J Bone Joint Surg Br* **2005,** *87* (2), 142-50.
33.Gugala, Z.; Gogolewski, S., Regeneration of segmental diaphyseal defects in sheep tibiae using resorbable polymeric membranes: a preliminary study. *J Orthop Trauma* **1999,** *13* (3), 187-95.
34.Huffer, W. E.; Benedict, J. J.; Turner, A. S.; Briest, A.; Rettenmaier, R.; Springer, M.; Walboomers, X. F., Repair of sheep long bone cortical defects filled with COLLOSS, COLLOSS E, OSSAPLAST, and fresh iliac crest autograft. *J Biomed Mater Res B Appl Biomater* **2007,** *82* (2), 460-70.

3 *In Vitro* Evaluation of Recombinant Bone Morphogenetic Protein-2 Bioactivity for Regenerative Medicine

Reprinted with edits, the definitive version of this chapter has been published in the following form: Fung, S. L.; Wu, X.; Maceren, J. P.; Mao, Y.; Kohn, J., *In Vitro* Evaluation of Recombinant Bone Morphogenetic Protein-2 Bioactivity for Regenerative Medicine. *Tissue Eng Part C Methods* **2019,** *25* (9), 553-559.

3.1 Introduction

Bone morphogenetic protein-2 (BMP-2) is a potent inducer of osteogenic differentiation.[1-4] It is currently the only Food and Drug Administration (FDA)-approved osteoinductive factor used clinically for bone fusion applications in the USA.[5] BMP-2 can be isolated from native bone, or more commonly, expressed as a recombinant human protein (rhBMP-2). The structure and function of the native human BMP-2 have been thoroughly addressed.[6] Mature, bioactive BMP-2 molecules are in the form of a dimer composed of two monomeric units linked by disulfide bonds. Reduction of these disulfide bonds results in the complete loss of bioactivity.[6] RhBMP-2 has been showed to increase alkaline phosphatase (ALP) expression through the Wnt signaling pathway in many cell types, making ALP expression a universal marker for measuring rhBMP-2 bioactivity *in vitro*.[7]

rhBMP-2 can be produced in various expression systems, including a mammalian source, such as the Chinese hamster ovary (CHO) or human embryonic kidney (HEK) cells;

or a bacterial source, such as *E.coli.*[7-8] Recombinant proteins produced in mammalian cells are glycosylated in their final form, whereas those produced in bacterial cells do not undergo this post-translational modification.[8] Although it has been reported that glycosylation is not essential for the biological activity of rhBMP-2,[9-11] the glycosylation influences the biological function of the protein, especially in its effect on interactions between the protein and its carrier and on its distribution once delivered in the body. For example, it was shown that despite small differences in the isoelectric point (pI) of the *E.coli*- and CHO-derived rhBMP-2, the pharmacokinetics (PK) varied significantly *in vivo* due to the reduced solubility of the non-glycosylated protein.[9] In the case of rhBMP-2 mixed with a fibrin carrier, the reduced solubility of non-glycosylated rhBMP-2 improved the healing rate of critical-sized defects in a rat calvarial model.[11]

Different cell lines have been used to measure rhBMP-2 bioactivity *in vitro*. W-20-17 cells are derived from the bone marrow of a W^{++} mouse strain. These cells express low basal levels of ALP, however, upon induction with >6 ng/mL rhBMP-2 for 24 hours, cells express higher than basal levels of ALP in a dose-dependent manner without an effect on cell proliferation.[12] The W-20-17 cell line has been used to determine the bioactivity of rhBMP-2 delivered in hydrogels and microspheres,[10, 13-14] and is also the cell line in the American Society for Testing and Materials (ASTM) Standard Test Method for *In vitro* Biological Activity of Recombinant Human Bone Morphogenetic Protein-2 (rhBMP-2) (F2131-02). rhBMP-2 also has the ability to redirect C2C12 cells, a myoblast cell line, down the osteogenic lineage.[1] ALP activity, osteocalcin production, and parathyroid hormone-induced 3',5'-cAMP production were all upregulated upon incubation with >100 ng/mL rhBMP-2, which suggests the emergence of an osteoblastic phenotype. These

concentrations were also sufficient to inhibit myotube formation. Transforming growth factor beta-1 (TGF-β1) induction resulted in a decrease in osteocalcin production and ALP activity, which confirms the specificity of rhBMP-2 in converting myoblasts towards the osteoblastic lineage.[1] Therefore, C2C12 cells are used as a model cell line to measure rhBMP-2 bioactivity in many studies.[15-18] Other cells such as osteoblast progenitor cells (MC3T3) have also been used to determine the bioactivity of BMP-2.[19-21]

In this study, we evaluated and compared the assay sensitivity of the most widely used rhBMP-2 bioactivity assays. We explored the dose-response of W-20-17, C2C12, and MC3T3 cells to the same batch of rhBMP-2 (*E.coli*-derived rhBMP-2). Next, we compared the bioactivity and stability of rhBMP-2 from different commercial sources. The results of our systematic study will help researchers to choose an appropriate bioactivity assay based on their research needs.

3.2 Materials and Methods

3.2.1 Cell Culture

C2C12 cells were (ATCC CRL-1772) cultured according to the manufacturer's instructions. Cells were maintained in DMEM (Dubecco's Modified Eagle Medium, Life Technologies) containing 10% fetal bovine serum (FBS, Atlanta Biologicals) and 35 µg/mL gentamicin (Sigma Aldrich). Cells were passaged prior to reaching confluence, and media was changed every 3-4 days. MC3T3-E1 cells (ATCC CRL-2593) were cultured in complete Alpha Minimum Essential Medium (αMEM, Life Technologies) containing 10% FBS and 35 µg/mL gentamicin. Cells were passaged upon reaching confluence, with media changes every 3-4 days. W-20-17 cells (ATCC CRL-2623) were cultured according to the

ASTM Standard Protocol (F2131-02). Basal media was prepared by dissolving 13.3 g of Dulbecco's modified Eagle's medium with 4500 mg/L glucose and 4.0 mM L-glutamine (Sigma Aldrich) and 2.226 g sodium bicarbonate (Sigma Aldrich) in 800 mL of purified water. The pH was adjusted to 7.3 ± 0.1 using 0.2 N HCl, and the final volume was brought to 1 L. The basal media was then sterile filtered through a 0.2 μm PES filter into sterile bottles, and then supplemented with heat inactivated FBS (10%), L-Glutamine (8 mM, Life Technologies), and gentamicin (50 μg/mL). Cells with the passage numbers between 3-6 were seeded at a 2 x 10^5 cells per T162 flask, and cultured for 4 days prior to seeding for bioactivity assays. All cells were cultured at 37^{o}C, 5% CO_2 and >95% humidity.

3.2.2 rhBMP-2 Sources

Recombinant human bone morphogenetic protein-2 (rhBMP-2) was obtained from East China University of Science and Technology (ECUST) or purchased from Peprotech, R&D Systems, or Humanzyme. The source information for the rhBMP-2 and international standard used is described in Table 3.1.

Table 3.1 Product information for commercially available rhBMP-2s and the international standard.

Manufacturer	Source	Lot #
National Institute for Biological Standards and Control, Blanche Lane, UK	CHO Cells	N/A
PeproTech, Inc. Rocky Hill, NJ	CHO Cells	0215595
R & D System, Inc. Minneapolis, MN	CHO Cells	MSA5216021
Medtronic, Minneapolis, MN	CHO Cells	N/A
Humanzyme, Inc. Chicago, IL	HEK293 Cells	0415-01
ECUST, Shanghai, China	*E. Coli*	N/A
R & D System, Inc. Minneapolis, MN	*E. Coli*	WN1415061
PeproTech, Inc. Rocky Hill, NJ	*E. Coli*	0614255

To dissociate samples from their manufacturers, rhBMP-2 derived from CHO cells is denoted C1/C2/C3 in text. HEK293-derived and *E. Coli*-derived rHBMP-2 is denoted H1 and E1/E2/E3, respectively. Proteins received as lyophilized powders were reconstituted according to manufacturers' instructions and stored at -80^{o}C. Prior to analysis, concentrations of each stock solution were determined using a micro bicinchoninic acid (BCA) Kit (Thermo Fisher Scientific) according to manufacturer's instructions. The dilution of each sample was performed based on the concentration determined by BCA assay.

3.2.3 Bioactivity Assays

The protocol for testing *in vitro* bioactivity of rhBMP-2 using C2C12 cells was adapted from the protocols described in the literature.[16] Maintenance media was prepared by adding FBS to a final concentration of 2% in DMEM (Life Technologies). C2C12 cells were plated at 1 x 10^4 cells/well in a 96-well tissue culture-treated polystyrene plate (Denville Scientific Inc.) and cultured in complete growth media (DMEM +10% FBS + 35 µg/mL gentamicin) at 37ºC for 24 hours. rhBMP-2 was diluted to 1369 ng/mL in maintenance media, then serially diluted at 4.3-fold dilutions (unless otherwise noted) in a 96-well plate. 7 dilutions were prepared. Growth media was removed, the monolayer of cells was washed twice with sterile PBS, and 100 µL of maintenance media was added to each well. 100 µL of the maintenance media containing rhBMP-2 from the dilution series was added, resulting in the highest concentration of the series being 684.5 ng/mL. Cells were cultured in the absence of rhBMP-2 to determine the background signal. Cells were incubated at 37ºC, 5% CO_2 for 72 ± 4 h unless otherwise noted. The media was removed from all wells. The plate was washed with 200 µL PBS. 50 µL purified water was added to each well, and the plate was frozen at -80ºC. Plates underwent two thaw-freeze cycles. The plate was brought to room temperature prior to development. The assay mix was prepared by dissolving 170 mg p-nitrophenyl phosphate (PNPP) in 50 mL glycine buffer, the glycine buffer was prepared according to ASTM (F2131-02). 50 µL assay mix was added to each well, and the plate was incubated at room temperature on an orbital shaker. Measurements of absorbance at 405 nm were taken every 30 minutes on a Tecan Spark 10M plate reader (TECAN) until the highest reading of the plate was at least 1.0 OD greater than the background signal. 100 µL 0.2 N NaOH was added to each well to stop the reaction.

Absorbance was measured again at 405 nm. The dose-response of MC3T3-E1 cells to rhBMP-2 induction was assayed using the same methods, with all cultures carried out using αMEM in place of DMEM.

The protocol for testing *in vitro* bioactivity of rhBMP-2 using W-20-17 cells was adapted from the ASTM Standard (F2131-02). Assay medium was prepared by adding FBS (final concentration 10%), L-Glutamine (final concentration 4 mM), and penicillin/streptomycin (Life Technologies, final concentration 1%) to the W-20-17 basal medium described above. W-20-17 cells were plated at 1.0 x 10^5 cells/well in 200 µL assay medium in a 96-well tissue culture-treated polystyrene plate. rhBMP-2 was diluted as described above. The media was removed from the monolayer of W-20-17 cells, and 200 µL of the assay media containing rhBMP-2 was added to each well. Assay media containing no rhBMP-2 was used as the background sample. Cells were incubated in the presence of rhBMP-2 for 24 ± 4 h unless otherwise noted. Takedown of the plates and development were performed as described above. Modifications to standard protocols: (1) To evaluate the dose-response at higher concentrations, rhBMP-2 stocks were diluted to 4096 ng/mL, then diluted 2-fold to achieve a final concentration range from 1 to 2048 ng/mL; (2) To determine the effect of incubation time on the dose-response, incubation times of 24 hours, 3 days, and 6 days were tested.

3.2.4 Analysis of Data

The background signal from the samples containing no rhBMP-2 was subtracted from the absorbance value of each test sample. The bioactivity of the sample was determined by fitting the data using a four-parameter logistic (4PL) equation model, where:

Y = measured optical density at 405 nm,

X = concentration of rhBMP-2,

A = minimum optical density,

B = slope at the inflection point,

C = ED50 (concentration that reflects that at half of the maximum concentration), and

D = maximum optical density

3.2.5 Storage Stability

To examine a correlation between the concentration and bioactivity of rhBMP-2, a 1 μg/mL solution of CHO-derived rhBMP-2 (C1) and *E. coli*-derived rhBMP-2 (E3) and EEBMP-2 was prepared in the assay medium of W-20-17 cells. The stock solution was divided into 500 μL aliquots in centrifuge tubes. The aliquots were incubated at 37°C, 5% CO_2, RH 75%. At 6 h, 12 h, Day 1, 2, 3, 5, 7 and 14, three aliquots were collected and stored at -80°C prior to enzyme-linked immunosorbent assay (ELISA, PeproTech) and bioactivity assay. The quantified concentrations from ELISA at each time point were normalized to those of Day 0. The bioactivity of rhBMP-2 at each time point was measured following the procedure from ASTM Standard (F2131-02) with minor modification, 2-fold dilutions were performed on each aliquot and incubated with W-20-17 cells directly for 24 hours.

To evaluate the stability of rhBMP-2 at physiological temperature, a 100 ng/mL solution, as calculated using BCA assay, of each rhBMP-2 was prepared in the assay media of W-20-17 cells. The stock solution was then aliquoted into 500 μL aliquots in centrifuge tubes. The aliquots were incubated at 37°C, 5% CO_2, RH 75%. At Day 1, 2, 3, 5, 7, 14, 21

and 28, three aliquots were collected for each rhBMP-2. The samples were stored at -80°C prior to ELISA (PeproTech). The quantified concentrations at each time point were normalized to those of Day 0.

3.2.6 Statistical Analysis

Single factor analysis of variance (ANOVA) was performed followed by a multiple comparison post-hoc test (Dunnett's test) with an established significance of $p \leq 0.05$. Data were reported as mean ± standard error (SE). All statistical analyses were carried out in GraphPad Prism 7 software.

3.3 Results and Discussion

Since rhBMP-2 is expressed in different biological systems and may come from different manufacturing processes, its bioactivity has to been measured and reported to facilitate the comparison of results from different laboratories. Further, for comparative studies, a generally-accepted bioactivity assay (used at a uniform concentration of rhBMP-2) is critically needed. Here, we report, for the first time, a direct comparison of different bioactivity assay parameters and an evaluation of the advantages and disadvantages of each assay. In addition, we compared the bioactivity of commercially available preparations of rhBMP-2 to an international standard, and assessed the effect of glycosylation on the stability of rhBMP-2s during incubation under physiological conditions.

3.3.1 RhBMP-2 Dose-Response of Model Cell Lines

The induction of ALP in W-20-17, C2C12, and MC3T3 cells was compared as a function of the concentration of an *E. coli*-derived rhBMP-2 obtained from ECUST. After 72 hours of incubation with a concentration range of 1 - 2048 ng/mL of rhBMP-2, ALP induction was measured with PNPP as a substrate (Figure 3.1).

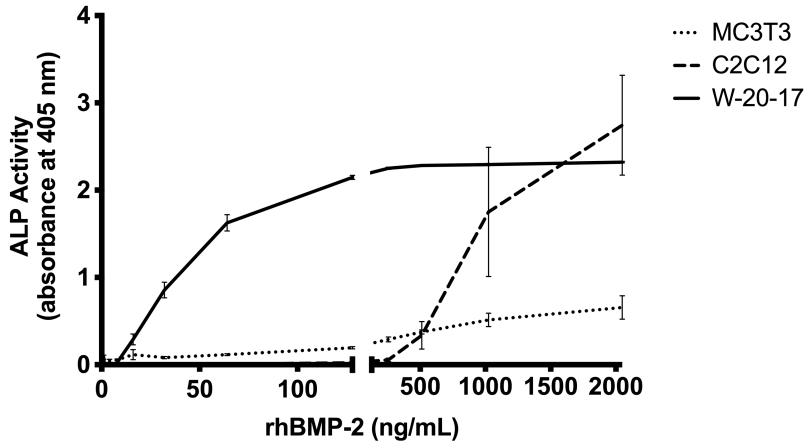

Figure 3.1 Dose-response of rhBMP-2 in different model cell lines. The activity of rhBMP-2 (obtained from ECUST) was measured in C2C12 (dashed), MC3T3 (dotted) or W-20-17 cells (solid) after 72 hours (3 days). Dose range from 1 ng/ml to 2048 ng/ml with 2-fold dilutions were tested in all three cell lines (n = 4).

C2C12 cells have a detection limit of about 200 ng/mL and show a strong dose-response at concentrations > 500 ng/mL and up to the highest concentration of rhBMP-2 used in this study. MC3T3 cells have a lower detection limit at about 60 ng/mL, but the MC3T3 cell-based assay is less sensitive to variations in rhBMP-2 concentration and may therefore be a less desirable assay when accurate quantification is required. W-20-17 cells

show the greatest sensitivity, with a detection limit at 10 ng/mL. A sharp dose-dependent response is observed up to 100 ng/mL, after which the signal reached saturation.

Currently in the literature, different cell lines (i.e., C2C12, W-20-17, MC3T3) and varying assay incubation times have been used to measure bioactivity of rhBMP-2. The varying responses from the three different model cell lines (Figure 3.1) highlight the importance of choosing the proper cell line when evaluating rhBMP-2 bioactivity *in vitro*. Each cell line analyzed in this study shows different rhBMP-2 response kinetics, making them suitable for different applications.

The ASTM Standard (F2131-02) uses the W-20-17 mouse stromal cell line, which has a very low detection limit of 2 ng/mL. This assay is best when rhBMP-2 is present only in low concentrations.[10, 13-14] C2C12 cells show little response at concentrations less than 200 ng/mL in agreement with previous reports,[1, 15-18] but a much greater response at higher concentrations (>500 ng/mL), a range at which the W-20-17 cells have already saturated in their signal output. C2C12 cells express constitutively high levels of Msx2, which suppresses the mRNA and enzymatic activity levels of ALP induced by rhBMP-2.[22] This explains why these cells require higher concentrations of rhBMP-2 to overcome the Msx2 suppression of ALP activity. As a myoblast cell line, the use of these cells to evaluate rhBMP-2 bioactivity can give key insight into the consequences of using rhBMP-2 above a certain concentration *in vivo*. The MC3T3 cells express a higher basal level of ALP activity compared to C2C12 and W-20-17 cells, and ALP is not upregulated to the same extent upon induction with rhBMP-2. However, the range over which the cells respond is much broader than either the C2C12 or W-20-17 cells, making it a better cell line to use if studying systems that take advantage of a broad concentration range.

3.3.2 Effect of Incubation Time on rhBMP-2 Dose-Response

Incubation time with rhBMP-2 is another variable reported in the literature, with many studies reporting incubation times ranging from 1-7 days.[15-18] The kinetics of ALP expression in response to rhBMP-2 induction may be different in different cell lines. In order to evaluate the effect of incubation time on the response to rhBMP-2, we compared the dose-dependent responses of C2C12 and W-20-17 cells to the same *E. coli*-derived rhBMP-2 as used before using a lower range of concentrations from 0 to 684.5 ng/mL (Figure 3.2).

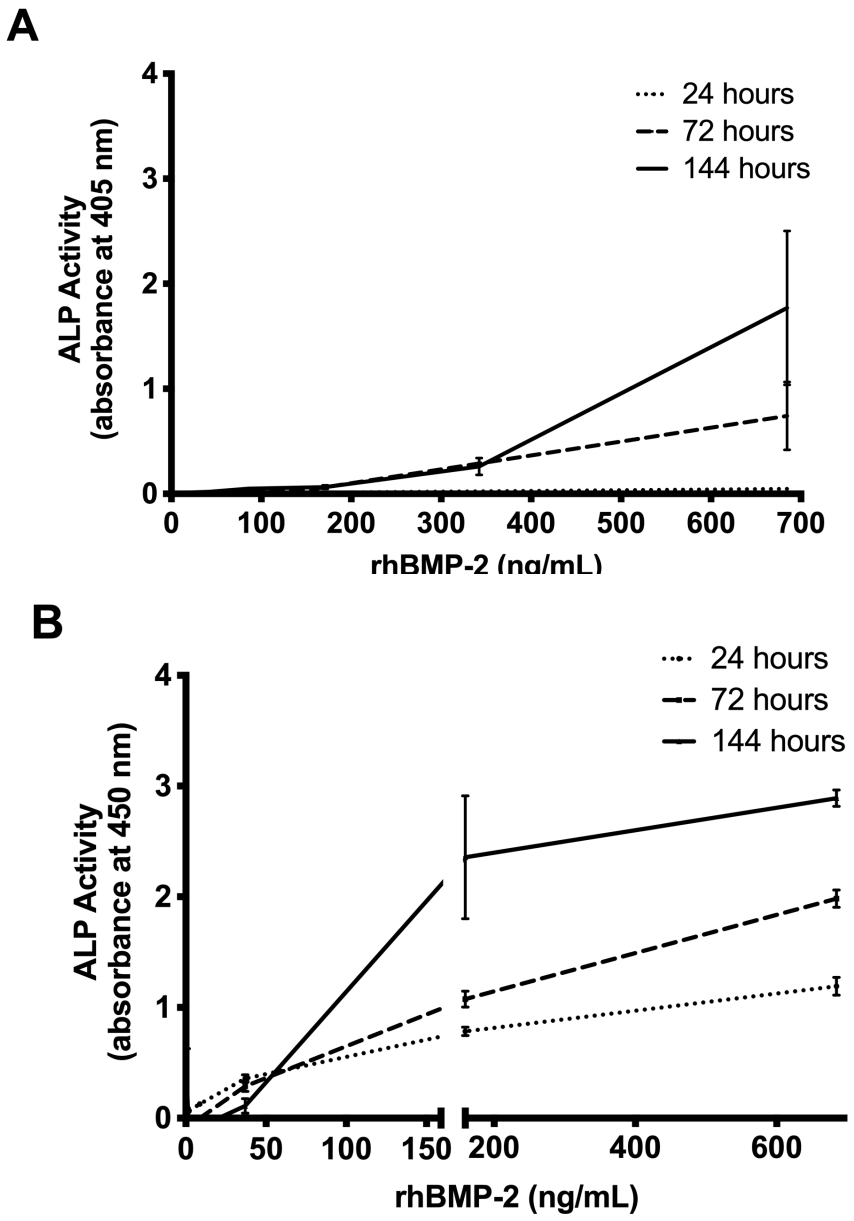

Figure 3.2 Effect of incubation time on rhBMP-2 dose-response. The rhBMP-2 activity was evaluated at the indicated period of time in C2C12 cells (A) and W-20-17 cells (B) for a low concentration range of 0 to 684.5 ng/mL of rhBMP-2 obtained from ECUST (n = 4).

As shown in Figure 3.2A, 24 hours of incubation with rhBMP-2 resulted in little ALP activity in the C2C12 cell line. Increasing the incubation time to 3 and 6 days increased the response at the highest concentrations (684.5 ng/mL), but did not improve the sensitivity of the cell line at lower concentrations. A different effect of incubation time was observed for W-20-17 cells. A 24-hour incubation with the same low concentration range of rhBMP-2 increased the sensitivity of the W-20-17 cell line, as the detection limit was reduced to ~2 ng/mL (Figure 3.2B). The slope of the linear response range decreased, making the cell line more responsive over a broader range of concentrations, but less sensitive to small differences in concentration. As incubation time increased to 3 and 6 days, the detection limit increased, but the slope of the linear range also increased, indicating an even narrower range of sensitivity.

3.3.3 Comparison of Commercially Available rhBMP-2

After choosing the W-20-17 cell line as the model cell line of choice and a 24-hour incubation as the incubation time, we validated the method using rhBMP-2 from commercial sources. The comparison of the commercially available BMP-2s with an international standard highlights the importance of the expression system used to produce the recombinant protein. We compared the bioactivity of rhBMP-2 obtained from different commercial sources, CHO-derived rhBMP-2 (C1, C2, C3), *E. coli*-derived rhBMP-2 (E1, E2, E3) and HEK-293-derived rhBMP-2 (H1) (Figure 3.3).

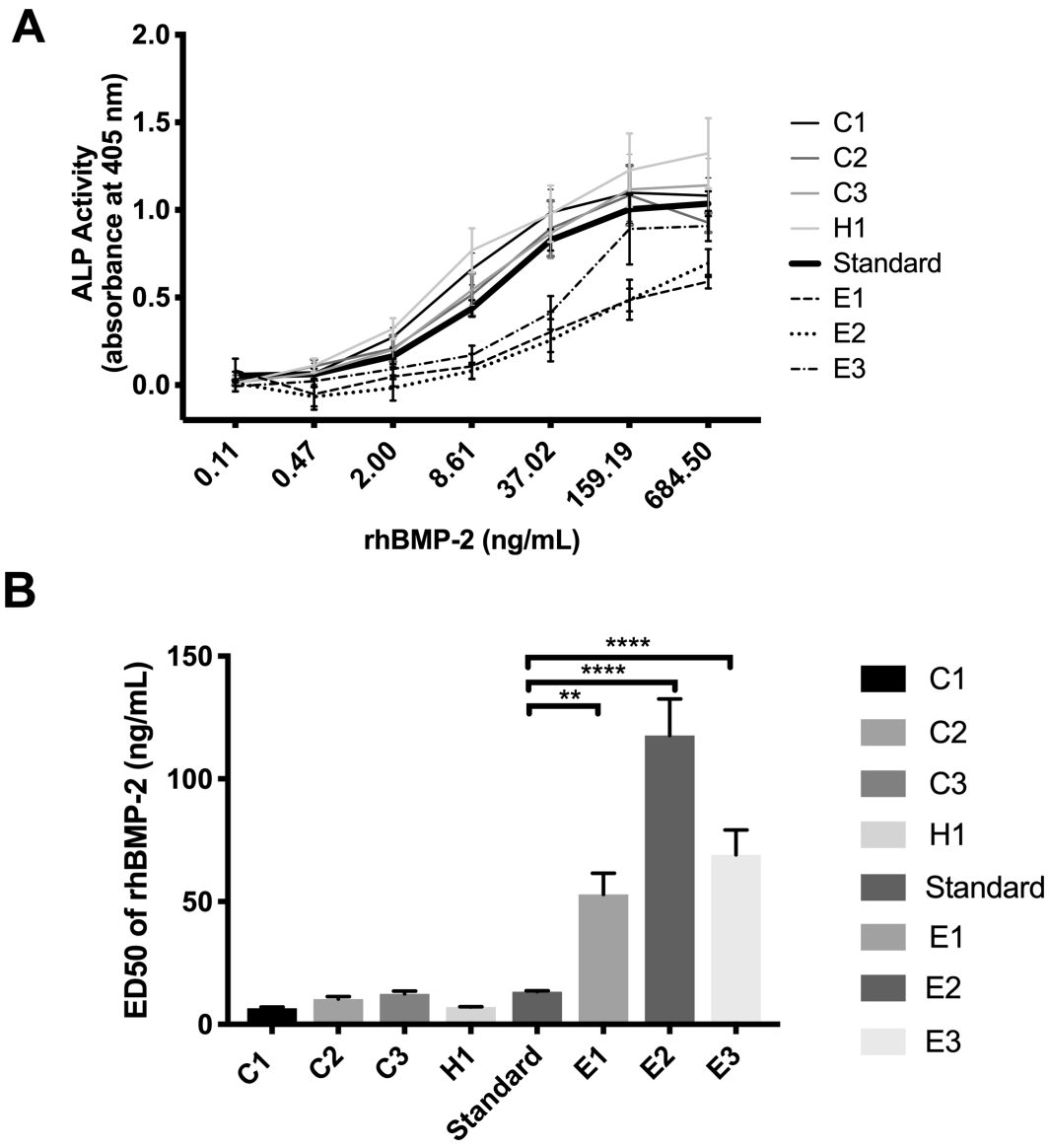

Figure 3.3 Bioactivity comparison of commercially available rhBMP-2. (A) RhBMP-2 dose-response curves obtained by incubating W-17-20 cells with rhBMP-2-containing media for 24 hours at the concentration range of 0.1-684.5 ng/mL. The international rhBMP-2 standard is indicated by the bolded line. (B) Quantification of ED50 values based on (A) (n = 3). ** indicates $p < 0.01$, **** indicates $p < 0.0001$.

As shown in Figure 3.3A, all tested samples of *E. coli*-derived rhBMP-2 triggered lower levels of ALP expression as compared to all of the samples of mammalian-derived rhBMP-2. This is also reflected by the ED50 values (Figure 3.3B) where higher values indicate lower bioactivity. These results confirm the common observation that mammalian cell-derived rhBMP-2 is more active *in vitro* than *E.coli*-derived forms of rhBMP-2. The most bioactive preparations among our test samples were C1 and H1, but the differences among all mammalian cell-derived rhBMP-2 samples were not statistically significant. The difference in bioactivities could arise from the lack of glycosylation of *E. coli*-derived rhBMP-2. The glycosylated form of the protein produced in mammalian cells is more hydrophilic, and the post-translational modification plays an important role in recognition of the protein by the cells.[23-24] On the other hand, it is worth noting that some studies demonstrate that *E.coli*-derived rhBMP-2 is able to trigger higher healing *in vivo*. This is probably because the lack of glycosylation increases the retention of *E. coli*-derived rhBMP-2 within the implanted carrier *in vivo* compared to that of the CHO-derived protein.[25]

3.3.4 Storage Stability

To define a correlation between the bioactivity of rhBMP-2 protein and protein concentration, a CHO-derived rhBMP-2 (C1) (Figure 3.4A) and an *E. coli*-derived rhBMP-2 (E3) (Figure 3.4B) solutions (1 μg/mL) were incubated in the assay medium of W-20-17 cells at 37°C for up to 14 days.

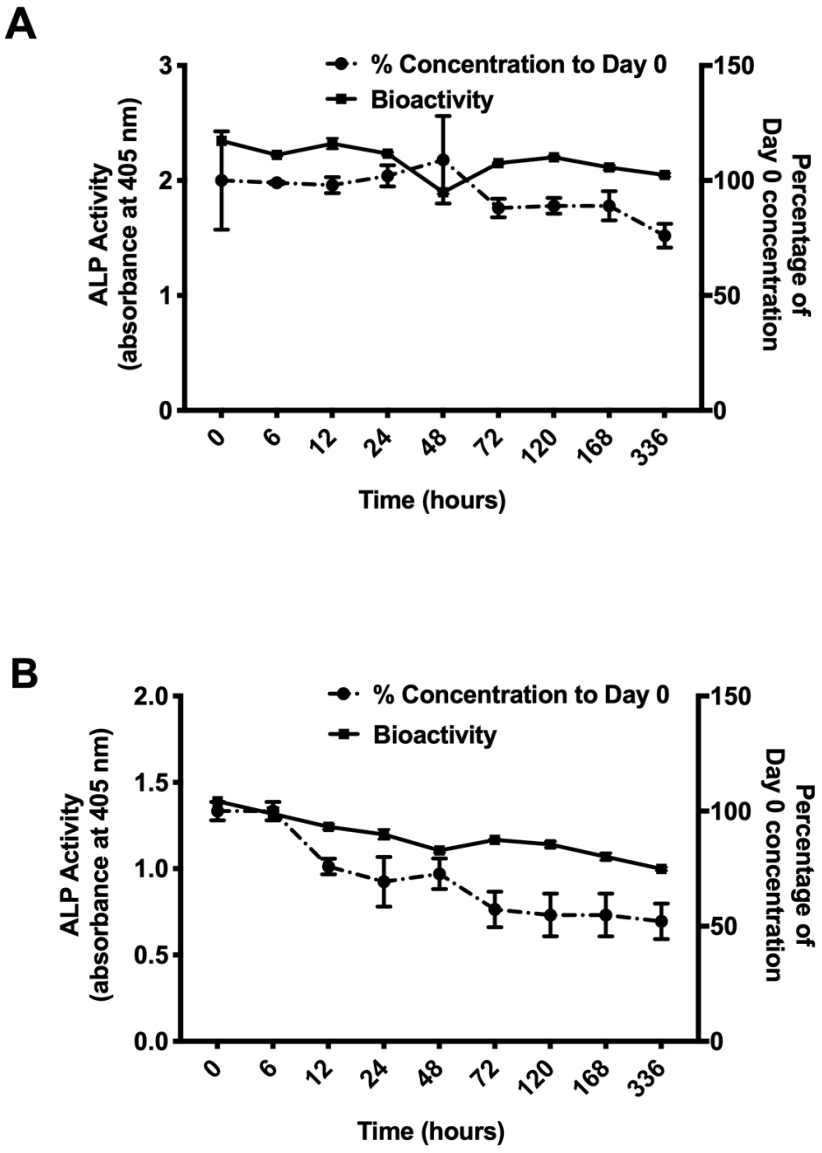

Figure 3.4 Stability of rhBMP-2 at 37°C over time. The concentration of rhBMP-2 in the medium was quantified using ELISA (dashed), and bioactivity by ALP induction was measured in response to rhBMP-2 stimulation (solid). CHO-derived rhBMP-2 (C1) (A) and *E. coli*-derived rhBMP-2 (E3) (B) were tested using W-20-17 cells (n = 3).

Both bioactivity and protein concentration in the assay medium was measured at different time points (Figure 3.4). For C1 (Figure 3.4) and E3 (Figure 3.4B), the decrease of bioactivity followed the decrease in rhBMP-2 concentration. These results indicate that the change of rhBMP-2 concentration can be used as an approximate indicator of a change in bioactivity. This may be useful in some experimental designs since it is easier to determine rhBMP-2 concentration by ELISA than bioactivity by ALP expression. The convenient measurement of rhBMP-2 concentration can be used to obtain an estimate of the bioactivity of the protein, assuming that rhBMP-2 is losing its bioactivity through denaturation or degradation that will render the epitopes unrecognizable by the antibodies of an ELISA.

To determine the storage stability of different rhBMP-2 preparations, the concentrations of the different rhBMP-2 proteins in solution were measured by ELISA over time (

Figure 3.5).

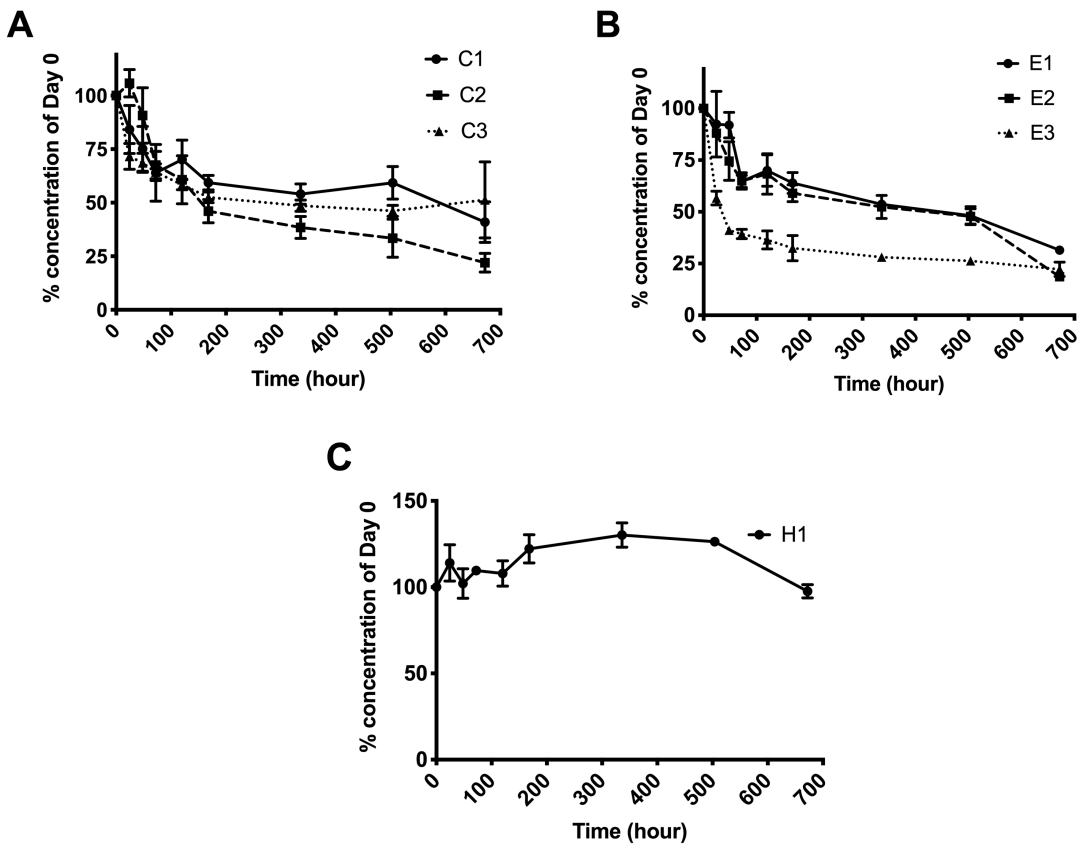

Figure 3.5 Stability of commercially available rhBMP-2 at 37°C. The concentration of CHO cell-derived rhBMP-2 (A), *E. coli* derived rhBMP-2 (B) and HEK-derived rhBMP-2 (C) at the indicated time points. The concentration was quantified by ELISA and normalized to that of Day 0 (n = 3).

We expected that the ELISA-measured concentrations of rhBMP-2 would decrease over time. This basic behavior was indeed observed for all tested samples with the exception of the HEK-derived rhBMP-2 (H1), which showed an unexpected degree of stability throughout the incubation time (

Figure 3.5C).

Figure 3.5 shows sample-specific variations in storage stability at 37 °C. There seems to be a general trend that the half-life of E. coli-derived BMP-2 (except for E3) was relatively longer compared to CHO-derived BMP-2 (

Figure 3.5B). However, we did not find generally applicable correlations between storage stability and the source of rhBMP-2, indicating that the storage stability of any given sample of rhBMP-2 needs to be verified.

3.4 Conclusion

We determined the different dose-responsive behaviors of W-20-17, MC3T3 and C2C12 cell lines. Among those cell lines, W-20-17 cells used as described in ASTM Standard (F2131-02) had the lowest limit of detection with a desirable dose-dependent response when low concentrations of rhBMP-2 were present. C2C12 cells have a detection limit of about 200 ng/mL and showed a strong dose-response at concentrations > 500 ng/mL and up to about 2000 ng/mL, the highest concentration of rhBMP-2 used in our study.

A bioactivity assay using C2C12 cells may be ideal when rhBMP-2 is present in higher concentrations and could be used, for example, as a quality test during the production of rhBMP-2 batches. Bioactivity assays using MC3T3 cells have a detection limit at about 60 ng/mL, but the MC3T3 cell-based assay is less sensitive to variations in rhBMP-2 concentration. On the other hand, incubation time is an important variable in all cell-based bioactivity assays. Assays based on C2C12 cells gave optimal results at long incubation times of up to 6 days, while assays using W-20-17 cells performed well for all incubation times ranging from 24 hours to 6 days.

We observed that rhBMP-2 generated from mammalian cells showed overall higher bioactivity than that from *E. coli*. Moreover, we established a relationship between bioactivity as measured by ALP induction and rhBMP-2 concentration as measured by

ELISA. Therefore, the concentration of rhBMP-2 being released from a delivery vehicle within the cellular dose responsive range can be used as an indicator of rhBMP-2 bioactivity. Our results provide guidance for the establishment of assays for the measurement of rhBMP-2 bioactivity under a wide range of experimental conditions.

3.5 References

1.Katagiri, T.; Yamaguchi, A.; Komaki, M.; Abe, E.; Takahashi, N.; Ikeda, T.; Rosen, V.; Wozney, J. M.; Fujisawa-Sehara, A.; Suda, T., Bone morphogenetic protein-2 converts the differentiation pathway of C2C12 myoblasts into the osteoblast lineage. *J Cell Biol* **1994,** *127* (6 Pt 1), 1755-66.
2.Yamaguchi, A.; Katagiri, T.; Ikeda, T.; Wozney, J. M.; Rosen, V.; Wang, E. A.; Kahn, A. J.; Suda, T.; Yoshiki, S., Recombinant human bone morphogenetic protein-2 stimulates osteoblastic maturation and inhibits myogenic differentiation in vitro. *J Cell Biol* **1991,** *113* (3), 681-7.
3.Ebara, S.; Nakayama, K., Mechanism for the action of bone morphogenetic proteins and regulation of their activity. *Spine (Phila Pa 1976)* **2002,** *27* (16 Suppl 1), S10-5.
4.Wozney, J. M.; Rosen, V.; Celeste, A. J.; Mitsock, L. M.; Whitters, M. J.; Kriz, R. W.; Hewick, R. M.; Wang, E. A., Novel regulators of bone formation: molecular clones and activities. *Science* **1988,** *242* (4885), 1528-34.
5.Gautschi, O. P.; Frey, S. P.; Zellweger, R., Bone morphogenetic proteins in clinical applications. *ANZ J Surg* **2007,** *77* (8), 626-31.
6.Scheufler, C.; Sebald, W.; Hulsmeyer, M., Crystal structure of human bone morphogenetic protein-2 at 2.7 A resolution. *J Mol Biol* **1999,** *287* (1), 103-15.
7.Kubler, N. R.; Reuther, J. F.; Faller, G.; Kirchner, T.; Ruppert, R.; Sebald, W., Inductive properties of recombinant human BMP-2 produced in a bacterial expression system. *Int J Oral Maxillofac Surg* **1998,** *27* (4), 305-9.
8.Demain, A. L.; Vaishnav, P., Production of recombinant proteins by microbes and higher organisms. *Biotechnol Adv* **2009,** *27* (3), 297-306.
9.Kim, I. S.; Lee, E. N.; Cho, T. H.; Song, Y. M.; Hwang, S. J.; Oh, J. H.; Park, E. K.; Koo, T. Y.; Seo, Y. K., Promising Efficacy of Escherichia coli Recombinant Human Bone Morphogenetic Protein-2 in Collagen Sponge for Ectopic and Orthotopic Bone Formation and Comparison with Mammalian Cell Recombinant Human Bone Morphogenetic Protein-2. *Tissue Eng Pt A* **2011,** *17* (3-4), 337-348.
10.Kisiel, M.; Ventura, M.; Oommen, O. P.; George, A.; Walboomers, X. F.; Hilborn, J.; Varghese, O. P., Critical assessment of rhBMP-2 mediated bone induction: An in vitro and in vivo evaluation. *J Control Release* **2012,** *162* (3), 646-653.
11.Schmoekel, H.; Schense, J. C.; Weber, F. E.; Gratz, K. W.; Gnagi, D.; Muller, R.; Hubbell, J. A., Bone healing in the rat and dog with nonglycosylated BMP-2 demonstrating low solubility in fibrin matrices. *J Orthopaed Res* **2004,** *22* (2), 376-381.
12.Thies, R. S.; Bauduy, M.; Ashton, B. A.; Kurtzberg, L.; Wozney, J. M.; Rosen, V., Recombinant Human Bone Morphogenetic Protein-2 Induces Osteoblastic Differentiation in W-20-17 Stromal Cells. *Endocrinology* **1992,** *130* (3), 1318-1324.
13.Kim, S.; Kang, Y. Q.; Krueger, C. A.; Sen, M. L.; Holcomb, J. B.; Chen, D.; Wenke, J. C.; Yang, Y. Z., Sequential delivery of BMP-2 and IGF-1 using a chitosan gel with gelatin microspheres enhances early osteoblastic differentiation. *Acta Biomaterialia* **2012,** *8* (5), 1768-1777.
14.Kempen, D. H. R.; Lu, L.; Hefferan, T. E.; Creemers, L. B.; Maran, A.; Classic, K. L.; Dhert, W. J. A.; Yaszemski, M. J., Retention of in vitro and in vivo BMP-2 bioactivities in sustained delivery vehicles for bone tissue engineering. *Biomaterials* **2008,** *29* (22), 3245-3252.

15.Hanseler, P.; Jung, U. W.; Jung, R. E.; Choi, K. H.; Cho, K. S.; Hammerle, C. H. F.; Weber, F. E., Analysis of hydrolyzable polyethylene glycol hydrogels and deproteinized bone mineral as delivery systems for glycosylated and non-glycosylated bone morphogenetic protein-2. *Acta Biomaterialia* **2012,** *8* (1), 116-123.
16.Zhou, H.; Qian, J.; Wang, J.; Yao, W.; Liu, C.; Chen, J.; Cao, X., Enhanced bioactivity of bone morphogenetic protein-2 with low dose of 2-N, 6-O-sulfated chitosan in vitro and in vivo. *Biomaterials* **2009,** *30* (9), 1715-24.
17.Smith, E.; Yang, J.; McGann, L.; Sebald, W.; Uludag, H., RGD-grafted thermoreversible polymers to facilitate attachment of BMP-2 responsive C2C12 cells. *Biomaterials* **2005,** *26* (35), 7329-38.
18.Crouzier, T.; Sailhan, F.; Becquart, P.; Guillot, R.; Logeart-Avramoglou, D.; Picart, C., The performance of BMP-2 loaded TCP/HAP porous ceramics with a polyelectrolyte multilayer film coating. *Biomaterials* **2011,** *32* (30), 7543-54.
19.Takuwa, Y.; Ohse, C.; Wang, E. A.; Wozney, J. M.; Yamashita, K., Bone morphogenetic protein-2 stimulates alkaline phosphatase activity and collagen synthesis in cultured osteoblastic cells, MC3T3-E1. *Biochem Biophys Res Commun* **1991,** *174* (1), 96-101.
20.Hiraki, Y.; Inoue, H.; Shigeno, C.; Sanma, Y.; Bentz, H.; Rosen, D. M.; Asada, A.; Suzuki, F., Bone morphogenetic proteins (BMP-2 and BMP-3) promote growth and expression of the differentiated phenotype of rabbit chondrocytes and osteoblastic MC3T3-E1 cells in vitro. *Journal of bone and mineral research : the official journal of the American Society for Bone and Mineral Research* **1991,** *6* (12), 1373-85.
21.Krishnan, L.; Priddy, L. B.; Esancy, C.; Klosterhoff, B. S.; Stevens, H. Y.; Tran, L.; Guldberg, R. E., Delivery vehicle effects on bone regeneration and heterotopic ossification induced by high dose BMP-2. *Acta Biomaterialia* **2017,** *49*, 101-112.
22.Kim, Y. J.; Lee, M. H.; Wozney, J. M.; Cho, J. Y.; Ryoo, H. M., Bone morphogenetic protein-2-induced alkaline phosphatase expression is stimulated by Dlx5 and repressed by Msx2. *J Biol Chem* **2004,** *279* (49), 50773-50780.
23.Hang, Q. L.; Zhou, Y.; Hou, S. C.; Zhang, D. M.; Yang, X. J.; Chen, J. P.; Ben, Z. Y.; Cheng, C.; Shen, A. G., Asparagine-linked glycosylation of bone morphogenetic protein-2 is required for secretion and osteoblast differentiation. *Glycobiology* **2014,** *24* (3), 292-304.
24.Ohtsubo, K.; Marth, J. D., Glycosylation in cellular mechanisms of health and disease. *Cell* **2006,** *126* (5), 855-67.
25.Uludag, H.; D'Augusta, D.; Golden, J.; Li, J.; Timony, G.; Riedel, R.; Wozney, J. M., Implantation of recombinant human bone morphogenetic proteins with biomaterial carriers: A correlation between protein pharmacokinetics and osteoinduction in the rat ectopic model. *J Biomed Mater Res* **2000,** *50* (2), 227-38.

4 Dopamine-Functionalized Tyrosine-Based Polycarbonates for Bone-Related Applications

4.1 Introduction

While scaffolds made of tyrosine-derived polycarbonates and calcium phosphates have been successfully utilized as carriers for recombinant human bone morphogenetic protein 2 (rhBMP-2) to trigger full bone regeneration in critical size bone defects, the scaffold alone treatments usually demonstrate moderate osteoconductivity *in vivo* due to the lack of strong biological cues in synthetic polymers.[1-3] In the meanwhile, the free carboxylic groups on the polycarbonate backbone allow for further functionalization via reaction with amines or alcohols. For example, amino-PEG-biotin was attached to the backbone of E1001(1k) for further biotinylated rhBMP-2 conjugation via the biotin-streptavidin interaction. Such surface-tethered osteogenic rhBMP-2 could further trigger the differentiation of mesenchymal stem cells (MSCs) *in vitro*.[4] Similarly, other functional amines could be introduced into the polymer backbone at altered mole percentages by varying the synthetic routes.

On the other hand, the versatile catechol chemistry opens possibilities for multiple biomedical applications. Catechol can be easily oxidized to *o*-quinone and then can undergo reactions with primary amines and thiol groups via Michael-type addition or Schiff base reaction, allowing for covalent modification of bioactive peptides and proteins on the material surfaces. It was also speculated that the interaction between catechol and proteins contributes to the enhanced cell attachment.[5-8] In addition, the redox chemistry of catechol could induce nano-sized silver deposition on catecholized surfaces,[9-10] while silver nanoparticles (AgNPs) have been widely recognized as an antibacterial agent against a broad range of bacteria

and fungi.[11] It is widely acknowledged that infection at the tissue-implant interface or biofilm formation causes implant failures. As a result, there is a growing interest in the development of functional biomaterials with proper antibacterial activity in the biomedical field.[12] Consequently, the catechol-mediated AgNP deposition on biomaterial raises many research interests for this purpose. So far, many trials have been performed on functionalized hydrogels like chitosan,[13] gelatin[14] and poly(ethylene glycol) (PEG),[15] but the reports on catechol-functionalized polymers films are relatively rare.[16] In summary, the chelation of bidentate catechol, the redox chemistry of catechol to *o*-quinone, the nucleophilic addition on *o*-quinone and the ability of catechol to reduce ionic silver to form AgNPs make catechol remarkably useful in the orthopedics field.

Catechol derivatives occur naturally in marine invertebrates, fruits, tea, and insects.[17] Molecules such as dopamine, L-DOPA and dihydrocaffeic acid can be applied as building blocks to generate catechol-containing polymers.[18-20] Dopamine, being a hormone and neurotransmitter, is the most frequently used building blocks of catechol-modified polymers.[5, 21] Among the vast amount of papers reported on the catechol-derived biomaterials, the majority of reports fall into four categories: (1) direct functionalization onto polymers like PEG and natural polysaccharides;[13, 22-24] (2) polymerization of catechol-containing monomers (like dopamine methacrylamide) with various monomers;[21, 25] (3) use of catechol-modified initiators to create end-functionalized polymers; [25-32] and (4) peptide synthesis using L-DOPA.[21, 26-38] Very few papers reported on the introduction into biodegradable polyesters and polycarbonates like PLA,[39] polycaprolactone (PCL)[40] and trimethylene carbonate-derived copolymers.[41-42]

In this chapter, dopamine was chosen as the catecholamine to directly functionalize tyrosine-derived polycarbonates through reaction with the carboxylic acid groups on the

backbone. Repeating units containing catechol side chains ranging from 5 to 40 mol%. The water contact angle measurement and Arnold's test were conducted on spin-coated polymer films to confirm the presence of surface-anchoring catechol groups. Cell-material interaction studies were conducted to examine the compatibility of functionalized polymers and their osteogenic potential. Lastly, the investigation of catechol-induced AgNPs deposition was conducted on the polymer films and the antibacterial effects of AgNPs decorated polymers were elaborated.

4.2 Material and Methods

4.2.1 Materials

Desaminotyrosyl-tyrosine ethyl ester (DTE) and desaminotyrosyl-tyrosine tert-butyl ester (DTtBu) were previously synthesized at New Jersey Center for Biomaterials. E1001(1k) was synthesized by Cyalume Technologies Holdings, Inc. (Ft. Lauderdale, FL, USA). 1-Ethyl-3-(3-dimethylaminopropyl)carbodiimide (EDC) was purchased from Kawaguchi Chemical Industry Co., LTD (Japan). N, N-Diisopropylethylamine (DIPEA) was purchased from TCI America (Portland, OR). Poly(ethylene glycol) (PEG) (Mw 1000 Da) is purchased from Alfa Aesar (Haverhill, MA). Dichloromethane (DCM) and ethanol (EtOH) were purchased from Fisher Scientific (Pittsburgh, PA). Agar was purchased from Becton Dickinson (Franklin Lakes, NJ). Dopamine hydrochloride, N-hydroxysuccinimide (NHS), anhydrous N, N-dimethylformamide (DMF), isopropanol (IPA), dimethylsulfoxide-d6 (DMSO-d6), bis(trichloromethyl)carbonate (triphosgene), silver nitrate solution ($AgNO_3$) solution (0.1 M), concentrate nitric acid (HNO_3), concentrate hydrochloric acid (HCl), sodium molybdate, sodium nitrite ($NaNO_2$), HPLC water, silver standard for ICP, tryptic soy broth (TSB), poly-L-

Lysine hydrobromide (PLL), β-glycerophosphate, ascorbic acid, dexamethasone and gentamicin solution were obtained from Sigma-Aldrich Corporation (St Louis, MO). *Escherichia coli* (*E. coli*, ATCC700928), *Staphylococcus aureus* (*S. aureus*, ATCC25923) and MC3T3-E1 cells (ATCC CRL-2593) are from American Type Culture Collection (City of Manassas, VA). Human osteoblasts-femoral (HO-f) are from ScienCell Research Laboratories (Carlsbad, CA). Human mesenchymal stem cells (hMSCs) are from RoosterBio Inc (Frederick, MD). Osteoblast culturing medium (ObM) comes from Cell Application, Inc. (San Diego, CA). Dulbecco's Modified Eagle Medium (DMEM), alpha Minimum Essential Medium (αMEM), fetal bovine serum (FBS), trypsin-EDTA (0.25%), Dulbecco's Phosphate Buffered Saline (DPBS) come from Thermo Fisher Scientific (Waltham, MA).

4.2.2 Polymer Synthesis

4.2.2.1 Synthesis of Exx01(1k)

Polycarbonates with the chemical structure of poly((99-xx)DTE-co-xx%DT-co-1%PEG_{1k} carbonate) (Figure 4.1) were synthesized following previously reported procedures.[2] Briefly, the DTE and DTtBu diols were copolymerized with PEG (molecular weight 1 kDa) using pyridine and bis(trichloromethyl)carbonate in DCM, followed by selective removal of the tert-butyl ester protecting groups using TFA. The resulting polymers were purified by precipitation in IPA for three times and dried under vacuum to evaporate solvents. These terpolymers are abbreviated as Exx01(1k) where E refers to the ethyl ester side chains, xx is the mole percent of DT, "01" represents the polymers are composed of 1 mol% of PEG units. The following polymers were used in this study: E1501(1k), E2001(1k), E3001(1k) and E5001(1k).

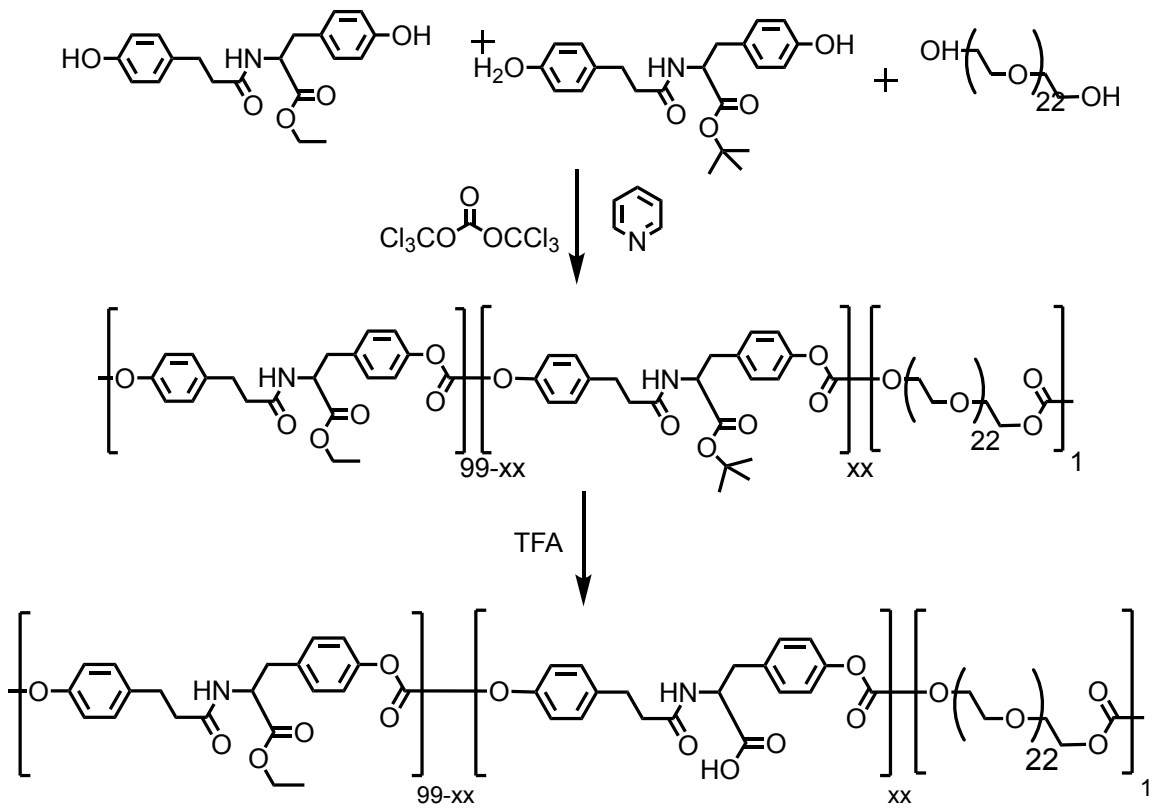

Figure 4.1 Synthetic scheme of tyrosine-derived polycarbonates with the chemical composition poly((99-xx)%DTE-co-xx%DT-co-1%PEG carbonate), the terpolymers were abbreviated as Exx01(1k), where E is the ethyl ester pendant chain, xx is the mol% of DT, 01 represents the polymers contain 1 mol% of PEG.

4.2.2.2 Synthesis of Catechol-Functionalized E1001(1k) Analogs

To make E1001(1k) analogs with catechol functionality, polymers with the chemical structure Exx01(1k) were selected and reacted with dopamine hydrochloride. A general procedure goes as follows (as illustrated in Figure 4.2): an Exx01(1k) polymer was loaded into a 3-neck round bottom flask, the flask was then purged with argon (Ar) and dissolved in anhydrous DMF (10 wt% solution). The solution was then degassed with Ar and added with EDC (1.05 equivalence to the moles of carboxylic groups in each polymer) and NHS (1.5 equivalence to the moles of carboxylic groups in each polymer). The reaction mixture was then kept stirring on ice for 1 h. After this, dopamine hydrochloride (1.05 equivalence to the targeted % mole of functionalization) dissolved in anhydrous DMF and DIPEA was added into the reaction under Ar atmosphere and allowed for stirring overnight under Ar protection. The remaining NHS ester (10 mol%) was hydrolyzed by the addition of 1 mL DI water and stirred for 1 h at room temperature. The resulting polymers were purified by precipitation in IPA for three times and blended in water to yield white polymer chunks. Finally, the chunks were dried under vacuum to evaporate solvents.

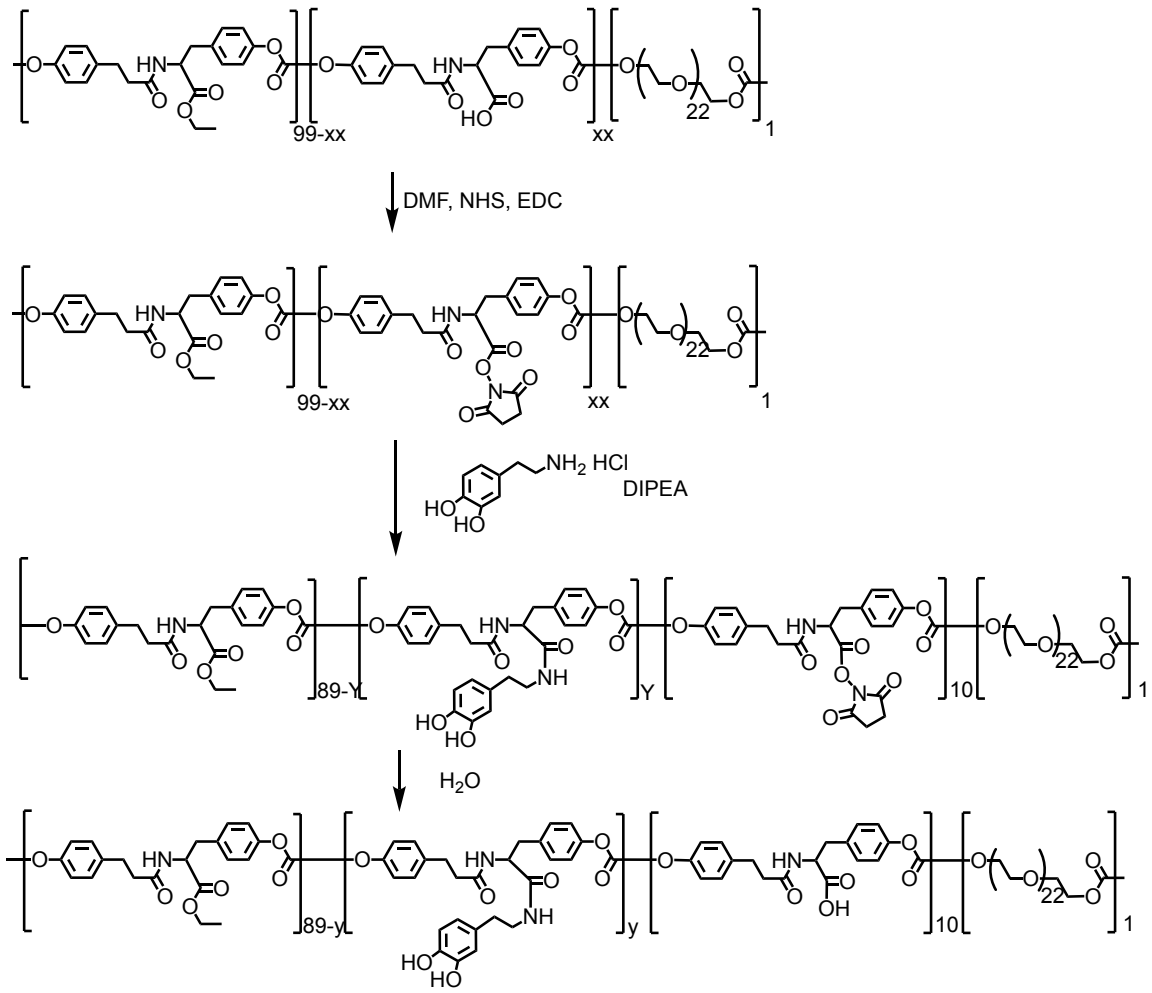

Figure 4.2 Catechol-modified E1001(1k) analogs with different mol % of catechol side chains.

4.2.3 Characterization of Polymers

The chemical composition of polymers was studied by ^{1}H NMR using 500 MHz Varian NMR instrument in DMSO-d_6 solutions. The calculation of mol% of catechol modification is presented as follows:

$$\%\text{of catechol} = \frac{\text{Normalized integration of aromatic protons from catechol}}{\text{Normalized integration of aromatic proton from the backbone and PEG}}$$

The number average molecular weight (M_n) and weight average molecular weight (M_w) of the polymers were measured by gel permeation chromatography (GPC, Waters) in DMF (0.1% TFA) as the mobile phase. The GPC calibration curve was created using polystyrene standards (Agilent Technologies, Santa Clara, CA) ranging from 4720 Da to 6,325,000 Da (M_w).

4.2.3.1 Spin Coating

2% (w/v) polymer solutions were prepared in 90:10 mixture of DCM/DMF and filtered through 0.45 μm PTFE filters. Glass cover slips were cleaned with 1M HCl and EtOH prior to use. To obtain thin films, ~90μL of the solution was placed on each 15 mm cover slip, and spin-coated at 3000 rpm for 30s on a Headway Research Inc. (Garland, TX) spin coater. All films were dried under vacuum for 48 h before use.

4.2.3.2 Water Contact Angle

The water contact angle was measured following ASTM C813-90 using NRL C. A. goniometer (rame-hart, Inc, Mountain Lakes, NJ, USA). Briefly, 15 mm cover slips coated with

polymer films were individually placed on the platform, then the syringe needle was brought into close proximity to the film surface and then, with the test surface in a horizontal position, a hypodermic syringe was used to force a 20 μL drop of ultrapure water onto the surface. The contact angle on the left and the right side of each drop was measured. By making left- and right-side determinations, the effect of a slightly nonlevel surface is alleviated. Three random spots were measured for each cover slip and 3 individual polymer films were measured for each sample. Test conditions: 23 ºC, 25% RH.

4.2.3.3 Visualization of Surface-Active Catechol Moieties

To qualitatively visualize the presence of surface-exposed catechol groups, Arnow's test was performed on the spin-coated polymer films.[43-44] Briefly, polymer-coated cover slips were placed individually into 24-well plate, then the following reagents were sequentially added into each well to generate a red/brown color on the polymer films with the presence of catechol: 200 μL 0.5 M HCl and 200 μL nitrite-molybdate (0.02 v/v%), 200 μL 1M NaOH and 200 μL DI water. Films were incubated for a couple of minutes and then the films were washed with DI water. Images were taken and contrast was manually adapted to highlight the differences between different groups.

4.2.4 Cell-Material Interaction

4.2.4.1 Interaction with Human Osteoblasts-Femoral (HO-fs)

In vitro HO-fs culture was conducted using cells from passages 3. HO-fs were cultured on those PLL-coated 10 cm cell culture dishes until they reached ~90% confluence. The cells were lifted using 0.25% trypsin-EDTA solution before use. Spin-coated polymer

films containing 0%, 5%, 10%, 20% and 40% catechol were sterilized by immersion in 70% IPA for 30 mins, then dried on sterile absorbent paper. The films were then individually transferred into each well of 24-well plates and washed with 1 mL 1X DPBS. Cell seeding was performed by adding 1 mL of cell suspension (8 x10^4 cells/mL) in serum-free DMEM (n =1) or 1 mL of cell suspension (4 x10^4 cells/mL) in ObM (n = 4). The cell-seeded films were incubated at 37°C, 5% CO_2 and 95% humidity.

To examine the cell adhesion, one film from each medium was fixed in 4 % paraformaldehyde (in PBS) after 2-h incubation with cell suspensions and stained with rhodamine phalloidin (Invitrogen, Carlsbad, CA), followed by counterstaining of 4',6-diamidino-2-phenylindole (DAPI, Invitrogen, Carlsbad, CA) following manufacturer's instructions. All films were imaged by a Zeiss Observer D1 using the DAPI filter (335–383 excitation, 420–470 emission), Alexa 555 filter (538–562 excitation, 570-640 emission) and an AxioCam MRm digital camera. To examine the proliferation and ALP expression of HO-fs, the cell suspension in ObM was removed after initial overnight incubation and continued culture in the same medium. The cell proliferation was measured by alamarBlue assay (Bio-Rad, Hercules, CA) on Day 1, 2 and 3. For the ALP expression experiment, cells were lysed on Day 3. The ALP level was quantified using Alkaline Phosphatase Activity Fluorometric Assay Kit (BioVision, Milpitas, CA). The dsDNA contents were measured using Quant-iT™ PicoGreen® dsDNA Kit (Invitrogen, Carlsbad, CA). All data obtained from Tecan SPARK M10 plate reader.

4.2.4.2 Interaction with MC3T3 cells

In vitro MC3T3 cell culture was conducted using cells from passages 6. MC3T3 cells were cultured in 10 cm cell culture dishes in αMEM containing 10% FBS (i.e., growth medium, GM) until they reached ~90% confluence. The cells were then harvested using 0.25% trypsin-EDTA solution before use. Polymer films containing 0%, 5%, 10%, 20% and 40% catechol were sterilized in 70% IPA as described in **Section 4.2.3.1**. After preconditioning the films in 1mL GM for 1 h at 37 ºC, 0.5 mL cell suspension in GM (4 x 10^4 cells/mL, n = 6) was added to each well and incubated at 37°C, 5% CO_2 and 95% humidity overnight. Then the cell suspension was removed and the cells were cultured in 1mL GM. The cell proliferation (Day 1, 4, 7, 14) ALP expression and DNA contents were measured (Day 7, 14) as described in **Section 4.2.3.1.**

4.2.4.3 Interaction with hMSCs

In vitro hMSCs culture was conducted using cells from passages 4. MSCs were cultured in 10 cm cell culture dishes in αMEM containing 10% FBS and 35 µg/mL gentamicin (Growth medium, GM) until they reached ~90% confluence, the cells were then harvested using 0.25% trypsin-EDTA solution before use. Polymer films containing 0%, 5%, 10% and 20% catechol were sterilized in 70% IPA as described in **Section 4.2.3.1**. After preconditioning the films in 1mL GM for 1 h at 37 ºC, 565 µL cell suspension in GM (1.8 x 10^4 cells/mL) was added to each well and incubated at 37°C, 5% CO_2 and 95% humidity overnight. Then the media was removed and the cells were cultured in 1mL GM or the same amount of osteogenic medium (OS, namely GM containing 20 mM β-glycerophosphate, 50 µg/ml of ascorbic acid and 100 nM dexamethasone). The ALP level

and DNA contents were measured as described in **Section 4.2.3.1** on Day 7 and Day 14 (n = 4).

4.2.5 Antibacterial Properties of E1001(1k) and Catechol Polymers

4.2.5.1 Ag Deposition on Spin-Coated Polymer Films

The catechol-assisted AgNPs deposition was conducted by immersion the films in $AgNO_3$ solutions at various concentrations. Briefly, a 100 mM $AgNO_3$ solution (Sigma) was diluted to the desired concentration using Milli Q water. Each spin-coated polymer film (15 mm) was then immersed in 2 mL solution and agitated for 24 h in the dark. The Ag-coated films were rinsed with Milli Q water and excess water was removed using KimWipe. All films were further dried under vacuum overnight before further tests.

4.2.5.2 SEM on the Ag-coated Films

Scanning electron microscopy (SEM, Phenom ProX) was used to observe the morphology of the Ag-coated polymer films. All films were mounted on alumina stubs using conductive carbon tapes and imaged without metal coating.

4.2.5.3 Quantification of $AgNO_3$ Uptake of E1001(1k) Films

To quantify the amount of $AgNO_3$ uptake of E1001(1k) films during catechol-assisted Ag deposition, spin-coated E1001(1k) films were first immersed in $AgNO_3$ solution ranging from 0 mM to 100 mM following the protocol described in **Section 4.2.4.1**. After this, the films were digested in 171 μL concentrate HNO_3 and diluted with HPLC water to give 2% HNO_3 solution (n = 4). The amount of silver ions was measured by

inductively coupled plasma optical emission spectrometry (ICP-OES, PerkinElmer ICP-OES Optima 7300 DV) and calculated against a silver standard for ICP (Sigma).

4.2.5.4 General Procedure for *In Vitro* Antibacterial Tests

The *in vitro* antibacterial activity of silver-decorated films was tested against *E. coli* (Gram-negative) and *S. aureus* (Gram-positive) using a spread plate method. Bacteria inoculum was performed by taking a single colony from a freshly streaked tryptic soy agar (TSA) plate with a loop and cultured in 1mL of sterile tryptic soy broth (TSB) at 37ºC and shaking until the optical density (OD) readings at 600 nm measured between 0.2-0.6, the bacteria inoculum was further diluted with sterile 1X DPBS to giving a concentration of 1 x 10^6 CFU/mL. The number of CFUs was estimated based on the fact that OD_{600} = 1.0 corresponds to 10^9 CFU/mL.[45] Before antibacterial tests, spin-coated polymer films were soaked in 70% IPA for 15 mins and rinsed in sterile DI water for 15 mins twice. The abovementioned bacteria solution in 1x DPBS was then dropped onto sterilized films at a density of 100 µL/cm^2. After 24 h incubation at 37 ºC, 100 µL of the dissociated bacteria suspension as well as their serial dilutions in TSB were inoculated onto TSA plates, respectively. The plates from *E. coli* tests were incubated for 24 h before CFU counts, whereas the plates from *S. aureus* tests were incubated for 48 h before CFU counts. For all experiments, sterile glass cover slips were used as negative controls. The antibacterial effect from silver was calculated as Log Reduction:

$$\text{Log Reduction} = \log 10\left(\frac{\text{CFU of controls}}{\text{CFU of experimental groups}}\right)$$

4.2.5.5 Influence of $AgNO_3$ Concentration Used for Coating on Antibacterial Properties

To assess the influence of $AgNO_3$ concentration used for Ag coating on the antibacterial effects, spin-coated E1001(1k) films and an E1001(1k) analog with 20% catechol were coated in $AgNO_3$ solution ranging from 0 mM to 100 mM following the protocol described in **Section 4.2.4.1**. Antibacterial tests against *E. coli* and *S. aureus* were conducted according to the protocol described in **Section 4.2.4.4** (n = 4).

4.2.5.6 Influence of Catechol Contents on Antibacterial Properties

To investigate the antibacterial properties of polymers with different catechol contents, spin-coated films containing 0-40% catechol were coated in 10 mM $AgNO_3$ following the protocol described in **Section 4.2.4.1**. Antibacterial tests against *E. coli* and *S. aureus* were conducted according to the protocol described in **Section 4.2.4.4** (n = 4).

4.2.6 Statistical Analysis

Single factor analysis of variance (ANOVA) was performed followed by a multiple comparison post-hoc test (Tukey's test) with an established significance of $p \leq 0.05$. Data were reported as mean ± standard error (SE). Data processed in GraphPad Prism 7 software.

4.3 Results and Discussion

4.3.1 Characterization of Exx01(1k)

The synthesis of E1501(1k), E2001(1k), E3001(1k) and E5001(1k) was done by condensation polymerization with coupling reagent triphosgene, the step-growth

polymerization yield polymers with M_w around 300 kDa, the molecular weight data and PDI was collected in Table 4.3. The chemical composition of each polymer was identified by ^{1}H NMR (Table 4.1). The % mole of each monomer component was calculated based on the integration of amide protons (D, I) at ~8.3 and ~8.2 ppm, aromatic protons (A) at ~7.2 ppm and methylene protons from PEG (K) at ~4.1, ~3.6 and ~3.5 ppm. The polymer compositions were within ± 1 mol% of the intended values (Table 4.2).

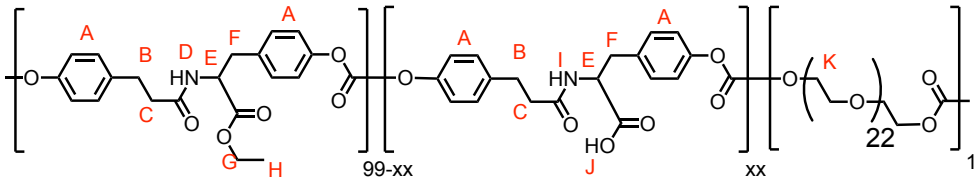

Figure 4.3 Chemical structure of Exx01(1k).

Table 4.1 Assignment of ^{1}H NMR chemical shifts of Exx01(1k).

Proton	Chemical Shift (ppm)	Proton	Chemical Shift (ppm)
A	7.2	G	4.0
B	2.4	H	1.1
C	2.7	I	8.2
D	8.3	J	12.8
E	4.4	K	3.5, 3.6, 4.1
F	2.8, 3.0		

Table 4.2 Chemical composition of Exx01(1k).

Polymer	Chemical composition (mol%)		
	%DTE	%DT	$\%PEG_{1k}$
E1501(1k)	83.2	15.8	1.0
E2001(1k)	79.8	18.5	0.8
E3001(1k)	70.0	29.0	1.0
E5001(1k)	49.6	49.6	0.8

4.3.2 Catechol-Modified E1001(1k) Analogs

The DT units in Exx01(1k) were partially functionalized with dopamine, a constant 10 mol% of DT unites was retained to assemble E1001(1k). The structure of catechol-modified polymers was determined by ^{1}H NMR and chemical shifts are illustrated in Figure 4.4, the presence of new amide peaks at 8.9 ppm (D) and 7.9 ppm (E) indicate successful functionalization of carboxylic groups from DT with dopamine. The phenolic protons at 8.6 and 8.7 ppm (A) and aromatic protons from catechol indicate the presence of catechol in the polymer chains. The retained amide peak at 8.2 ppm (C) indicates the presence of DT units after functionalization. The amides from DT had been partially downshifted due to the increased number of amide bones and resulting hydrogen bonding. Owing to the increase of hydrogen bonding between polymer chains after functionalization, the mol% of catechol modification was calculated from aromatic protons of catechol at 6.5 – 6.6 ppm, aromatic protons from the backbone at ~7.2 ppm and methylene protons from PEG at ~4.1, ~3.6 and ~3.5 ppm. The catechol % and molecular weight data were summarized in Table 4.3. The calculated % of catechol modification is close to theoretical values.

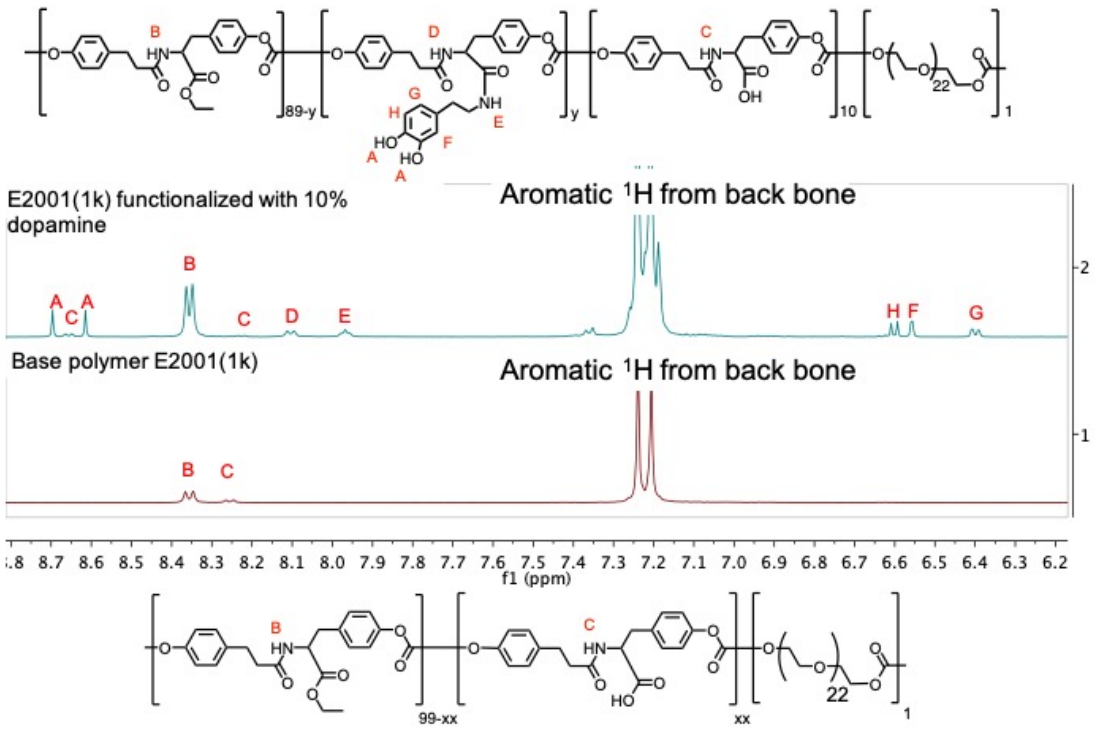

Figure 4.4 Chemical structure and ^{1}H NMR chemical shift assignment for catechol-modified polymers, the modification of E2001(1k) with 10 mol% of catechol was demonstrated here.

Table 4.3 Mol% of catechol modification calculated from ^{1}H NMR spectra and molecular weights of polymers before/after functionalization.

Base Polymer	Intended Y% Catechol	% Catechol by 1H NMR Estimation	M_w/PDI Before Functionalization	Mw/PDI After Functionalization
E1501(1k)	5	6.o	303kDa/1.5	298kDa/1.7
E2001(1k)	10	10.9	208kDa/1.5	263kDa/1.6
E3001(1k)	20	22.5	215kDa/1.5	269kDa/1.7
E5001(1k)	40	39.7	310kDa/1.5	363kDa/2.0

4.3.3 Surface-Active Catechol Moieties

As illustrated in Figure 4.5, the chemical modification of dopamine was done in bulk, and to allow for interaction with cell and further functionalization on surfaces, it is critical to have surface accessible catechol moieties from dopamine when the polymers are processed for further applications. Therefore, water contact measurements and Arnow's test were conducted to qualitatively confirm the presence of surface-active catechol moieties on spin-coated films.

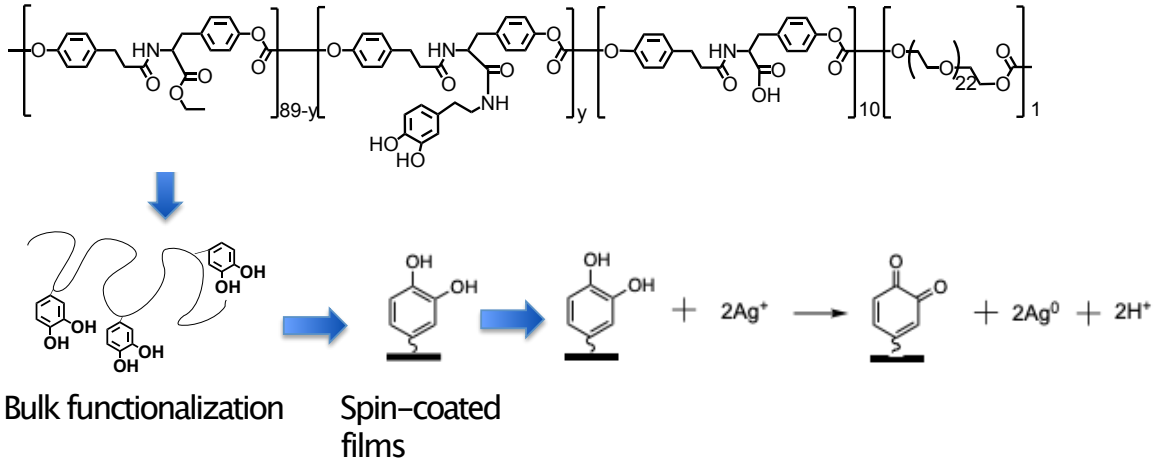

Figure 4.5 Illustration of catechol-assisted silver deposition on polymer films.

Table 4.4 Water contact angles of polymers with different catechol contents.

Catechol %	0	5	10	20	40
Contact angle	68.8 ± 0.3	67.9 ± 0.3	67.8 ± 0.3	64.5 ± 0.7	62.2 ± 0.4

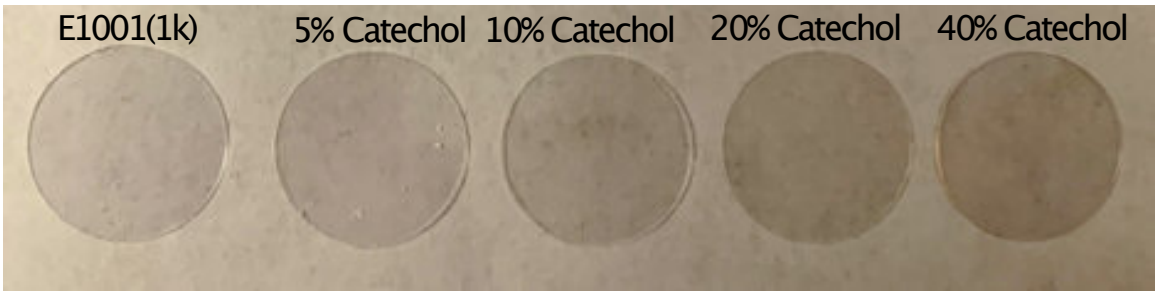

Figure 4.6 Arnow's test showing surface-active catechol moieties on spin-coated films, the presence of catechol indicated by increased brown tone.

Water contact angle measurement (

Table 4.4) showed that the incorporation of 5% and 10% catechol side chains did not significantly influence the surface hydrophilicity. However, when the catechol content increased to 20% and above, the contact angle dropped significantly. This is due to the presence of more catechol groups on the surface and thus increased the hydrophilicity of polymer surfaces. Also, the color change from Arnow's test (Figure 4.6) demonstrates that as the catechol mol % increase in the bulk polymer, the resulting films had more catechol moieties present on the surface, yielding deeper brown color. Both experiments indicated that dopamine-modified polymers can be used for catechol-mediated functionalization and could potentially interact with cells.

Catechol %	0	5	10	20	40
Contact angle	68.8 ± 0.3	67.9 ± 0.3	67.8 ± 0.3	64.5 ± 0.7	62.2 ± 0.4

4.3.4 Cell-Material Interactions

4.3.4.1 Catechol-HO-f Interaction

To examine if the catechol-modification could potentially enhance the cell attachment and alter tyrosine-based polycarbonates more bioactive, HO-fs were cultured on spin-coated polymer films and examined for proliferation as well as ALP expression. As shown in Figure 4.7, HO-fs have different degrees of initial adhesion behaviors in the serum-free medium. The actin network spreads out more as the catechol content increases, suggesting an interaction between the cell membrane and surface-active catechol moieties. This finding agrees with the literature report,[40] where enhanced fibroblast adhesion was observed on catechol decorated PCL nanofibers in a serum-free medium. However, the

HO-fs adhesion appeared similar in ObM containing serum proteins (Figure 4.7) regardless of catechol contents. It could be attributed to the nonspecific protein adsorption on hydrophobic polymer surfaces overwhelming the reaction between catechol and actin networks.[46] For the HO-fs proliferation, no significant difference was found between E1001(1k) and catechol functionalized analogs at all time points (Figure 4.8). However, HO-fs grown on films containing 10% and 20% catechol have more ALP expression compared to those on E1001(1k) films (Figure 4.9), suggesting that those two kinds of polymers could have helped the maintenance of osteoblasts. No significant difference was found within the rest groups.

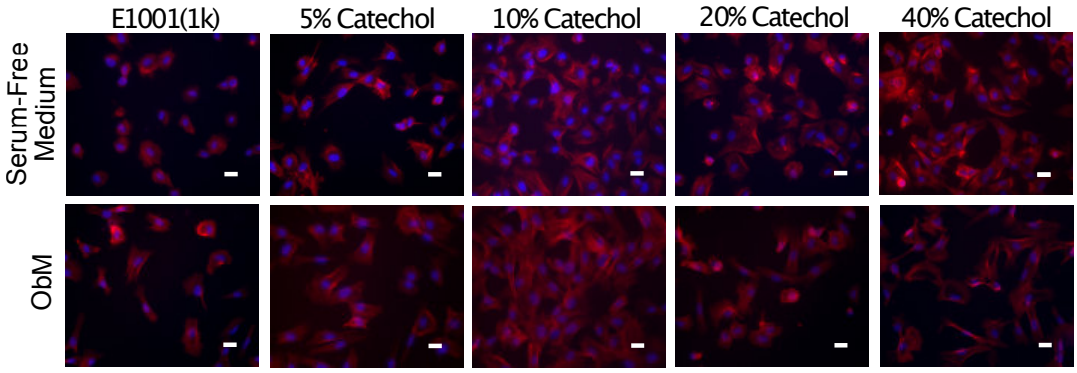

Figure 4.7 HO-fs adhesion on catechol-containing polymer films in a serum-free medium and a complete medium (ObM). Cells are stained with actin (red) and DAPI (blue). Scale bars are 100 μm.

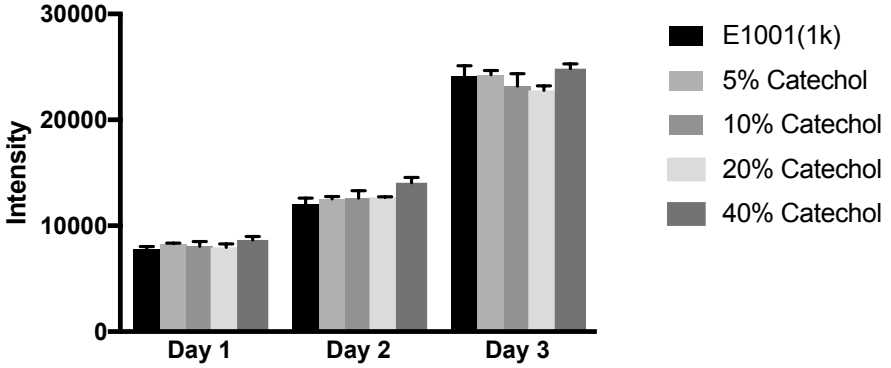

Figure 4.8 Proliferation of HO-fs on polymer films containing different mol% of catechol (n = 3).

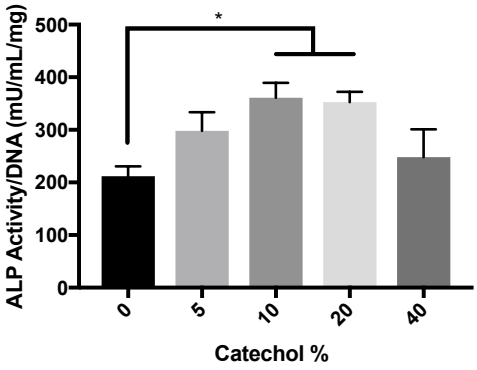

Figure 4.9 ALP expression from HO-fs after a 3-day culture on catechol-modified polymer films (n = 3). * indicates $p<0.05$.

4.3.4.2 Catechol-MC3T3 cell Interaction

The cellular response from MC3T3 cells to the presence of catechol moieties was studied in the same way as HO-fs studies. The initial attachment of MC3T3 cells was similar across all polymers in a complete medium. This observation is consistent with that of HO-fs attachment in ObM. The cell proliferation data are presented in Figure 4.10, all polymers were able to support cell proliferation until Day 7. No significance was found between Day 7 and Day14, indicating that cells reached confluency and those cells on films containing 40% catechol had significant metabolic activity drop compared to other groups on Day 14.

The ALP activity was quantified to assess the osteogenic differentiation of MC3T3 cells. As demonstrated in Figure 4.11, MC3T3 grown on all polymers had significantly higher ALP expression at Day 14. Cells on catechol-containing films behaved similarly to E1001(1k) on Day 7. Cells on polymers containing 5% and 10% catechol had comparable ALP activity to those on E1001 (1k), whereas the ALP activity from cells on 20% and 40% catechol had significantly lower ALP expression compared to E1001(1k), 5% and 10% catechol groups at Day 14. These results revealed that the introduction of catechol groups into tyrosine-derived polycarbonate backbones has minimal effects on the proliferation of MC3T3 cells. However, the sole presence of catechol functionality does not stimulate the osteogenic differentiation of MC3T3 as the catechol contents increases.

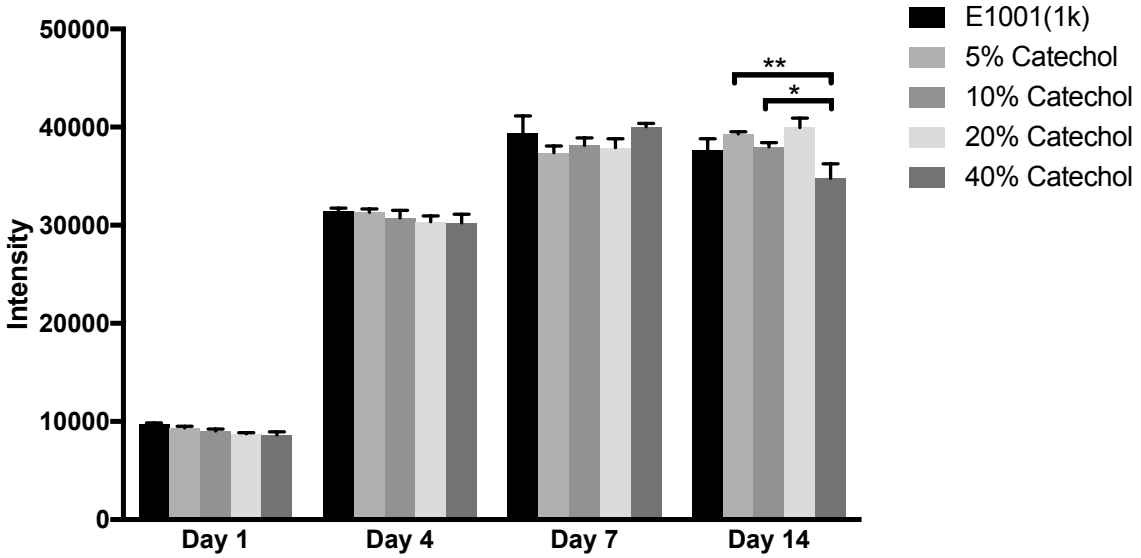

Figure 4.10 Proliferation of MC3T3 cells on polymer films containing different mol% of catechol (n = 3). * indicates $p<0.05$, ** indicates $p<0.01$, *** indicates $p<0.001$, **** indicates $p<0.0001$.

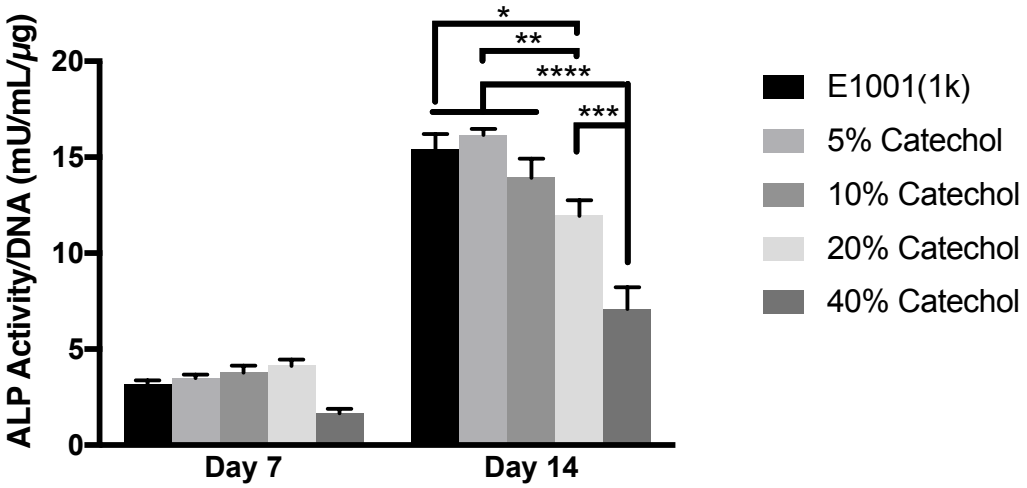

Figure 4.11 ALP expression from MC3T3 cells after 7-day and 14-day culture on catechol-modified polymer films (n = 3). * indicates $p<0.05$, ** indicates $p<0.01$, *** indicates $p<0.001$, **** indicates $p<0.0001$.

4.3.4.3 Catechol-hMSCs Interaction

The interaction between hMSCs and surface-active catechol moieties was investigated based on the aforementioned studies. Since the cell viability on catechol-modified polymer films is not deteriorated and polymers with 40% catechol seemed to decrease the ALP expression in MC3T3 cells on Day 14, only the ALP activity was investigated for E1001(1k) as well as its analogs containing 5 - 20% catechol side chains.

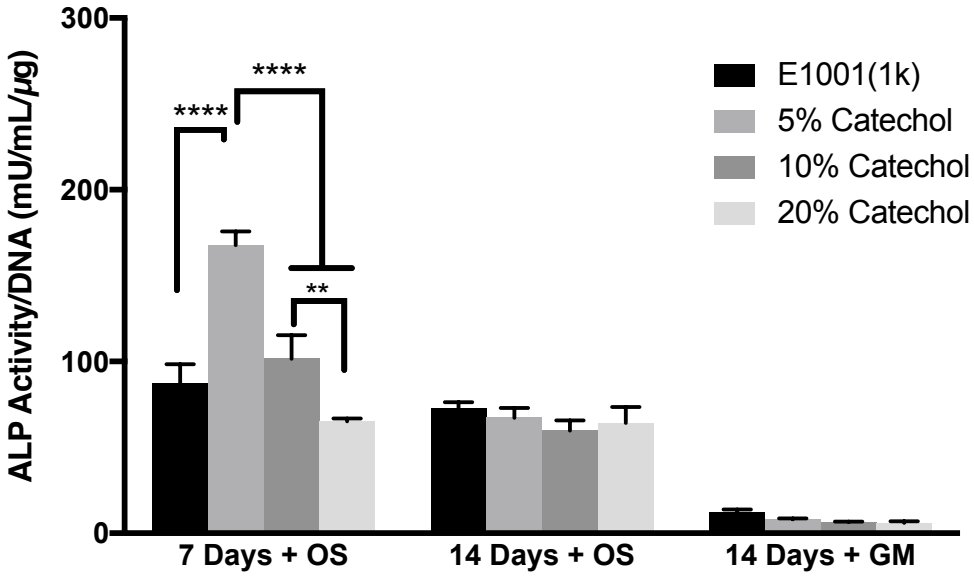

Figure 4.12 ALP expression from hMSCs after 7-day and 14-day cultures in osteogenic medium (OS) and growth medium (GM) on catechol-modified polymer films (n = 4). ** indicates $p<0.01$, **** indicates $p<0.0001$.

It was found that hMSCs maintained in OS had higher ALP expression than those in GM on Day 14, the presence of catechol itself did not affect the osteogenic differentiation of MSCs in GM and OS media on Day 14 (Figure 4.12). hMSCs on polymer films with 5% and 10% catechol side chains have higher ALP activity on Day 7 than Day 14 in OS, no difference was found between E1001(1k) and polymer with 20% catechol

side chains. Moreover, the highest ALP activity was detected from cells on polymers with 5% catechol groups on Day7 in OS, polymers with 10-20% catechol groups have comparable ALP activities to the E1001(1k) group.

The series of cell-material interaction studies showed that the surface-active catechol moieties have a limited osteogenic effect on hMSCs or MC3T3 cells, and only enhanced HO-fs adhesion in a serum-free medium. This is likely due to the intense serum protein adsorption on the polymer surface in complete media,[46] the dramatic differences in concentrations and dimensions between serum proteins and catechol groups impeded direct contact of catechol moieties with living cells. It can be concluded that secondary functionality (i.e., transition metal ions, peptides, proteins, nanoparticles) needs to be introduced via catechol groups to make the base polymers more bioactive.

4.3.5 Antibacterial Properties of E1001(1k) and Catechol Polymers

The unique catechol redox chemistry allows for nano-sized silver deposition on functionalized surfaces (Figure 4.5). In this section, the catechol-assisted AgNPs deposition on E1001(1k) analogs were investigated and the antibacterial properties of the Ag-decorated polymer films were tested against model gram-negative bacteria (*E. coli*) and gram-positive bacteria (*S. aureus*).

4.3.5.1.1 Quantification of $AgNO_3$ Uptake of E1001(1k) Films

Since the deposition of Ag is performed by immersing the films in $AgNO_3$ solutions for 24 h, the polymer films would absorb a trace amount of $AgNO_3$ through water uptake.

Preliminary studies on the antibacterial properties of catechol-modified polymer suggest that E1001(1k) films have certain an antibacterial activity after soaking in $AgNO_3$ solutions, whereas the untreated polymer films showed no killing of *E. coli* and *S.aureus* (Figure 4.14). Furthermore, SEM images of the soaked E1001(k) films showed no Ag aggregates on the surface (Figure 4.15). Those observations lead to the speculation of $AgNO_3$ incorporation into E1001(1k) films by water uptake during Ag deposition. Herein, the Ag contents in E1001(1k) films were measured by ICP-OES. As indicated in Figure 4.13, the amount of $AgNO_3$ detected is proportional to the $AgNO_3$ concentration used for soaking. Since Ag^+ and metallic AgNPs have comparable antibacterial activities and the effective concentration range of Ag^+ is super low,[47-48] the existence of Ag^+ in E1001(1k) renders the antibacterial effect from catechol-assisted AgNPs indistinguishable from controls. Therefore, the determination of a proper $AgNO_3$ concentration range for AgNPs deposition is crucial.

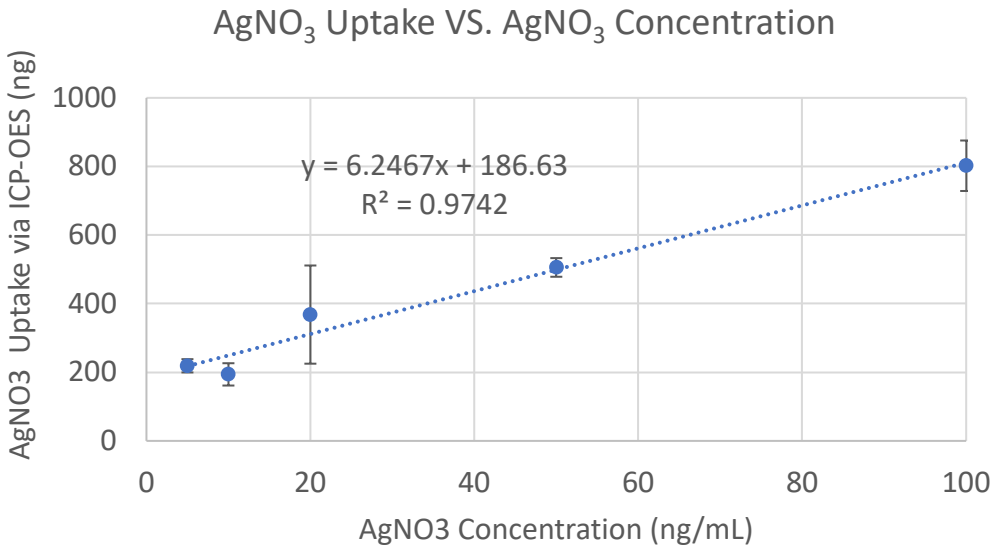

Figure 4.13 $AgNO_3$ uptake into E1001(1k) films during immersion coating of AgNPs measured by ICP-OES.

4.3.5.2 Antibacterial Properties of Uncoated Polymer Films

The antibacterial tests on untreated polymer films suggested that both E1001(1k) and E1001(1k) analog with 20% catechol are not intrinsically active against *E. coli.* While the polymer with 20% catechol demonstrates a slight antibacterial activity against *S. aureus* compared to the glass control, E1001(1k) shows no killing effect of the model gram-positive strain (Figure 4.14).

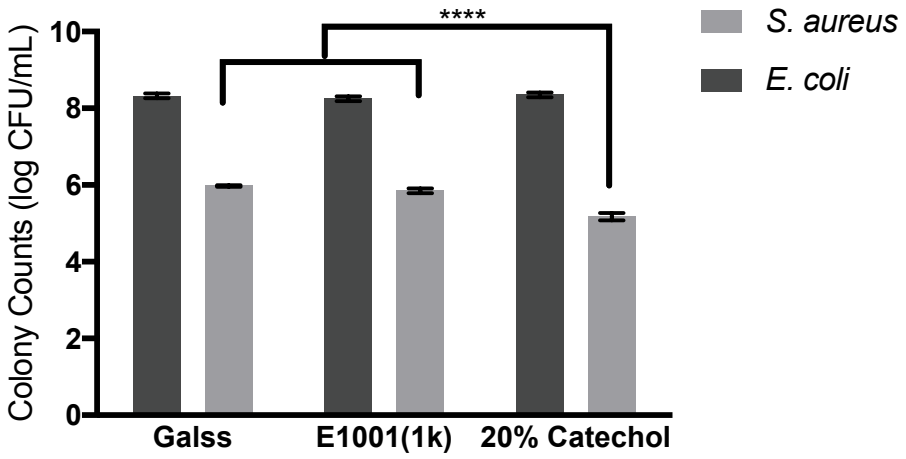

Figure 4.14 Antibacterial tests against *E. coli* and *S. aureus* on unmodified polymer films. Glass is used as a control (n = 4). **** indicates $p<0.0001$.

4.3.5.3 Effects of $AgNO_3$ Concentration for AgNPs Deposition

To investigate the best $AgNO_3$ concentration for AgNPs deposition, E1001(1k) films and films containing 20% catechol were immersed separately in a gradient of $AgNO_3$ solutions. SEM images (Figure 4.15) showed that the 5 mM $AgNO_3$ solution yielded sparse AgNPs (< 100 nm) deposited as bright spots, and as the concentration goes up, AgNPs started to distribute more uniformly on the surfaces. However, when the concentration exceeds 50 mM, the emergence of Ag aggregates on the order of microns accompanied by

the decrease of AgNPs was observed. On the contrary, E1001(1k) films showed smooth surfaces throughout the concentration gradient tested.

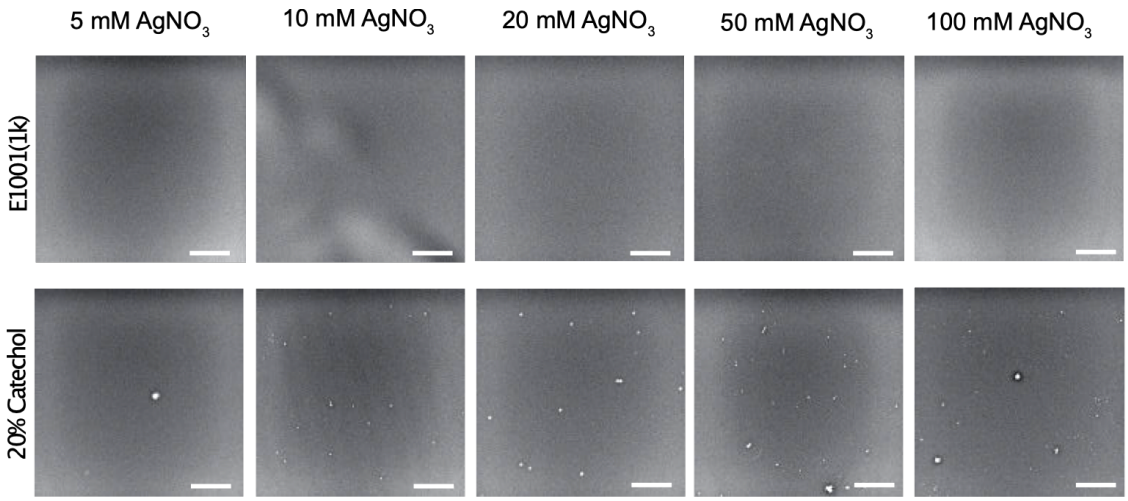

Figure 4.15 SEM images of catechol-assisted AgNPs deposition on polymer films through dip-coating in different $AgNO_3$ concentrations. Scale bars are 10 μm.

For antibacterial tests, films with 20% catechol showed a nearly full reduction of *E. coli* in all $AgNO_3$ concentrations used, whereas treated E1001(1k) films illustrated a concentration-dependent killing effect. Significant differences between the activities against *E. coli* was observed in the range of 5-20 mM $AgNO_3$ (Figure 4.16A). On the other hand, *S. aureus* appeared more resistant to silver species, a significant difference between the activities against *S. aureus* was observed for 10 and 50 mM $AgNO_3$ (Figure 4.16B). Representative agar plates coated with bacteria suspension cultured on films were collected in Figure 4.17 and Figure 4.18.

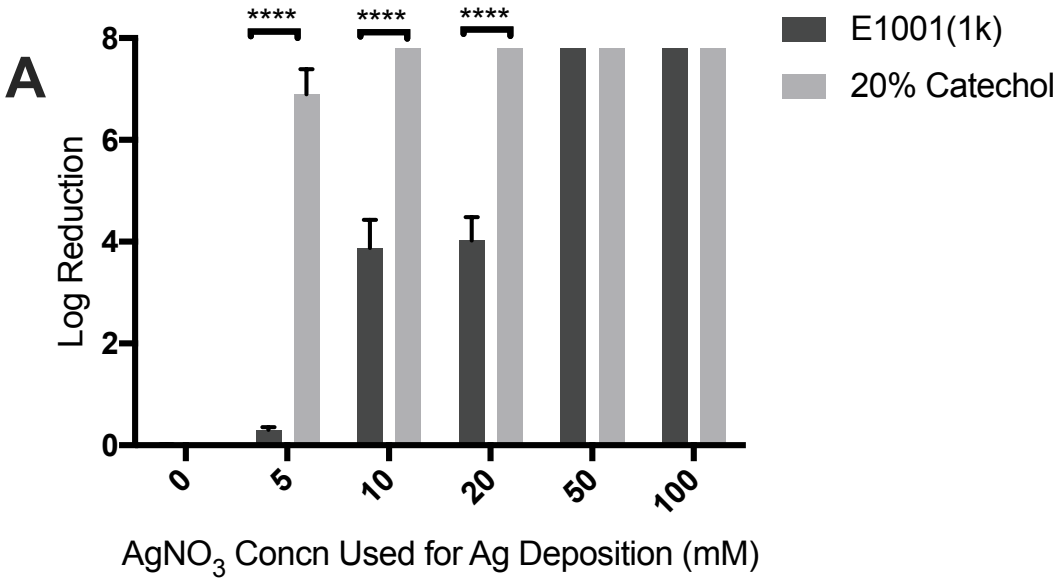

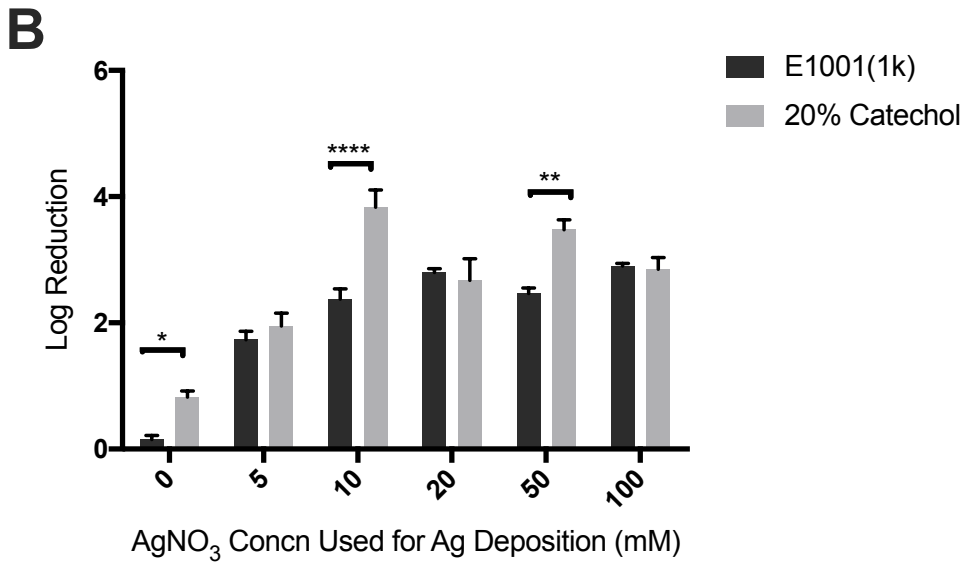

Figure 4.16 The influence of altering $AgNO_3$ concentration used for dip-coating on the antibacterial properties of E1001(1k) and E1001(1k) analog with 20% catechol against *E. coli* (A) and *S. aureus* (B) (n = 4). * indicates $p<0.05$, ** indicates $p<0.01$, **** indicates $p<0.0001$.

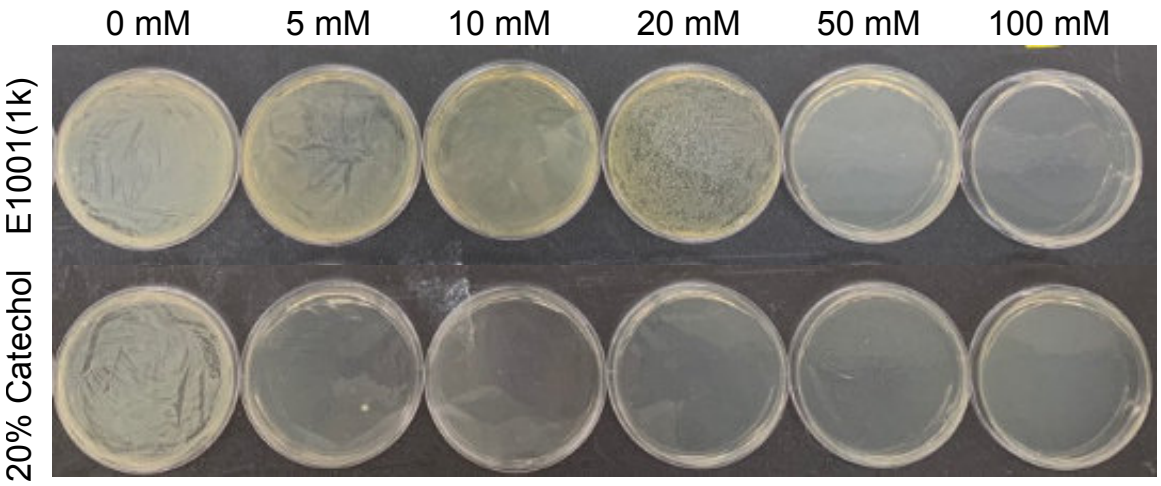

Figure 4.17 Representative TSA plates coated with *E. coli* suspension without dilution.

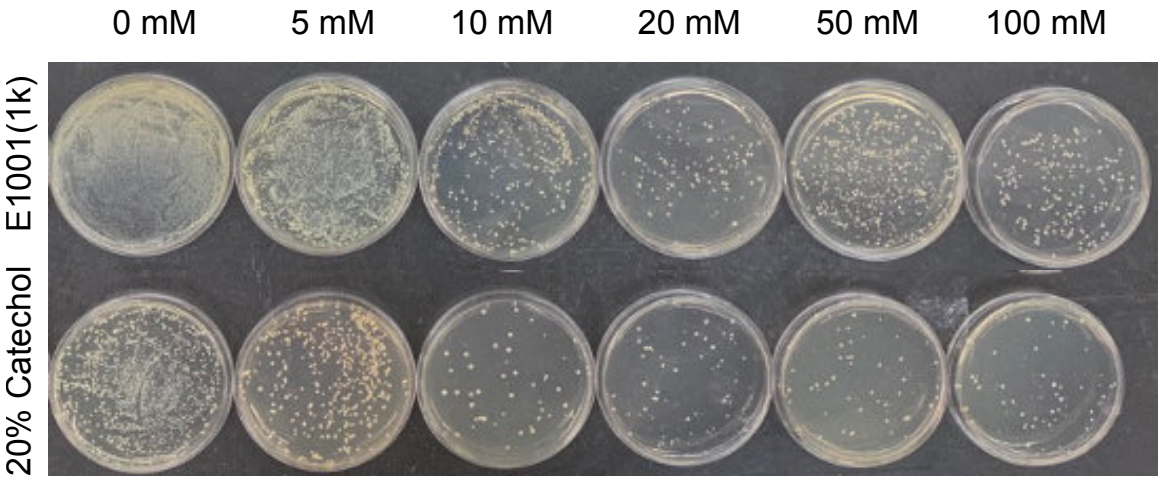

Figure 4.18 Representative TSA plates coated with *S. aureus* suspension without dilution.

4.3.5.4 Influence of Catechol Contents on Antibacterial Strength

Based on the studies discussed in **Section 4.3.3.3**, 10 mM $AgNO_3$ was chosen as the proper concentration for AgNPs deposition. The antibacterial properties of polymers with different catechol contents were investigated in this section. The presence of surface-active catechol is able to facilitate AgNPs formation (< 100 nm) on all modified polymer films, as the catechol content increases to 40 mol%, larger aggregates started to appear (Figure 4.19).

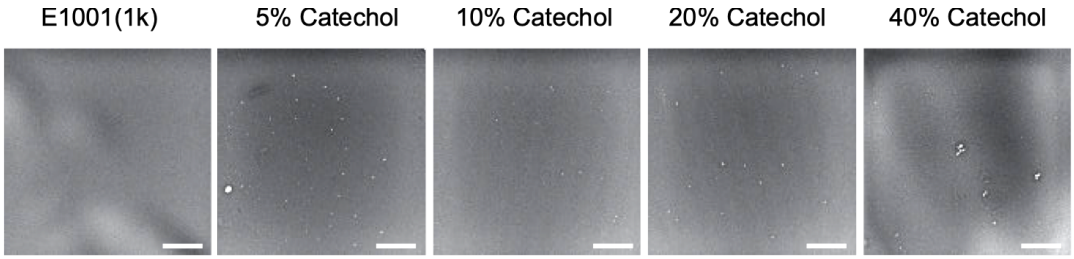

Figure 4.19 SEM images of catechol-assisted AgNPs deposition on polymer films containing different mol% of catechol side chains, all films were dip-coated in 10 mM $AgNO_3$ solution. Scale bars are 10 μm.

Antibacterial tests revealed strong activities of polymers containing 20% and 40% catechol against *E. coli* (log reduction ~8, Figure 4.20A). Polymers with 5% and 10% catechol showed equal or less of a killing effect of *E. coli* to E1001 (1k). According to Figure 4.20B, the polymers containing 20% and 40% catechol have significantly higher log reduction (3~4) than the other three groups, the log reduction of 5% and 10% catechol groups were not significantly different from the E1001(1k) control. It can be concluded from these results that only polymers with 20-40% catechol will have enough antibacterial

activity at 10 mM coating concentration. Representative agar plates coated with bacteria suspension cultured on films were collected in Figure 4.21.

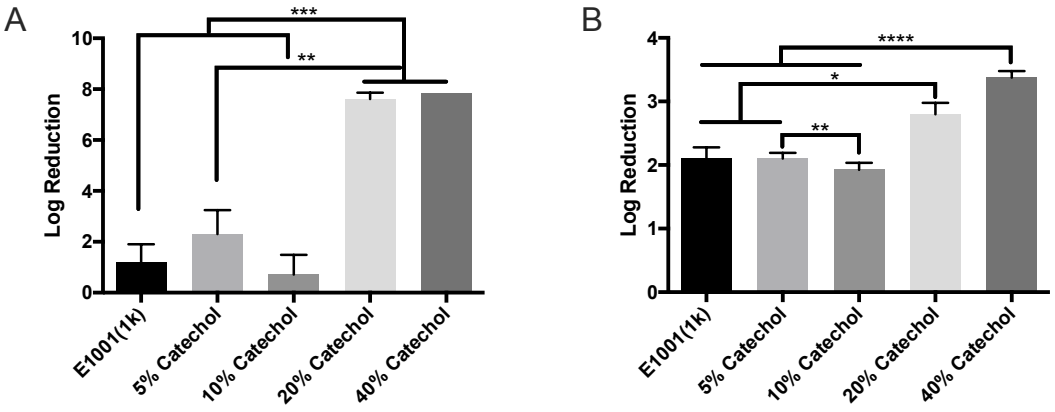

Figure 4.20 The influence of catechol contents on the antibacterial properties of polymers against *E. coli* (A) and *S. aureus* (B) (n = 4) when dip-coating in 10 mM $AgNO_3$. * indicates $p<0.05$, ** indicates $p<0.01$, *** indicates $p<0.001$, **** indicates $p<0.0001$.

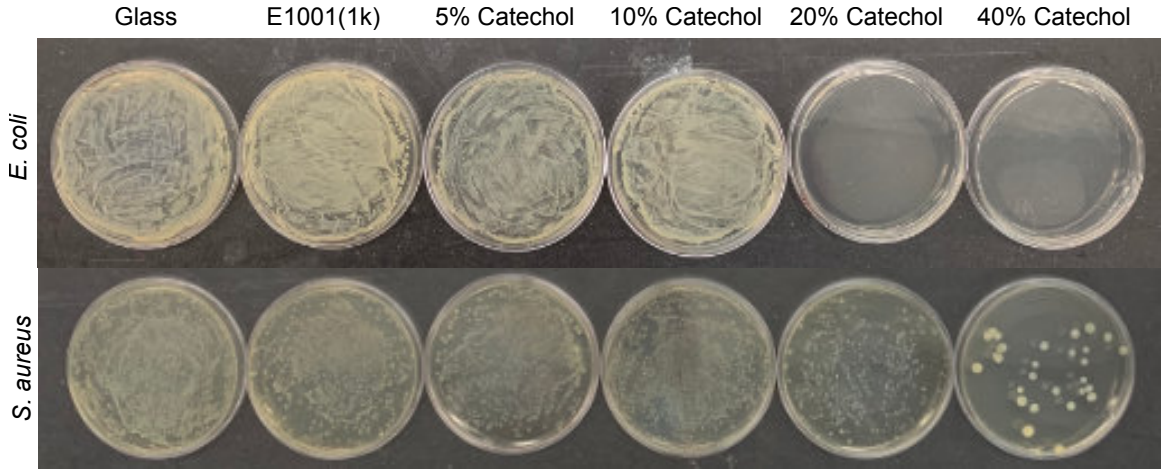

Figure 4.21 Representative agar plates coated with bacteria suspension without dilution.

4.4 Conclusion

With the intention to improve the bioactivity of E1001(1k), dopamine was successfully modified as side chains onto tyrosine-derived polycarbonates. Surface-active catechol moieties from dopamine side chains were confirmed with water contact angle measurement and Arnow's test. *In vitro* cell studies revealed that the catechol modification maintains good cell viability of the resulting polymers compared to E1001(1k). However, the sole presence of catechol has limited stimulation on osteogenic cell differentiation. Secondary biofunctionalization mediated by catechol is necessary to improve the bioactivity of these polymers. On the other hand, it was found that the surface anchoring catechol moieties could assist nano-sized silver deposition on surface, the decorated surface could be readily performed on all catechol-modified polymers, with proper coating condition screened out, polymers with 20% and 40% catechol were found to possess strong antibacterial activity against *E. coli* and *S. aureus*.

4.5 References

1.Kim, J.; Magno, M. H.; Alvarez, P.; Darr, A.; Kohn, J.; Hollinger, J. O., Osteogenic differentiation of pre-osteoblasts on biomimetic tyrosine-derived polycarbonate scaffolds. *Biomacromolecules* **2011,** *12* (10), 3520-7.
2.Magno, M. H. R.; Kim, J.; Srinivasan, A.; McBride, S.; Bolikal, D.; Darr, A.; Hollinger, J. O.; Kohn, J., Synthesis, degradation and biocompatibility of tyrosine-derived polycarbonate scaffolds *J. Mater. Chem.* **2010,** *20*, 8885-8893.
3.Chen, S. S.; Ortiz, O.; Pastino, A. K.; Wu, X.; Hu, B.; Hollinger, J. O.; Bromage, T. G.; Kohn, J., Hybrid Bone Scaffold Induces Bone Bridging in Goat Calvarial Critical Size Defects Without Growth Factor Augmentation. *Regen. Eng. Transl. Med.* **10.1007/s40883-019-00144-z**.
4.Bushman, J. S.; Raynor, J. E.; Kohn, J. B., Molecular surface design of tyrosine-derived polycarbonates for attachment of biomolecules. Google Patents: 2015.
5.Yang, J.; Stuart, M. A. C.; Kamperman, M., Jack of all trades: versatile catechol crosslinking mechanisms. *Chem Soc Rev* **2014,** *43* (24), 8271-8298.
6.Ding, Y. H.; Yang, Z. L.; Bi, C. W. C.; Yang, M.; Zhang, J. C.; Xu, S. L.; Lu, X.; Huang, N.; Huang, P. B.; Leng, Y., Modulation of protein adsorption, vascular cell selectivity and platelet adhesion by mussel-inspired surface functionalization. *J Mater Chem B* **2014,** *2* (24), 3819-3829.
7.Saiz-Poseu, J.; Mancebo-Aracil, J.; Nador, F.; Busque, F.; Ruiz-Molina, D., The Chemistry behind Catechol-Based Adhesion. *Angewandte Chemie (International ed. in English)* **2019,** *58* (3), 696-714.
8.Yang, Z.; Tu, Q.; Zhu, Y.; Luo, R.; Li, X.; Xie, Y.; Maitz, M. F.; Wang, J.; Huang, N., Mussel-inspired coating of polydopamine directs endothelial and smooth muscle cell fate for re-endothelialization of vascular devices. *Adv Healthc Mater* **2012,** *1* (5), 548-59.
9.Black, K. C. L.; Liu, Z. Q.; Messersmith, P. B., Catechol Redox Induced Formation of Metal Core-Polymer Shell Nanoparticles. *Chem Mater* **2011,** *23* (5), 1130-1135.
10.Baron, R.; Zayats, M.; Willner, I., Dopamine-, L-DOPA-, adrenaline-, and noradrenaline-induced growth of Au nanoparticles: Assays for the detection of neurotransmitters and of tyrosinase activity. *Anal Chem* **2005,** *77* (6), 1566-1571.
11.Zhang, X. F.; Liu, Z. G.; Shen, W.; Gurunathan, S., Silver Nanoparticles: Synthesis, Characterization, Properties, Applications, and Therapeutic Approaches. *Int J Mol Sci* **2016,** *17* (9).
12.Orapiriyakul, W.; Young, P. S.; Damiati, L.; Tsimbouri, P. M., Antibacterial surface modification of titanium implants in orthopaedics. *J Tissue Eng* **2018,** *9*.
13.Ryu, J. H.; Hong, S.; Lee, H., Bio-inspired adhesive catechol-conjugated chitosan for biomedical applications: A mini review. *Acta Biomaterialia* **2015,** *27*, 101-115.
14.Le Thi, P.; Lee, Y.; Hoang Thi, T. T.; Park, K. M.; Park, K. D., Catechol-rich gelatin hydrogels in situ hybridizations with silver nanoparticle for enhanced antibacterial activity. *Mater Sci Eng C Mater Biol Appl* **2018,** *92*, 52-60.
15.Sanborn, T. J.; Messersmith, P. B.; Barron, A. E., In situ crosslinking of a biomimetic peptide-PEG hydrogel via thermally triggered activation of factor XIII. *Biomaterials* **2002,** *23* (13), 2703-10.

16.Kim, S. H.; Lee, S.; In, I.; Park, S. Y., Synthesis and antibacterial activity of surface-coated catechol-conjugated polymer with silver nanoparticles on versatile substrate. *Surface and Interface Analysis* **2016,** *48* (9), 995-1001.
17.Huang, W. Y.; Cai, Y. Z.; Zhang, Y., Natural phenolic compounds from medicinal herbs and dietary plants: potential use for cancer prevention. *Nutr Cancer* **2010,** *62* (1), 1-20.
18.Zhang, C.; Ma, M. Q.; Chen, T. T.; Zhang, H.; Hu, D. F.; Wu, B. H.; Ji, J.; Xu, Z. K., Dopamine-Triggered One-Step Polymerization and Codeposition of Acrylate Monomers for Functional Coatings. *ACS Appl Mater Interfaces* **2017,** *9* (39), 34356-34366.
19.Takeshima, H.; Satoh, K.; Kamigaito, M., Scalable Synthesis of Bio-Based Functional Styrene: Protected Vinyl Catechol from Caffeic Acid and Controlled Radical and Anionic Polymerizations Thereof. *Acs Sustain Chem Eng* **2018,** *6* (11), 13681-13686.
20.Shi, D. J.; Shen, J. L.; Zhao, Z. H.; Shi, C.; Chen, M. Q., Studies on Preparation of Poly(3,4-Dihydroxyphenylalanine)-Polylactide Copolymers and the Effect of the Structure of the Copolymers on Their Properties. *Polymers-Basel* **2016,** *8* (3).
21.Kord Forooshani, P.; Lee, B. P., Recent approaches in designing bioadhesive materials inspired by mussel adhesive protein. *J Polym Sci A Polym Chem* **2017,** *55* (1), 9-33.
22.Lee, B. P.; Dalsin, J. L.; Messersmith, P. B., Synthesis and gelation of DOPA-modified poly(ethylene glycol) hydrogels. *Biomacromolecules* **2002,** *3* (5), 1038-47.
23.Huang, K.; Lee, B. P.; Ingram, D. R.; Messersmith, P. B., Synthesis and characterization of self-assembling block copolymers containing bioadhesive end groups. *Biomacromolecules* **2002,** *3* (2), 397-406.
24.Mehdizadeh, M.; Weng, H.; Gyawali, D.; Tang, L.; Yang, J., Injectable citrate-based mussel-inspired tissue bioadhesives with high wet strength for sutureless wound closure. *Biomaterials* **2012,** *33* (32), 7972-7983.
25.Zhang, H.; Zhao, T. Y.; Newland, B.; Liu, W. G.; Wang, W.; Wang, W. X., Catechol functionalized hyperbranched polymers as biomedical materials. *Prog Polym Sci* **2018,** *78*, 47-55.
26.Liu, J.; Yang, W.; Zareie, H. M.; Gooding, J. J.; Davis, T. P., pH-Detachable polymer brushes formed using titanium− diol coordination chemistry and living radical polymerization (RAFT). *Macromolecules* **2009,** *42* (8), 2931-2939.
27.Zobrist, C.; Sobocinski, J.; Lyskawa, J.; Fournier, D.; Miri, V.; Traisnel, M.; Jimenez, M.; Woisel, P., Functionalization of titanium surfaces with polymer brushes prepared from a biomimetic RAFT agent. *Macromolecules* **2011,** *44* (15), 5883-5892.
28.Fan, X.; Lin, L.; Messersmith, P. B., Cell fouling resistance of polymer brushes grafted from Ti substrates by surface-initiated polymerization: effect of ethylene glycol side chain length. *Biomacromolecules* **2006,** *7* (8), 2443-2448.
29.Fan, X.; Lin, L.; Dalsin, J. L.; Messersmith, P. B., Biomimetic anchor for surface-initiated polymerization from metal substrates. *Journal of the American Chemical Society* **2005,** *127* (45), 15843-15847.
30.Gao, C.; Li, G.; Xue, H.; Yang, W.; Zhang, F.; Jiang, S., Functionalizable and ultra-low fouling zwitterionic surfaces via adhesive mussel mimetic linkages. *Biomaterials* **2010,** *31* (7), 1486-1492.
31.Li, G.; Cheng, G.; Xue, H.; Chen, S.; Zhang, F.; Jiang, S., Ultra low fouling zwitterionic polymers with a biomimetic adhesive group. *Biomaterials* **2008,** *29* (35), 4592-4597.

32.Ye, Q.; Wang, X.; Li, S.; Zhou, F., Surface-initiated ring-opening metathesis polymerization of pentadecafluorooctyl-5-norbornene-2-carboxylate from variable substrates modified with sticky biomimic initiator. *Macromolecules* **2010,** *43* (13), 5554-5560.
33.Kuang, J.; Messersmith, P. B., Universal surface-initiated polymerization of antifouling zwitterionic brushes using a mussel-mimetic peptide initiator. *Langmuir* **2012,** *28* (18), 7258-7266.
34.Hu, B.-H.; Messersmith, P. B., Protection of 3, 4-dihydroxyphenylalanine (DOPA) for Fmoc solid-phase peptide synthesis. *Tetrahedron letters* **2000,** *41* (31), 5795-5798.
35.Sever, M. J.; Wilker, J. J., Synthesis of peptides containing DOPA (3, 4-dihydroxyphenylalanine). *Tetrahedron* **2001,** *57* (29), 6139-6146.
36.Behnam, M. A.; Sundermann, T. R.; Klein, C. D., Solid phase synthesis of C-terminal boronic acid peptides. *Organic letters* **2016,** *18* (9), 2016-2019.
37.Miller, S. M.; Simon, R. J.; Ng, S.; Zuckermann, R. N.; Kerr, J. M.; Moos, W. H., Comparison of the proteolytic susceptibilities of homologous L-amino acid, D-amino acid, and N-substituted glycine peptide and peptoid oligomers. *Drug Development Research* **1995,** *35* (1), 20-32.
38.Statz, A. R.; Meagher, R. J.; Barron, A. E.; Messersmith, P. B., New peptidomimetic polymers for antifouling surfaces. *Journal of the American Chemical Society* **2005,** *127* (22), 7972-7973.
39.Jenkins, C. L.; Siebert, H. M.; Wilker, J. J., Integrating Mussel Chemistry into a Bio-Based Polymer to Create Degradable Adhesives. *Macromolecules* **2017,** *50* (2), 561-568.
40.Choi, J. S.; Messersmith, P. B.; Yoo, H. S., Decoration of electrospun nanofibers with monomeric catechols to facilitate cell adhesion. *Macromol Biosci* **2014,** *14* (2), 270-9.
41.Yang, C.; Ding, X.; Ono, R. J.; Lee, H.; Hsu, L. Y.; Tong, Y. W.; Hedrick, J.; Yang, Y. Y., Brush-like polycarbonates containing dopamine, cations, and PEG providing a broad-spectrum, antibacterial, and antifouling surface via one-step coating. *Adv Mater* **2014,** *26* (43), 7346-51.
42.Becker, G.; Wurm, F. R., Functional biodegradable polymers via ring-opening polymerization of monomers without protective groups. *Chem Soc Rev* **2018,** *47* (20), 7739-7782.
43.Spaans, S.; Fransen, P. P. K. H.; Ippel, B. D.; de Bont, D. F. A.; Keizer, H. M.; Bax, N. A. M.; Bouten, C. V. C.; Dankers, P. Y. W., Supramolecular surface functionalization via catechols for the improvement of cell-material interactions. *Biomaterials Science* **2017,** *5* (8), 1541-1548.
44.Arnow, L. E., Colorimetric determination of the components of 3, 4-dihydroxyphenylalanine-tyrosine mixtures. *J. biol. Chem* **1937,** *118* (2), 531-537.
45.Mao, Y.; Hoffman, T.; Singh-Varma, A.; Duan-Arnold, Y.; Moorman, M.; Danilkovitch, A.; Kohn, J., Antimicrobial Peptides Secreted From Human Cryopreserved Viable Amniotic Membrane Contribute to its Antibacterial Activity. *Sci Rep* **2017,** *7* (1), 13722.
46.Szleifer, I., Polymers and proteins: interactions at interfaces. *Current Opinion in Solid State and Materials Science* **1997,** *2* (3), 337-344.
47.Kim, J. S.; Kuk, E.; Yu, K. N.; Kim, J. H.; Park, S. J.; Lee, H. J.; Kim, S. H.; Park, Y. K.; Park, Y. H.; Hwang, C. Y.; Kim, Y. K.; Lee, Y. S.; Jeong, D. H.; Cho, M. H., Antimicrobial effects of silver nanoparticles. *Nanomedicine* **2007,** *3* (1), 95-101.

48.Ning, C.; Wang, X.; Li, L.; Zhu, Y.; Li, M.; Yu, P.; Zhou, L.; Zhou, Z.; Chen, J.; Tan, G.; Zhang, Y.; Wang, Y.; Mao, C., Concentration ranges of antibacterial cations for showing the highest antibacterial efficacy but the least cytotoxicity against mammalian cells: implications for a new antibacterial mechanism. *Chem Res Toxicol* **2015,** *28* (9), 1815-22.

5 Conclusion and Future Perspectives

This doctoral research aimed to investigate the efficacy of physically and chemically incorporated components in the development of scaffold-based bone tissue engineering strategies. Critical components of bone tissue microenvironment including the scaffold phase and the osteogenic GFs phase were investigated and addressed in detail.

The conventional BGS developed in the Kohn lab involves a porous composite scaffold made from a polycarbonate (i.e., E1001(1k)) and various calcium phosphate minerals as well as a physically incorporated osteogenic growth factor (i.e., rhBMP-2) to mimic the bone microenvironment. **Chapter 2** of this thesis focused on expanding the *in vivo* tests of E1001(1k)/β-TCP scaffolds from craniofacial defects to long bone defects in a critical size large animal model. The comparable performance of E1001(1k)/β-TCP scaffolds to the clinically relevant BGS chronOS® and more physiological morphology of new bone within the scaffolds make E1001(1k)/β-TCP scaffolds a promising candidate for large bone defect reconstruction. It should be noted that the long bone reconstruction is a prolonged process, fully functional tibial bone could have been obtained given a longer period of the *in vivo* study. More importantly, the dose of rhBMP-2 applied in this study is the lowest ever reported for acellular scaffolds, the *in vivo* bone void filling could have been improved further with slightly elevated doses.

Though rhBMP-2-containing devices have been approved by FDA for treatment of multiple bone injuries, adverse effects have been observed in clinical applications due to supraphysiological levels of rhBMP-2 present in the devices. In **Chapter 3**, a systematic study on *in vitro* rhBMP-2 bioactivity assays was conducted to help address the proper rhBMP-2 dosing for *in vitro* and *in vivo* studies. The determined optimal dose-response

ranges and rhBMP-2 induction time using W-20-17, MC3T3 and C2C12 cell assays can be useful in terms of the selection of proper cell lines for evaluation of rhBMP-2 release *in vitro*. The ED50 values of rhBMP-2 expressed from *E. coli,* CHO cells and HEK 293 cells will assist the evaluation of rhBMP-2 efficacy *in vitro* and eventually lead to the determination of proper doses for *in vivo* studies. In addition, it was observed that the bioactivity quantified from the W-20-17 cellular assay is proportional to the concentration of rhBMP-2 quantified by ELISA upon incubation at 37 ºC. Therefore, the bioactivity retention of rhBMP-2 during *in vitro* studies could be indicated by the concentration quantified through ELISA. The methodology and rhBMP-2 bioactivity data reported in this chapter bring insight into the development of bone tissue engineering strategies using rhBMP-2 as the signaling phase.

In **Chapter 4**, the polycarbonate used for bone scaffold fabrication was further investigated with chemically functionalized catechol side chains to create a more bioactive polymeric platform. Though the modified polymers were able to support HO-fs, MC3T3 cells and hMSCs growth, the catechol functionality has limited osteogenic effects on MSCs and MC3T3 cells. Therefore, secondary functionalization on surface-anchoring catechol moieties with osteogenic GFs or peptides through the Michael-type addition on oxidized quinones might be necessary for stronger osteogenic stimulation. Another application that arises from surface-active catechol moieties is their ability to assist nano-sized silver deposition on the polymeric surface through the redox reaction between catechol and silver ions in aqueous solutions. It was found that the antibacterial strength of Ag-decorated films is proportional to the $AgNO_3$ used for AgNPs deposition as well as the mol% of catechol side chains in the E1001(1k) analogs. The antibacterial activities of E1001(1k) analog

polymers introduced by catechol functionalization could beneficial in the field of antibacterial coating on orthopedic implants. Moreover, given the versatile nature of catechol chemistry, the catechol-modified polycarbonates could potentially have bone-related applications in facilitating the biomineralization of calcium phosphate through the chelation between calcium ions and catechol, and bioconjugation of bioactive molecules on the polymeric surfaces for important physiological events during bone injury healing such as angiogenesis.